Estimating Subsurface Stresses

An Investigation on Obtaining the Minimum Horizontal Stress from Hydraulic Stress Test Data

AESM7000: Master Thesis Applied Earth Sciences

W.L. Horeman

Delft University of Technology

TU Delft

Estimating Subsurface Stresses

An Investigation on Obtaining the Minimum Horizontal Stress from Hydraulic Stress Test Data

by

W.L. Horeman

Student Number: 4726669

Master Thesis Applied Earth Sciences

Daily Supervisor:	Lennart Hanemaaijer
Academic Supervisors:	Auke Barnhoorn, Phil Vardon
Advisor:	Javier Mozas
Assessment Committee:	Hadi Hajibeygi, Auke Barnhoorn, Phil Vardon
Project Duration:	August, 2025 - March, 2026
Faculty:	Faculty of Civil Engineering & Geosciences, TU Delft

TU Delft

Preface

Hereby I present my thesis for the Applied Earth Sciences programme at Delft University of Technology. I would like to express my sincere gratitude to my parents for their unconditional support throughout my life, and to my girlfriend for her continuous encouragement during this period.

I would also like to thank my supervisors at EBN, Lennart Hanemeijer, Marc Hettema, and in particular Adriaan Janszen, who kindly took the time to proofread this thesis. Furthermore, I am grateful to Phil Vardon and Auke Barnhoorn for their guidance and supervision, and to Hadi Hajibeygi for serving on my assessment committee. Finally, I would like to thank Javier Mozas for his support and valuable input throughout the past half year.

W.L. Horeman
The Hague, March 2026

Abstract

Accurate estimation of the minimum horizontal stress $S_{h\,\min}$ is essential for well design, drilling safety, and predicting induced seismicity. In many regions of the Netherlands, however, only formation integrity tests (FIT) and leak-off tests (LOT) are available, raising the question of whether these drilling tests can be used to reliably infer $S_{h\,\min}$. This study evaluates the reliability of stress estimation from hydraulic fracturing data, with a particular focus on the differences between fracture initiation and closure pressures.

A comprehensive dataset of extended leak-off tests (XLOT), micro-fracture tests, and conventional LOT/FIT data is analysed. Multiple closure interpretation methods are compared, and their variability, bias, and applicability are quantified. In addition, initiation-based pressures are evaluated within a mechanical framework, including sensitivity analyses and stress consistency checks.

The results show that closure-derived pressures provide the most reliable estimate of $S_{h\,\min}$, whereas initiation-based pressures are strongly influenced by near-wellbore effects and operational conditions. Closure interpretation is inherently method-dependent, with inter-method differences up to 25 bar, significantly exceeding the repeatability within a single method. Among the evaluated techniques, the semilog max method demonstrates the best balance between robustness and applicability.

Measured pressures from FIT and LOT tests often exceed closure-derived $S_{h\,\min}$ and exhibit large variability, including non-physical results in a significant fraction of cases. While these pressures can be interpreted as upper or lower bounds within a mechanical framework, their quantitative reliability is limited. Furthermore, an offset data case study from nearby wells did not provide a reliable predictor the $S_{h\,\min}$.

This study establishes a hierarchical interpretation framework in which closure-derived pressures form the primary estimate of $S_{h\,\min}$, while initiation-based pressures provide only supplementary constraints.

Contents

Nomenclature

Common Abbreviations

Abbreviation	Definition
FIT	Formation Integrity Test
LOT	Leak-Off Test
XLOT	Extended Leak-Off Test
FBP	Fracture Breakdown Pressure
FRP	Fracture Re-opening Pressure
FCP	Fracture Closure Pressure
LEFM	Linear Elastic Fracture Mechanics
ISIP	Instantaneous Shut-In Pressure
SCAN	Seismische Campagne Aardwarmte Nederland

Symbols

Symbol	Definition	SI Unit
K_0	Effective stress ratio, $K_0 = \frac{\sigma'_h}{\sigma'_v} = \frac{S_h - \alpha p}{S_v - \alpha p}$	[-]
E	Young's modulus, stiffness in uniaxial compression ($E = \sigma_{11}/\varepsilon_{11}$)	[Pa]
K	Bulk modulus, stiffness under hydrostatic compression ($K = \sigma_{kk}/\varepsilon_{kk}$)	[Pa]
G	Shear modulus, ratio of shear stress to shear strain ($G = \sigma_{13}/2\varepsilon_{13}$)	[Pa]
β	Compressibility, reciprocal of bulk modulus ($\beta = K^{-1}$)	[Pa^{-1}]
S_{ijkl}	Stiffness tensor (relating stress to strain, $\sigma_{ij} = S_{ijkl}\varepsilon_{kl}$)	[Pa]
C_{ijkl}	Compliance tensor (relating strain to stress, $\varepsilon_{ij} = C_{ijkl}\sigma_{kl}$)	[Pa^{-1}]
ν	Poisson's ratio, ratio of lateral expansion to acial shortening, ($\nu = \varepsilon_{33}/\varepsilon_{11}$)	[-]
α	Biot coefficient, quantifies the fraction of pore pressure that contributes to effective stress in porous rock, ($\alpha = 1 - K_b/K_g$)	[-]
S_v	Vertical total stress (overburden stress)	[Pa]
$S_{h,\min}$	Minimum horizontal total stress	[Pa]
$S_{H,\max}$	Maximum horizontal total stress	[Pa]
σ_{ij}	Effective stress tensor components	[Pa]
$\sigma_{\theta\theta}$	Tangential (hoop) stress around the wellbore wall	[Pa]
P_0	Far-field pore pressure	[Pa]
P_w	Wellbore pressure	[Pa]
P_p	Pore pressure	[Pa]
P_f	Fracture pressure	[Pa]
V	Fluid volume	[m^3]
t	Time	[s]
K_I	Mode-I stress intensity factor at the fracture tip	[Pa $m^{1/2}$]
K_{IC}	Mode-I fracture toughness	[Pa $m^{1/2}$]
T_0	Tensile strength of the rock	[Pa]

1

Introduction

As the Netherlands accelerates its transition away from large-scale natural gas production, geothermal energy is expected to become an increasingly important component of sustainable district heating in urban areas. Recent national outlooks adopt an upper bound of 100 PJ geothermal heat production by 2040 and 200 PJ by 2050 and 2060, compared to only 6.5 PJ realised in 2023 (Planbureau voor de Leefomgeving, 2025). Achieving this projected thirty-fold increase implies widespread deployment of geothermal energy, often in densely populated regions. In contrast to conventional hydrocarbon operations, geothermal projects are therefore commonly situated close to residential and industrial infrastructure, where even low-magnitude induced seismic events may have significant societal and political consequences, as demonstrated during and after the Groningen earthquakes (Van der Voort & Vanclay, 2015). Under these conditions, reliable characterization of subsurface stress conditions is not merely a technical requirement, but a prerequisite for safe well design, regulatory approval, and public acceptance.

In structurally complex basins such as the West Netherlands Basin, where pre-existing faults are abundant and may be critically stressed, uncertainty in the in-situ stress field directly propagates into uncertainty in fault reactivation potential and induced seismic hazard (Zoback, 2010). In response, Dutch regulation now mandates a Seismic Hazard and Risk Analysis (SHRA) for geothermal permitting, which relies on key geomechanical inputs to assess seismic hazard (Mijnbouwwet, 2023). SHRA methodologies explicitly require quantitative estimates of in-situ stresses to evaluate fault stability under operational pressure changes. Because SHRA models rely on Mohr–Coulomb failure criteria and slip tendency calculations, the minimum horizontal stress is a first-order control on predicted fault stability. Even modest deviations in $S_{h\,\mathrm{min}}$ may alter whether a fault segment is classified as stable, critically stressed, or unstable under operational pressure conditions. Consequently, epistemic uncertainty in $S_{h\,\mathrm{min}}$ propagates directly into increased variability in seismic risk classification, mitigation measures, and operational envelopes.

Accurate estimation of S_{hmin} remains a technical and practical challenge. Despite the central role of $S_{h\,\mathrm{min}}$ in both seismic hazard assessment and well design, there is currently no standardized national workflow for interpreting hydraulic stress tests in Dutch geothermal wells. Closure pressures derived from XLOT or micro-fracture tests are commonly interpreted as estimates of S_{hmin}, yet they depend strongly on the selected interpretation methodology. FIT and LOT measurements, while widely used in drilling operations, were not designed for stress characterization. As a result, current practice often relies on pragmatic assumptions rather than validated stress constraints, leading to inconsistent interpretations across operators and projects.

Hydraulic stress testing methods - including *leak-off tests* (LOTs), *extended leak-off tests* (XLOTs), *micro-frac* tests, and, to a lesser extent, *formation integrity tests* (FITs) - are the primary field-based tools for inferring S_{hmin}. Among these, XLOTs and micro-frac tests are generally considered the most reliable, as they capture both fracture initiation and closure pressures under controlled conditions (Haimson & Cornet, 2003). However, their high cost and operational complexity often preclude their use in routine

geothermal drilling programs (Widodo et al., 2003). The reliance on routinely acquired LOT and FIT data is therefore driven not only by availability, but also by economic considerations associated with rig time and dedicated stress testing operations.

As a result, project developers often rely on more routinely available LOT and FIT data, despite ambiguity regarding their suitability as proxies for S_{hmin}. In micro-frac and XLOT tests, the *fracture closure pressure* is a key parameter for determining $S_{h\mathrm{min}}$ (Zoback, 2010), but LOTs and FITs are terminated before closure is reached. Instead, the *leak-off pressure* (LOP) is recorded, which may deviate significantly from the true closure stress due to hoop stresses, pre-existing fractures, wellbore inclination and permeability in general (Verweij, 2015; Zang & Stephansson, 2010; Zoback, 2010).

Furthermore, FIT and LOT measurements are generally acquired for operational purposes rather than for geomechanical analysis. In the absence of more suitable data, these tests are often repurposed for geomechanical interpretation and caprock integrity assessment. However, they are frequently poorly documented, with incomplete metadata on mud weight, temperature, and injection rate, which complicates comparison with more controlled datasets such as XLOT and micro-frac measurements. Closure analysis of XLOTs and micro-fracs is further challenged by the lack of standardized interpretation procedures. In addition, pressure records may suffer from insufficient resolution or be affected by operational artifacts, such as premature pumping shutdowns or unintended fracturing of the rock–cement interface. Without the application of specialized interpretation methods, the estimation of closure stress from such datasets remains subject to significant uncertainty.

In the Netherlands, the SCAN ("Seismische Campagne Aardwarmte Nederland") project has recently provided a valuable step forward in addressing this gap. By systematically acquiring high-quality seismic and geomechanical data (including FIT, LOT and XLOT tests) and integrating it with wellbore information, SCAN improves the regional resolution of subsurface models, particularly in areas relevant for geothermal development. This provides a more robust geological framework within which stress test data can be interpreted, reducing epistemic uncertainty in S_{hmin} estimations.

Against this backdrop, this research investigates how hydraulic stress tests work, how their results should be interpreted, and how useful FIT and LOT tests can be for determining S_{hmin}. The study draws mainly on well data from SCAN geothermal research wells and public source NLOG. By improving the reliability and accessibility of S_{hmin} estimation, the research aims to contribute to safer, more cost-effective, and scalable geothermal energy deployment in the Netherlands, in line with international efforts to enhance subsurface stress characterization in sedimentary basins.

Chapter 2 presents the theoretical background required to interpret hydraulic stress test data, including stress theory, fracture mechanics, and the physical principles underlying different test types. Chapter 3 describes the research methodology, including data preprocessing, characteristic pressure identification, closure interpretation methods, and stress inference. Chapter 4 presents the results of the stress test analyses, including closure method comparison and the offset-data case study. Chapter 5 discusses the mechanical interpretation of the findings, evaluates methodological uncertainty, and answers the research questions. Finally, Chapter 6 summarises the main conclusions and provides recommendations for future research and practical application.

Research objective

The primary objective of this research is to evaluate how the minimum horizontal stress, S_{hmin}, can be reliably constrained using hydraulic stress test data in the Dutch geothermal context. Specifically, closure pressures derived from XLOT and micro-fracture tests are treated as mechanically defensible reference estimates of S_{hmin} and systematically compared with leak-off pressures obtained from LOT and FIT measurements. By assessing the methodological variability in closure picking, the mechanical interpretation of initiation-based pressures, and the predictive value of offset data, this study develops a structured and practically applicable workflow for stress estimation. The aim is to reduce epistemic uncertainty in S_{hmin} interpretation and to support more consistent input for seismic hazard assessment and well design in geothermal operations.

Research questions

The main research question is:

To what extent can the S_{hmin} be reliably estimated in regions for which only FIT and/or LOT data is available in the Netherlands?

This overarching question is addressed through the following sub-questions:

1. *What are the underlying physical principles governing hydraulic stress tests, and how are the hydraulic stress tests different from each other?*
2. *What methods can be used to determine the S_{hmin} from hydraulic stress tests using the closure pressure, which method is most preferred and why?*
3. *To what extent do FIT and LOT measurements provide a reliable constraint on the S_{hmin} when compared with XLOT and micro-fracture data from the same well?*
4. *Can the S_{hmin} be constrained based on offset LOT and FIT data?*

2

Background & literature review

This chapter provides the conceptual framework required to interpret hydraulic stress test data and to evaluate the reliability of stress estimates derived from such tests. The emphasis is placed on the minimum horizontal stress $S_{h\,\min}$. Because the stress state cannot be observed directly, $S_{h\,\min}$ must be inferred from pressure–time responses recorded during field tests, which introduces uncertainty that depends strongly on test design, wellbore geometry, and formation properties.

The chapter first reviews the fundamentals of in-situ stress magnitudes and directions in relation to tectonic regime and borehole observations. It then introduces the mechanical basis of rock failure, which underpins hydraulic fracturing and fault reactivation. Next, the main hydraulic stress test types are described within a unified terminology framework, and the characteristic pressures used in interpretation are defined and placed in their mechanical context. Afterwards, the governing physical models for fracture initiation and shut-in behaviour are introduced, including elastic stress concentration (Kirsch), fracture-mechanics-based propagation (LEFM), poro-elastic effects, diffusion-controlled leak-off, and fracture closure mechanics. At last, the assumptions used within this study are stated. Together, these elements establish the background needed for the methodological choices and interpretations presented in later chapters.

2.1. Theoretical basics

2.1.1. Stress basics & directions

The in-situ stress state describes the magnitude and orientation of forces acting on a rock mass before any disturbance by drilling or injection. It is defined by three mutually perpendicular principal stresses - vertical (S_v), maximum horizontal ($S_{H\,\max}$), and minimum horizontal ($S_{h\,\min}$) - for which all shear components vanish. Their relative magnitudes determine the tectonic regime (Anderson, 1951):

- **Normal faulting:** $S_v > S_{H\,\max} > S_{h\,\min}$
- **Strike-slip:** $S_{H\,\max} > S_v > S_{h\,\min}$
- **Reverse faulting:** $S_{H\,\max} > S_{h\,\min} > S_v$

In the Dutch subsurface, regional compilations and case studies indicate a predominantly normal-faulting stress regime, with a consistent NW–SE orientation of the maximum horizontal stress ($S_{H\,\max}$) at the regional scale (Heidbach et al., 2025; Muntendam-Bos et al., 2022). Local deviations from this regional pattern are nevertheless expected: in the vicinity of salt structures and major faults, both the stress regime and the principal stress directions may be significantly perturbed.

The vertical stress (S_v) is primarily controlled by the weight of the overburden and can be obtained by integrating bulk density with depth. The horizontal stresses arise from Poisson's effect associated with vertical loading, pore pressure, and superimposed tectonic strain. Stress orientations are commonly inferred from borehole image logs, where borehole breakouts typically align with $S_{h\,\min}$ and drilling-induced tensile fractures align with $S_{H\,\max}$. These observations are often complemented by regional

compilations such as the World Stress Map (WSM) (Heidbach et al., 2025).

The $S_{H\,\max}$ represents the largest compressive stress in the horizontal plane (for a normal faulting regime) and is more difficult to quantify than $S_{h\,\min}$. In contrast to $S_{h\,\min}$, it cannot be measured directly using standard hydraulic fracture stress tests. Instead, $S_{H\,\max}$ may be constrained indirectly through borehole observations (e.g. breakouts and drilling-induced tensile fractures combined with rock strength data), wellbore stability analyses, and regional fault-mechanics considerations (Zoback, 2010). In this study, $S_{H\,\max}$ is therefore treated as a governing parameter for fracture orientation and propagation rather than as a primary target of estimation, and its magnitude is not explicitly determined.

The $S_{h\,\min}$, which is the focus of this study, defines the least compressive stress and is of primary importance for hydraulic fracturing, wellbore stability, and fault stability analysis, which is needed to quantify the likelihood of induced seismicity. It can be estimated most robustly from diagnostic hydraulic fracture tests by interpreting the fracture closure pressure (FCP) during shut-in, once the induced fracture has propagated beyond the near-wellbore stress concentration zone. Under these conditions, fracture closure reflects equilibrium with the far-field minimum horizontal stress, such that P_{FCP} provides a defensible proxy for $S_{h\,\min}$ (Nolte, 1979). More elaboration on this can be found in section 2.5. This study therefore focuses on estimating $S_{h\,\min}$ from such tests, as it forms a key input for geomechanical modelling and induced seismicity assessment.

2.1.2. Modes of fracturing

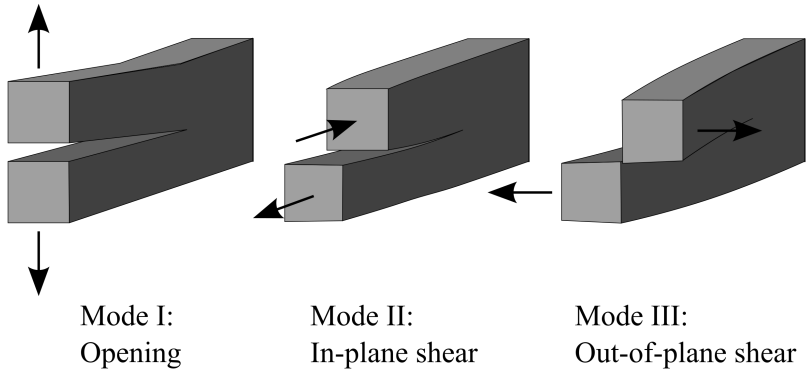

Figure 2.1: The three fundamental fracture modes: Mode I (tensile opening), Mode II (in-plane shear), and Mode III (out-of-plane shear), after Irwin (1957).

Fracturing in rocks occurs when the stress acting on a plane exceeds the material's strength, causing the rock to fail and displace along that plane. In fracture mechanics, three fundamental fracture modes are distinguished, each describing a specific form of displacement between the two fracture faces (Irwin, 1957) (See Figure 2.1):

- **Mode I – Tensile (opening) mode:** Characterized by displacement that is normal to the fracture plane. The opposing faces move directly apart, driven by tensile stress perpendicular to the fracture. This mode is dominant in hydraulic fracturing and forms the physical basis for estimating the minimum horizontal stress ($S_{h\,\min}$) from hydraulic fracture tests. Fracture initiation for an ideal planar crack occurs when the fluid pressure exceeds the least principal stress plus the tensile strength of the rock:

$$P_f \geq S_{h\,\min} + T_0, \tag{2.1}$$

  where P_f is the fluid pressure and T_0 the tensile strength. Note that this formula can change based on the geometry of the wellbore, as hoop stresses come into play. It is also dependent on whether perforations are present. More elaboration on this can be found in subsection 2.3.1.
- **Mode II – In-plane shear mode:** Characterized by sliding displacement parallel to the fracture front and within the fracture plane. Failure occurs when the shear stress exceeds the frictional

resistance along a pre-existing plane of weakness, consistent with the Mohr–Coulomb criterion:

$$\tau = c + \sigma_n \tan \phi, \tag{2.2}$$

where τ is the shear stress, c the cohesion, σ_n the effective normal stress, and ϕ the friction angle. σ_n can be calculated from:

$$\sigma_n = \frac{\sigma_1 + \sigma_3}{2} + \frac{\sigma_1 - \sigma_3}{2} \cos(2\theta) \tag{2.3}$$

Where σ_1 is the magnitude of the largest stress tensor, σ_3 is the magnitude of the smallest stress tensor, and θ is the angle between σ_1 and the fault plane. The difference between stress and effective stress is given by:

$$\sigma = S - \alpha P_p \tag{2.4}$$

Where P_p is the pore pressure. Notation varies throughout literature, but for clarity purposes, the notation as proposed above is the notation which will be used in this study. The Biot constant 'α' is assumed to be 1 throughout this study.

The Mode II failure is relevant to the reactivation of pre-existing faults during injection, depletion, and most relevantly, cooling induced by geothermal operations (Buijze et al., 2021). In Figure 2.2 one can observe what the effect is of a reduction in the $S_{h\,\min}$ caused by cooling, and what the relation is to fault reactivation.

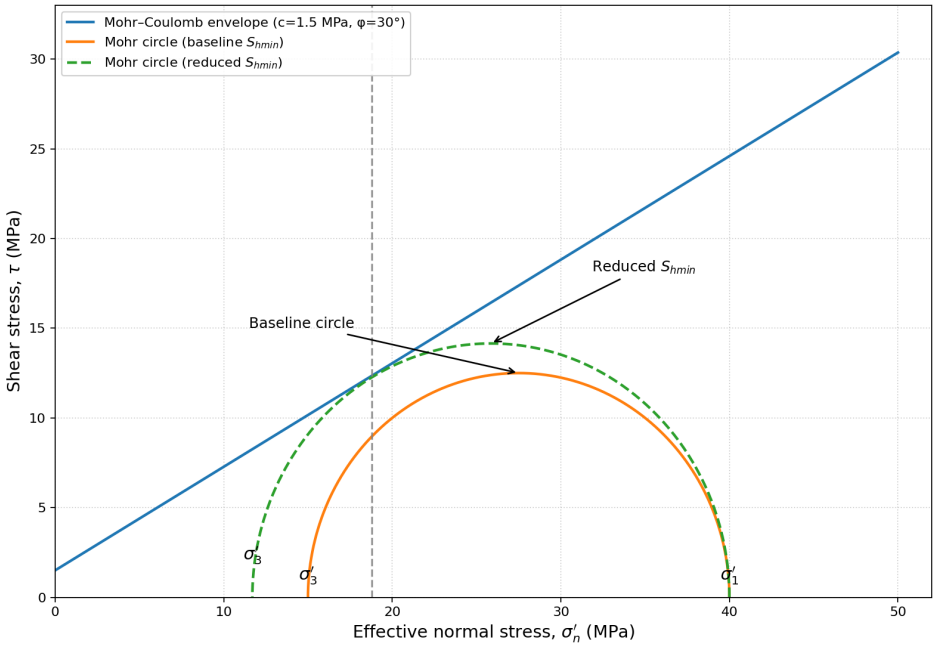

Figure 2.2: The Mohr–Coulomb failure criterion and Mohr's circle representation of stress states. One can see the reduction of $S_{h\,\min}$ due to cooling can lead to fault reactivation, as the Mohr circle meets the failure criterion here, located on the grey dashed line.

- **Mode III – Out-of-plane shear (tearing) mode:** Involves displacement perpendicular to the fracture front, producing a twisting or tearing motion of the fracture surfaces. Although less common in subsurface settings, Mode III can occur at fracture tips or along heterogeneous interfaces where local stress perturbations create complex mixed-mode propagation (for instance for wellbore breakouts). This failure mode is not relevant for this study.

During hydraulic fracture tests, the Mode I mechanism is of primary interest, as it provides a direct measure of the far-field $S_{h\,\min}$. Shear-dominated modes (II and III) are, however, critical for understanding potential fault reactivation and induced seismicity in geothermal and hydrocarbon reservoirs.

The remainder of this chapter first introduces hydraulic test types and characteristic pressures, then explains fracture initiation theory, later discusses diffusion and closure relevant for $S_{h\,\min}$ estimation, and finishes with the assumptions used in this study.

2.2. Hydraulic stress tests

A hydraulic stress test is an in-situ geomechanical experiment for which fluid is injected into a wellbore interval to deliberately perturb the local stress state and observe the mechanical response of the formation. By increasing pressure in a controlled manner, the test exploits the fact that rock failure and fracture behaviour are governed by the effective stresses acting around the wellbore. When the injection pressure approaches the minimum principal stress, tensile failure (Mode I failure) is initiated, resulting in fracture opening and fluid leak-off into the formation. The subsequent pressure response during shut-in and decline reflects fracture closure and stress re-equilibration. From these pressure–time signatures, key parameters such as the minimum horizontal stress and leak-off pressure can be inferred.

Hydraulic stress tests are conducted for different purposes. Some tests are diagnostic, designed specifically to characterise the in-situ stress state and formation behaviour (e.g. micro-fracture tests or extended leak-off tests). Others are primarily operational (e.g. leak-off tests and formation integrity test), performed to verify the maximum allowable mud weight or casing shoe integrity in order to safely continue drilling the next well section. While both rely on the same physical principles, their data quality, test design, and suitability for stress interpretation differ substantially.

Operational tests (FIT/LOT) primarily constrain the maximum allowable equivalent mud weight (EMW) at the casing shoe, often expressed as a fracture gradient (see Figure 2.4). Together with pore pressure, this defines the drilling pressure window. Diagnostic tests (XLOT/micro-frac) go further by enabling estimation of $S_{h\,\min}$ via closure behaviour.

Figure 2.3: BakerHughes micro-frac wireline tool, later to be used for performing a micro-frac test at the DEL-GT-02 well in Delft. Note the blue protection, which denote the packers on the tool.

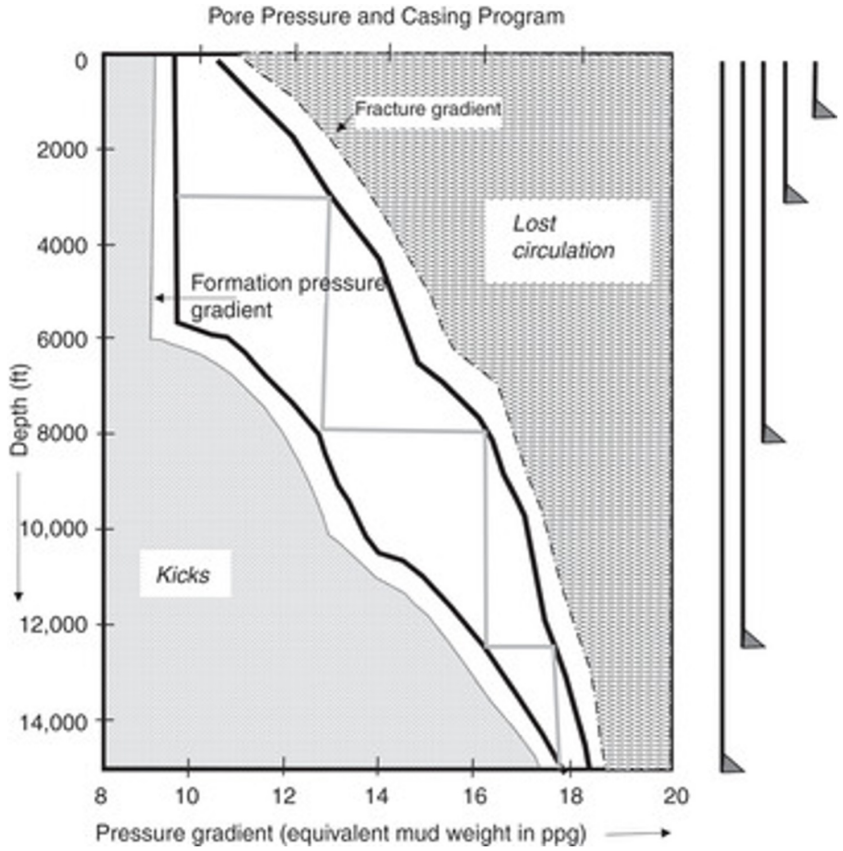

Figure 2.4: Schematic drilling pressure window. The safe operational window lies between pore pressure and the fracture/integrity limit. FIT and LOT measurements at casing shoes constrain the upper bound for equivalent mud weight in drilling operations. From Dutta et al. (2021).

2.2.1. Test design

A typical hydraulic stress test consists of injecting fluid into a wellbore interval at a controlled rate to progressively increase the downhole pressure and deliberately perturb the local stress state. During the early stage of injection, pressure rises approximately linearly as the wellbore, casing, and surrounding rock respond elastically. As injection continues, the pressure may deviate from linearity as fluid begins to leak into the formation and a hydraulic fracture is initiated at the borehole wall. With further pressurisation, the fracture breaks down and propagates, and the measured pressure reflects a combination of in-situ stresses, hoop stresses, and viscous pressure losses within the wellbore and fracture.

When injection is terminated (shut-in), flow decays and dynamic pressure losses rapidly dissipate. The subsequent pressure response is governed by fluid leak-off into the formation and progressive fracture closure. Analysis of the resulting pressure–time (or pressure–derivative) behaviour allows characteristic pressures to be identified, each corresponding to a distinct mechanical stage of the test. These characteristic pressures, recorded during injection and shut-in, form the basis for test interpretation and are highlighted later in subsection 2.2.3.

The design of a hydraulic stress test strongly controls both the quality of the interpreted stress parameters and the operational risks associated with the test. In particular, the depth of the test interval and the mechanical stratigraphy of the surrounding formations play a decisive role in governing fracture initiation, propagation, and containment.

Hydraulic stress tests are preferentially conducted at depths that are representative of the stress conditions relevant for subsequent drilling, completion, or reservoir operations. From a geomechanical perspective, the selected depth should be sufficiently removed from the surface to ensure a well-developed in-situ stress regime and to minimise near-surface effects such as stress relaxation, weathering, or the presence of unconsolidated sediments, all of which can complicate stress interpretation.

Equally important is the placement of the test interval within a mechanically favourable stratigraphic setting that promotes fracture containment. Preferred practice is to locate the interval within, or adjacent to, formations bounded by layers exhibiting a clear contrast in strength or stiffness. Such contrasts tend to limit vertical fracture height growth, as strong and stiff layers, such as carbonates or well-cemented sandstones, can act as mechanical barriers to fracture propagation. Effective fracture containment improves the interpretability of the pressure response by maintaining a relatively simple fracture geometry and reducing the risk of fracture communication with unintended intervals. Conversely, neglecting mechanical stratigraphy may lead to uncontrolled fracture growth, complex leak-off behaviour, and increased uncertainty in the estimation of the minimum horizontal stress (Economides & Nolte, 2000).

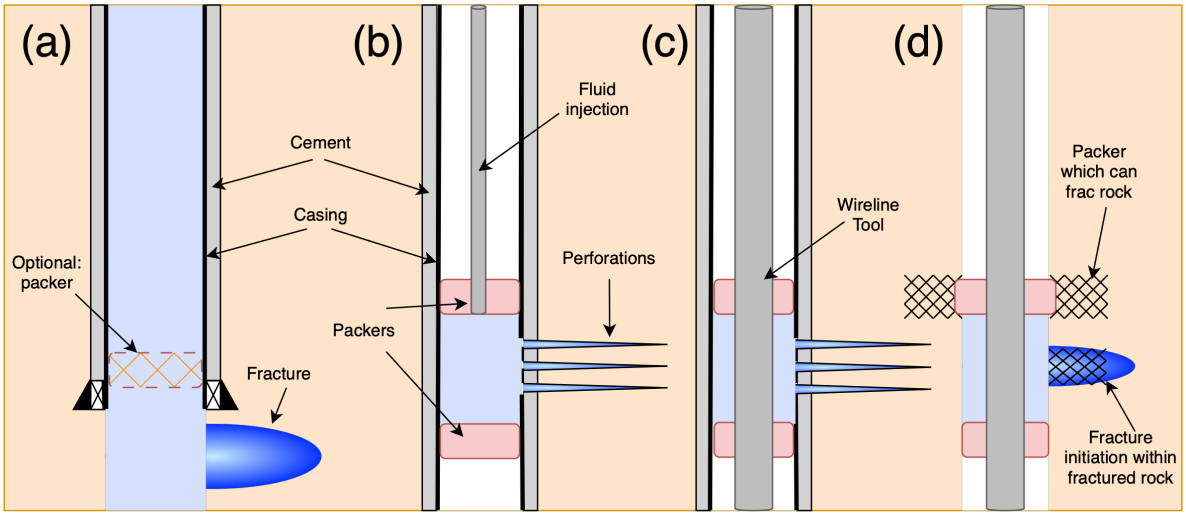

Figure 2.5: Schematic borehole configuration during (a) an open-hole leak-off test, (b) cased hole extended leak-off test, (c) wireline tool in cased hole or (d) wireline tool which can fracture rock in open-hole.

Cased versus uncased test intervals Hydraulic stress tests may be conducted either in cased-and-perforated intervals or in uncased (open-hole) sections, and this distinction has important implications for both fracture initiation and pressure interpretation. In uncased intervals, fluid is injected directly against the borehole wall, and fracture initiation is governed by the local hoop stress concentration around the open hole and the tensile strength. In this configuration, fracture initiation typically occurs at a pressure close to the tensile strength–controlled breakdown condition, and the near-wellbore stress state is relatively well defined. In contrast, cased tests rely on perforations to provide hydraulic communication with the formation. The presence of casing, cement, and perforation tunnels modifies the local stress field and introduces additional pressure losses between the wellbore and the fracture initiation point. As a result, fracture initiation in cased tests is strongly influenced by perforation geometry, cement integrity, and the damaged zone, and the measured surface or downhole pressure may significantly exceed the actual fracture-tip pressure. While cased tests are often operationally convenient and safer in deep wells, these additional complexities increase uncertainty in the identification of fracture initiation pressures and reduce the reliability of parameters that depend on early-time behaviour, such as the leak-off pressure. More elaboration follows in section 2.3.

Reservoir versus shale intervals (high- versus low-permeability formations) The permeability of the tested formation exerts a first-order control on fluid leak-off, pressure evolution, and fracture stability during a hydraulic stress test. In relatively high-permeability reservoir rocks, such as sandstones or fractured carbonates, fluid leak-off into the formation is substantial, leading to strong pressure damping during injection and rapid pressure decline during shut-in. In these settings, fracture initiation may be poorly defined, and test interpretation often relies more heavily on shut-in behaviour and pressure-derivative analysis. Conversely, in low-permeability formations such as shales or tight mudstones, leak-off is limited and pressure builds up rapidly, resulting in sharper pressure signatures associated with fracture initiation and propagation. These conditions tend to produce clearer identification of characteristic pressures, but they also increase the likelihood of unstable fracture growth if injection rates

are not carefully controlled. Consequently, stress tests in shale formations are generally more sensitive to fracture mechanics and toughness effects, whereas tests in reservoir rocks are more strongly influenced by fluid flow and diffusion processes. Recognising this distinction is essential when comparing test results across lithologies or when extrapolating stress estimates from one stratigraphic unit to another.

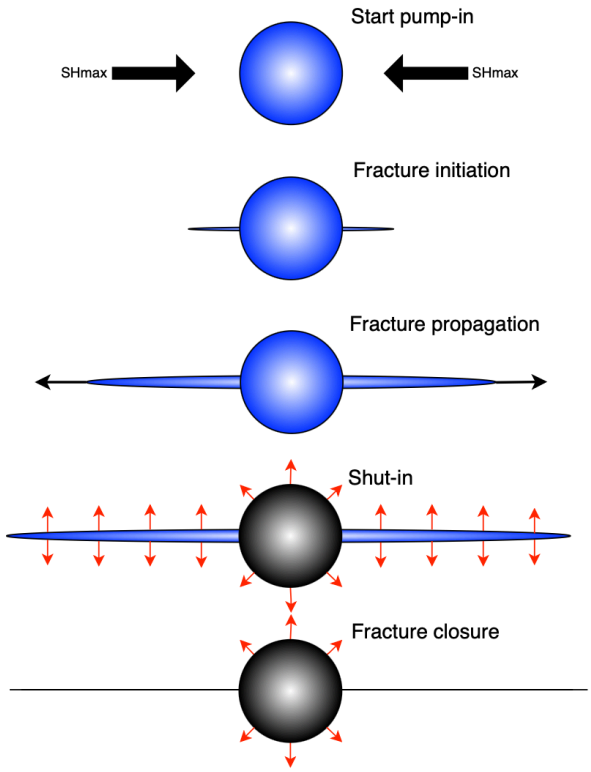

Figure 2.6: Schematic cross-section of hydraulic fracture development around a vertical wellbore during an injection test. From top to bottom: (1) start of pump-in, (2) fracture initiation at the wellbore wall once the tensile criterion is exceeded in the direction of $S_{H\,\max}$, (3) fracture propagation, (4) shut-in leading to pressure dissipation from wellbore storage, and (5) progressive fracture closure as fluid pressure declines and in-situ stresses dominate. Fractures don't necessarily have to be mirrored, but can also be one-sided.

2.2.2. Types of tests

A wide range of hydraulic stress tests is reported in the literature under different names, including FIT, LOT, XLOT, and micro-fracture tests. Following the terminology framework proposed by McClure (2017), these tests are best understood not as fundamentally different experiments, but as points along a continuum of increasingly diagnostic hydraulic fracture calibration tests. The physical processes involved are elastic pressurisation, fracture initiation, propagation, shut-in, and closure, and are similar in all cases. The practical distinction between test types lies primarily in their operational context, injected volume and rate, and the extent to which fracture closure behaviour is intentionally captured (McClure & Horne, 2014). Within this continuum, FITs and LOTs are classified as cheaper operational drilling tests intended to define safe drilling margins, whereas XLOTs, micro-fracture, and mini-fracture tests are more expensive diagnostic stress measurements designed to estimate fracture closure pressure and the minimum horizontal stress.

An additional practical distinction between these test types lies in the nature of the injected fluid. FITs, LOTs, and many open-hole XLOTs are typically conducted using particle-rich drilling fluids, whose rheology and filtration behaviour can be complex and variable. In contrast, SCAN-type XLOTs and micro- and mini-fracture tests are generally performed with more controlled injection fluids, allowing better constraint of fluid properties and improving the interpretability of the pressure response.

Formation Integrity Test (FIT) A Formation Integrity Test (FIT) represents the simplest end-member of this continuum. Fluid is injected below a casing shoe to verify that the formation can withstand the planned mud weight for the next drilling section. Injection is terminated before leak-off or fracturing occurs, and the pressure response remains within the linear elastic regime. FITs are purely operational tests and are not meant to provide diagnostic information on in-situ stresses. The use of drilling fluid further limits their interpretability, as fluid losses and filter-cake development can obscure the true formation response.

Leak-Off Test (LOT) A Leak-Off Test (LOT) extends a FIT by continuing injection until the pressure–volume response deviates from linearity, which is interpreted as the onset of leak-off pressure (LOP). LOTs are commonly used to define an upper bound on allowable mud weight. However, stress estimates derived from LOTs are generally unreliable, as emphasised by Addis et al. (1998) and Raaen et al. (2006). The observed LOP is strongly influenced by near-wellbore conditions, tensile strength, cement integrity, formation permeability, and the complex behaviour of particle-laden drilling fluids, and does not necessarily correspond to fracture initiation in intact rock. This will be elaborated on later in this chapter.

Extended Leak-Off Test (XLOT) An Extended Leak-Off Test (XLOT) deliberately extends a LOT beyond leak-off to include fracture breakdown, propagation, shut-in, and pressure decline. Within McClure's framework, an XLOT is mechanically equivalent to a small-scale fracture calibration test performed at or near a casing shoe. This is however not necessarily the case, as the XLOTs used for this study were often performed at perforations along a cased well. XLOTs are diagnostic rather than purely operational, and are commonly used to estimate fracture closure pressure and the minimum horizontal stress. These diagnostics could be used for frac design, if one would like to stimulate production.

In practice, XLOTs are often performed with multiple injection and shut-in cycles. Repeated cycling reduces the influence of near-wellbore stress fields and allows the interpreted closure pressure to converge toward the far-field stress state, improving the reliability of the stress estimate. However, when performed with drilling fluids (as in conventional or open-hole XLOTs), interpretation may still be complicated by fluid–formation interactions. In contrast, SCAN-type XLOTs, which use better-controlled injection fluids, generally yield more reliable and interpretable pressure responses.

Micro-fracture and Mini-fracture tests Micro-fracture and mini-fracture, or micro-frac and mini-frac tests, occupy the same diagnostic portion of the continuum as XLOTs, differing primarily in scale rather than in physical principle. Micro-fracture tests typically involve injection of approximately 2–100 gallons (8–380 L) at rates of 1–10 gal/min (4–38 L/min), whereas mini-fracture tests inject on the order of 10–100 barrels (1,590–15,900 L) at rates of 5–10 bbl/min (800–1600 L/min). Both test types intentionally create and propagate a hydraulic fracture followed by shut-in and pressure decline analysis.

A key advantage of these tests is the ability to control injection fluid properties, which reduces uncertainty associated with fluid rheology, leak-off behaviour, and near-wellbore effects. As a result, pressure transient interpretation is generally more reliable than for drilling-based tests such as FITs and LOTs.

Micro-fracture tests can be conducted using wireline-deployed tools (see Figure 2.3), allowing stress measurements to be obtained at discrete depths without the need for full wellbore isolation or surface pumping equipment. This capability makes micro-fracture tests particularly suitable for resolving stress variations with depth at relatively fine vertical resolution. In some tool configurations, inflatable packers are used not only to isolate the test interval but also to locally elevate the near-wellbore stress state, thereby promoting fracture initiation. This approach is especially useful in high-permeability formations where fracture initiation by surface injection is difficult due to rapid leak-off; however, it is generally limited to uncased (open-hole) wells. Mini-fracture tests, by contrast, interrogate larger rock volumes and are better suited for assessing stress uniformity, leak-off behaviour, and fracture containment over thicker stratigraphic intervals. From a mechanical perspective, however, both tests rely on the same fracture initiation, propagation, and closure processes as XLOTs.

Table 2.1: Overview of interpreted hydraulic stress tests, their definitions, purposes, typical conditions, test purpose, and whether key characteristic pressures are reached. Definitions adapted from McClure (2017) and Zoback (2010).

Test Type	Definition / Purpose	Typical Conditions	Test purpose	Characteristic pressures reached				
				LOP	FBP	FRP	ISIP	FCP
Formation Integrity Test (FIT)	Pressure test just below the casing shoe without intentionally fracturing the formation. Verifies formation integrity; sets a lower bound for safe mud weight. Relatively cheap.	After setting and cementing casing; prior to drilling the next section. Open-hole test.	Drilling	–	–	–	–	–
Leak-Off Test (LOT)	Injection at the casing shoe until deviation from linear pressurisation indicates leak-off. Sets an upper bound for safe mud weight. Relatively cheap.	After setting and cementing casing; prior to drilling the next section. Open-hole test.	Drilling	✓	–/✓[a]	–	–	–
Extended Leak-Off Test (XLOT)	LOT extended beyond leak-off to include breakdown, fracture propagation, shut-in, and pressure decline; enables estimation of fracture closure pressure and S_{hmin}. Relatively expensive.	Selected intervals for stress characterisation; often multiple injection cycles. Can be both open-hole at bottom of borehole, or at selected closed-hole interval through perforations.	Diagnostic	✓	✓	✓	✓	✓
Micro-Fracture Test (Micro-frac)	Small-volume hydraulic fracture test used to initiate and propagate a short fracture followed by shut-in. Relatively expensive.	Open-hole or perforated intervals, commonly prior to stimulation. Not often done at bottom of borehole.	Diagnostic	✓	✓	✓	✓	✓

Legend: ✓ = typically reached or interpreted; – = not reached.
[a] Formation breakdown pressure may occasionally be reached during a LOT.

2.2.3. Characteristic pressures

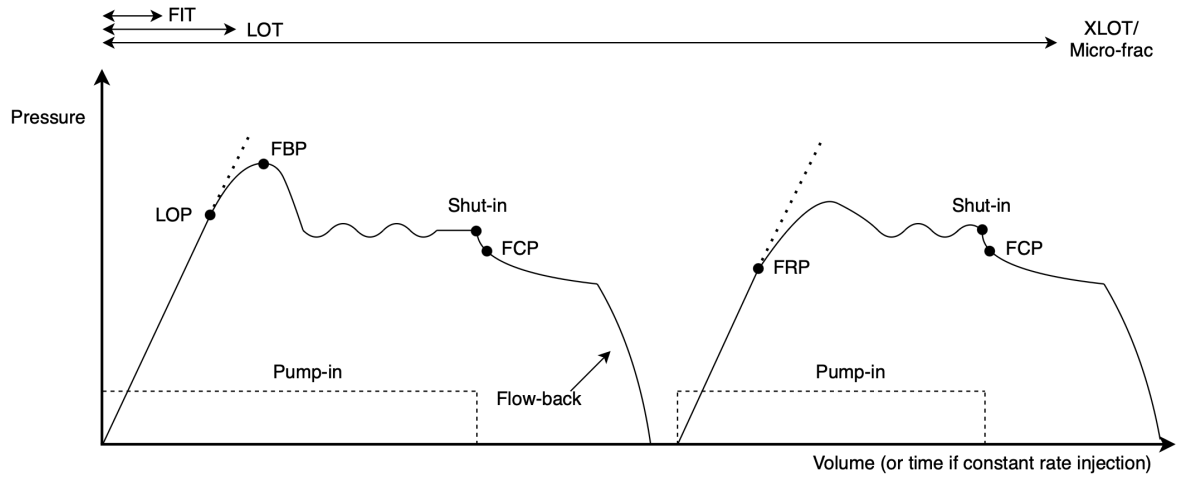

Figure 2.7: Characteristic pressures during a hydraulic stress test.

This subsection will go into the definition of the characteristic pressures, as recorded during a stress test. These characteristic pressures, are visually highlighted in Figure 2.7:

- **Leak-Off Pressure (LOP)** — the first sustained deviation from the linear pressure–volume trend

during injection, indicating that fluid begins to enter the formation and/or a tensile fracture initiates at the borehole wall. However, it could also be that fluid is simply leaking into a permeable formation, or behind the cement in a perforation. This is the reason why it is called leak-off pressure, and not fracture initiation pressure, as one cannot be fully certain what causes the deviation in linearity. Note that pressure–volume is preferred; pressure–time can mislead when rate varies. As Andrews et al. (2016) note, LOP is a somewhat arbitrary value: it may fall between the minimum stress (S_{hmin}) and the Formation Breakdown Pressure (FBP), but not consistently. By definition, the LOP reflects near-wellbore conditions and the tensile strength, rather than the true in-situ stress state. The LOP can also simply denote leak-off into a permeable formation, before a fracture has been created. Thus, unlike Fracture Closure Pressure (FCP), the LOP is a system-dependent, or even graph dependent parameter rather than an intrinsic property of the formation.

It is noted that the term *Fracture Initiation Pressure* (FIP) is used inconsistently in the literature. In drilling practice, FIP is sometimes equated to the leak-off pressure (LOP), whereas in other contexts it is used to denote the pressure at which a tensile fracture first opens, which may precede or coincide with the formation breakdown pressure (FBP). In this work, FIP is used strictly to denote the onset of tensile fracture opening at the borehole wall, recognising that it sometimes difficult to resolve separately from LOP or FBP in field data.

Several studies have further shown that LOP is not a reliable estimator of in-situ stress. For example, analyses of repeated XLOT cycles on the Norwegian Continental Shelf indicate that LOP can converge toward ISIP, with differences often within a few percent once near-wellbore effects have been mitigated. This behaviour reinforces the view that LOP is controlled primarily by local conditions and test history rather than by the far-field stress state (Addis et al., 1998; Raaen et al., 2006).

In some tests, the volume of fluid leaked off into the formation or fracture may be negligible relative to the injected volume, making leak-off difficult or impossible to identify on pressure–volume or pressure–time plots. In such cases, LOP and FIP picks become highly uncertain or purely interpretive (Zoback, 2010). For further elaboration, see section 2.3.

Nonlinear compressibility of the injected fluid or the wellbore system does not fundamentally complicate LOP interpretation, as these effects tend to increase the pressure–volume slope rather than decrease it. In contrast, leak-off or fracture initiation is associated with a reduction in slope. Nevertheless, because multiple mechanisms can cause such a deviation, LOP remains a system-dependent and graph-dependent parameter rather than a robust indicator of in-situ stress.

- **Formation Breakdown Pressure (FBP)** — the peak pressure at which a fracture grows uncontrollably from the borehole wall. It depends on in-situ stresses, wellbore geometry, injection rate, fluid properties, and the fracture toughness, and is therefore considered a system-dependent parameter rather than an intrinsic formation property. The FBP can simply be defined as the moment in time where the amount volume created in the fracture is larger than the amount of volume injected into the fracture:

$$\frac{\Delta V_{fracture}}{\Delta t} > \frac{\Delta V_{injected}}{\Delta t} \tag{2.5}$$

  The relationship between LOP and FBP depends on wellbore configuration. In uncased openhole intervals, LOP and FBP may be closely related and are sometimes indistinguishable. In contrast, in cased and perforated wells, LOP commonly reflects perforation friction, cement integrity, or near-wellbore damage, and should not be interpreted as equivalent to formation breakdown.

- **Fracture Re-opening Pressure (FRP)** — the pressure at which a previously created fracture re-opens during a subsequent injection cycle. The FRP should be lower than the initial LOP, if this value denotes fracture initiation, as tensile strength has already been overcome and the fracture surfaces are mechanically weakened. The FRP is controlled primarily by hoop stress and residual fracture roughness, and may be used to place constraints on tensile strength when compared with initial initiation pressures. During repeated cycles, injection pressure must exceed

FRP sufficiently to prevent rapid fracture closure and premature shut-in, otherwise the fracture may close before meaningful propagation occurs, resulting in estimates of near-wellbore stresses.

- **Fracture Propagation Pressure (FPP)** — the relatively stable pressure required to sustain fracture extension once breakdown has occurred. By definition, the wellbore pressure during propagation must exceed the minimum horizontal stress ($S_{h\,\min}$), since additional energy is needed to (i) overcome viscous pressure losses as fluid flows along the fracture and (ii) supply the fracture toughness at the tip.

  For laminar flow between parallel plates (the "cubic law"), the viscous pressure drop is given by:

$$\Delta P_{\text{visc}} = \frac{12\mu Q L}{w^3 h} \tag{2.6}$$

  where μ is the fluid viscosity, Q the injection rate, L the fracture half-length, w the fracture aperture, and h the fracture height. This expression shows that viscous losses increase for narrower or longer fractures, higher injection rates, and more viscous fluids.

  Accordingly, the wellbore-measured propagation pressure can be written as:

$$P_{\text{FPP,wb}} = S_{h\,\min} + P_{\text{toughness}} + \Delta P_{\text{visc}} \tag{2.7}$$

  After shut-in, the viscous term ΔP_{visc} dissipates rapidly, which is why the instantaneous shut-in pressure (ISIP) provides a better approximation of the average fracture pressure than the measured FPP plateau. The FPP will not be considered in this study, but is important for understanding the test.

- **Instantaneous Shut-In Pressure (ISIP)** — the wellbore pressure recorded during shut-in following cessation of injection. In the literature and in practice, the definition of ISIP is not clear. Some authors define ISIP as the pressure at the moment pumping is stopped, although this transition may take several seconds. Others define ISIP as the pressure when the flow rate has fully decayed to zero. A more physically rigorous definition identifies ISIP as the pressure at which wellbore storage effects have dissipated and the pressure measured at the gauge location equals the pressure inside the fracture.

  In this study, ISIP is defined as the pressure at the onset of flow-rate decline, i.e. the point at which shut-in begins. This definition is adopted for two practical and physical reasons. First, in low-permeability formations or in tests with short fractures, fracture closure may initiate rapidly, such that by the time the measured flow rate reaches zero the fracture may already be partially or fully closed. Second, in many field datasets a clear wellbore storage dissipation signature cannot be identified, preventing the use of a more rigorous storage-corrected definition. Defining ISIP at the onset of flow decline therefore provides a consistent and reproducible reference point across tests.

- **Fracture Closure Pressure (FCP)** — the pressure at which an induced fracture closes during shut-in, interpreted as the minimum horizontal stress (S_{hmin}). Closure occurs when the fracture faces can no longer be held open against the ambient least principal stress. This physical argument underpins the modern interpretation of FCP as the most reliable measure of S_{hmin}.

  In practice, closure is identified from the pressure decline following shut-in using diagnostic time transformation techniques such as the G-function method, square-root-of-time plots, in combination with methods for picking closure like the the system stiffness/compliance approach. These methods detect the transition from a hydraulically open to a mechanically closed fracture. Because this transition may occur over a finite pressure interval, FCP is sometimes expressed with an uncertainty range. More on this in chapter 3.

Table 2.2: Characteristic pressures in hydraulic stress testing: physical meaning and key pitfalls. Where possible, gauge pressures are corrected to the fracture mouth (perforations or open hole).

Parameter	Physical meaning / typical use	Notes / pitfalls (storage, hoop, tip)
LOP (Leak-Off Pressure)	First sustained fluid entry into formation or fracture; operational mud-weight limit	Strongly controlled by near-wellbore hoop stress and local permeability; ambiguous mechanism; may not be visible if leak-off volume is negligible.
FBP (Formation Breakdown Pressure)	Peak pressure preceding unstable fracture propagation; operational limit	Near-wellbore phenomenon; not equal to FIP; sensitive to rate, fluid, and borehole condition; in open hole may approach LOP, but in cased/perforated wells LOP $\neq$ FBP.
FPP (Fracture Propagation Pressure)	Plateau pressure sustaining fracture growth	Always exceeds $S_{h\min}$ due to viscous and toughness contributions; overestimates stress if tip losses ignored; linked to Carter leak-off and fracture geometry.
FRP (Fracture Re-opening Pressure)	Pressure required to re-open an existing fracture during subsequent cycles	Lower than initial LOP; tensile strength already overcome; requires sufficient overpressure to prevent rapid re-closure during repeated cycles.
ISIP (Instantaneous Shut-In Pressure)	Pressure at onset of shut-in; diagnostic reference / upper bound for closure	Definition-dependent; still contains residual net pressure; early falloff often dominated by wellbore storage and compliance; not equal to far-field $S_{h\min}$.
FCP (Fracture Closure Pressure)	Best estimator of $S_{h\min}$; transition from open to closed fracture	Closure occurs over a pressure interval; contact vs full closure distinction; accounting for wellbore storage is essential to avoid premature or biased picks.

2.3. Fracture initiation

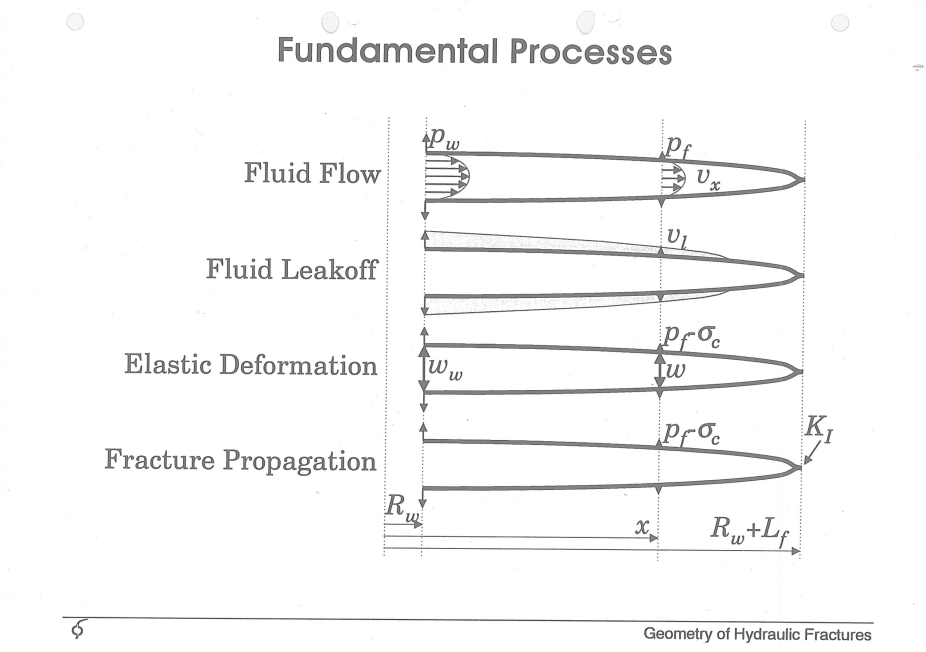

Figure 2.8: Fundamental physical process occurring in fracture during pump-in. From Weijers (1995).

Fracture initiation and propagation around a wellbore result from the interaction between the in-situ stress state, rock mechanical properties, and injection-induced pore pressure changes. Different modelling approaches capture different parts of this interaction. This section discusses the Kirsch stress concentration model, the deviated model and Linear Elastic Fracture Mechanics (LEFM), with emphasis on their governing equations, assumptions, and relevance for the interpretation of hydraulic stress test data.

2.3.1. Kirsch model

The Kirsch model describes the elastic stress distribution around a circular cylindrical opening in an infinite, homogeneous, isotropic medium subjected to far-field stresses. For a vertical wellbore of radius R, the effective stresses in polar coordinates (r, θ) are given by Jaeger and Cook (1979) and Kirsch (1898):

$$\sigma_{rr}(r,\theta) = \frac{1}{2}\left(S_{H\,\max} + S_{h\,\min} - 2P_0\right)\left(1 - \frac{R^2}{r^2}\right) + \frac{1}{2}\left(S_{H\,\max} - S_{h\,\min}\right)\left(1 - 4\frac{R^2}{r^2} + 3\frac{R^4}{r^4}\right)\cos 2\theta + \frac{P_0 R^2}{r^2}, \tag{2.8}$$

$$\sigma_{\theta\theta}(r,\theta) = \frac{1}{2}\left(S_{H\,\max} + S_{h\,\min} - 2P_0\right)\left(1 + \frac{R^2}{r^2}\right) - \frac{1}{2}\left(S_{H\,\max} - S_{h\,\min}\right)\left(1 + 3\frac{R^4}{r^4}\right)\cos 2\theta - \frac{P_0 R^2}{r^2} - \sigma^{\Delta T}, \tag{2.9}$$

$$\tau_{r\theta}(r,\theta) = \frac{1}{2}\left(S_{H\,\max} - S_{h\,\min}\right)\left(1 + 2\frac{R^2}{r^2} - 3\frac{R^4}{r^4}\right)\sin 2\theta. \tag{2.10}$$

where P_0 is the far-field pore pressure, and θ is the angle relative to the $S_{H\,\max}$ azimuth.

The thermoelastic contribution to the tangential (hoop) stress at the borehole wall is given by (Stephens & Voight, 1982):

$$\sigma_{\theta\theta}^{\Delta T} = \frac{\alpha_t E\,\Delta T}{1-\nu} \tag{2.11}$$

where:

- $\sigma_{\theta\theta}^{\Delta T}$ is the thermally induced tangential (hoop) stress change at the borehole wall,
- α_t is the linear coefficient of thermal expansion of the rock (1/K),
- E is Young's modulus of the rock (Pa or GPa),
- ΔT is the temperature change at the borehole wall relative to the undisturbed formation temperature (K or °C),
- ν is Poisson's ratio of the rock (dimensionless).

This expression assumes linear elastic, isotropic thermoelastic behaviour under plane strain conditions around the borehole. A temperature decrease ($\Delta T < 0$, cooling) induces tensile hoop stress, whereas heating induces compressive hoop stress.

Physically, the term $\alpha_t \Delta T$ represents the free thermal strain that the rock would undergo if unconstrained. Because the surrounding formation constrains radial expansion or contraction, this strain is converted into stress. The factor $\frac{E}{1-\nu}$ reflects the elastic stiffness of the material under plane strain conditions and governs how strongly thermal strain translates into stress.

The thermoelastic stress increment $\sigma_{\theta\theta}^{\Delta T}$ must be superimposed on the mechanically induced hoop stress from the Kirsch solution before applying the tensile failure criterion.

At the wellbore wall ($r = R$), the tangential total stress reduces to:

$$\sigma_{\theta\theta}(R,\theta) = \left(S_{H\,\max} + S_{h\,\min}\right) - 2\left(S_{H\,\max} - S_{h\,\min}\right)\cos 2\theta - 2P_0 - \Delta P - \sigma^{\Delta T}. \tag{2.12}$$

where ΔP is the difference between the wellbore pressure P_w and the near-field pore pressure P_p.

Solving for the required wellbore pressure yields the initiation pressure that depends explicitly on the in-situ stresses and tensile strength, which is the leak-off pressure. Importantly, the Kirsch solution contains no stress singularity and therefore cannot describe fracture propagation. It represents a stress-based initiation criterion at a smooth borehole wall and neglects fracture toughness and crack growth. The most simplified version becomes (Zoback, 2010):

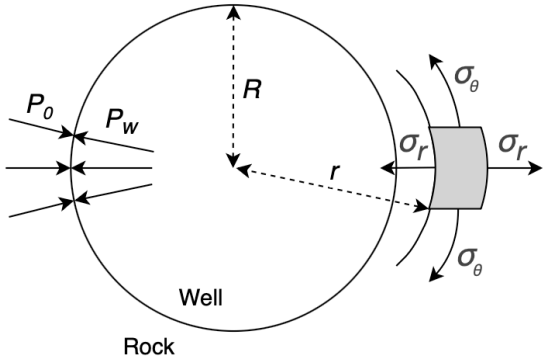

Figure 2.9: Schematic illustration of stresses acting around a circular wellbore. The well of radius R is subjected to far-field stress P_0 and wellbore pressure P_w. At a radial distance r from the well center, the rock experiences radial stress σ_r and tangential (hoop) stress σ_θ. The figure highlights the stress distribution in the surrounding rock and the definition of the radial and circumferential stress components used in wellbore stress analysis.

$$P_w = FIP = 3S_{h\,\min} - S_{H\,\max} - P_p = -T_0 \tag{2.13}$$

It is assumed here that the pore pressure at the wall is equal to the far-field pore pressure.

Figure 2.11 illustrates the tangential (hoop) stress at the wellbore wall as a function of azimuth for increasing wellbore pressure. The angular variation of the hoop stress is controlled by the far-field horizontal stress anisotropy, with the most tensile stresses developing in the direction of the maximum horizontal stress. Increasing wellbore pressure results in a uniform downward shift of the hoop-stress distribution, progressively unloading the rock at the borehole wall. Within the Kirsch framework, fracture initiation occurs when the minimum hoop stress reaches the tensile strength of the rock. The figure therefore visualises how rising injection pressure drives the system toward tensile failure while preserving the characteristic azimuthal stress pattern imposed by the in-situ stress field. In the next subsection the initiation model for deviated wells will be discussed.

2.3.2. Stress around deviated wellbores

The classical Kirsch solution describes stresses around a vertical wellbore drilled in a far-field stress state aligned with the principal stress directions. In practice, however, many wells are deviated and oriented obliquely with respect to the in-situ stress tensor. Under such conditions, the stress state at the borehole wall must be obtained through coordinate transformation of the far-field principal stresses into the local wellbore coordinate system.

For a well deviated by inclination angle I and azimuth θ_w, the far-field stress tensor must be rotated into the borehole coordinate system. The rotation introduces shear components even if the far-field stress tensor is principal.

Denoting the azimuthal difference between the wellbore and the maximum horizontal stress direction as

$$\Delta\theta = \theta_w - \theta_{H\,\max},$$

the transformed stress components acting in the plane perpendicular to the wellbore axis become functions of I and $\Delta\theta$. As a result, both normal and shear stresses act at the borehole wall.

For a deviated well, the far-field stress tensor is first rotated into the local borehole coordinate system. Let σ_{11}, σ_{22}, and σ_{12} denote the effective far-field stress components transformed into the plane perpendicular to the borehole axis. These represent the in-plane normal and shear effective stresses acting in the cross-sectional plane of the well.

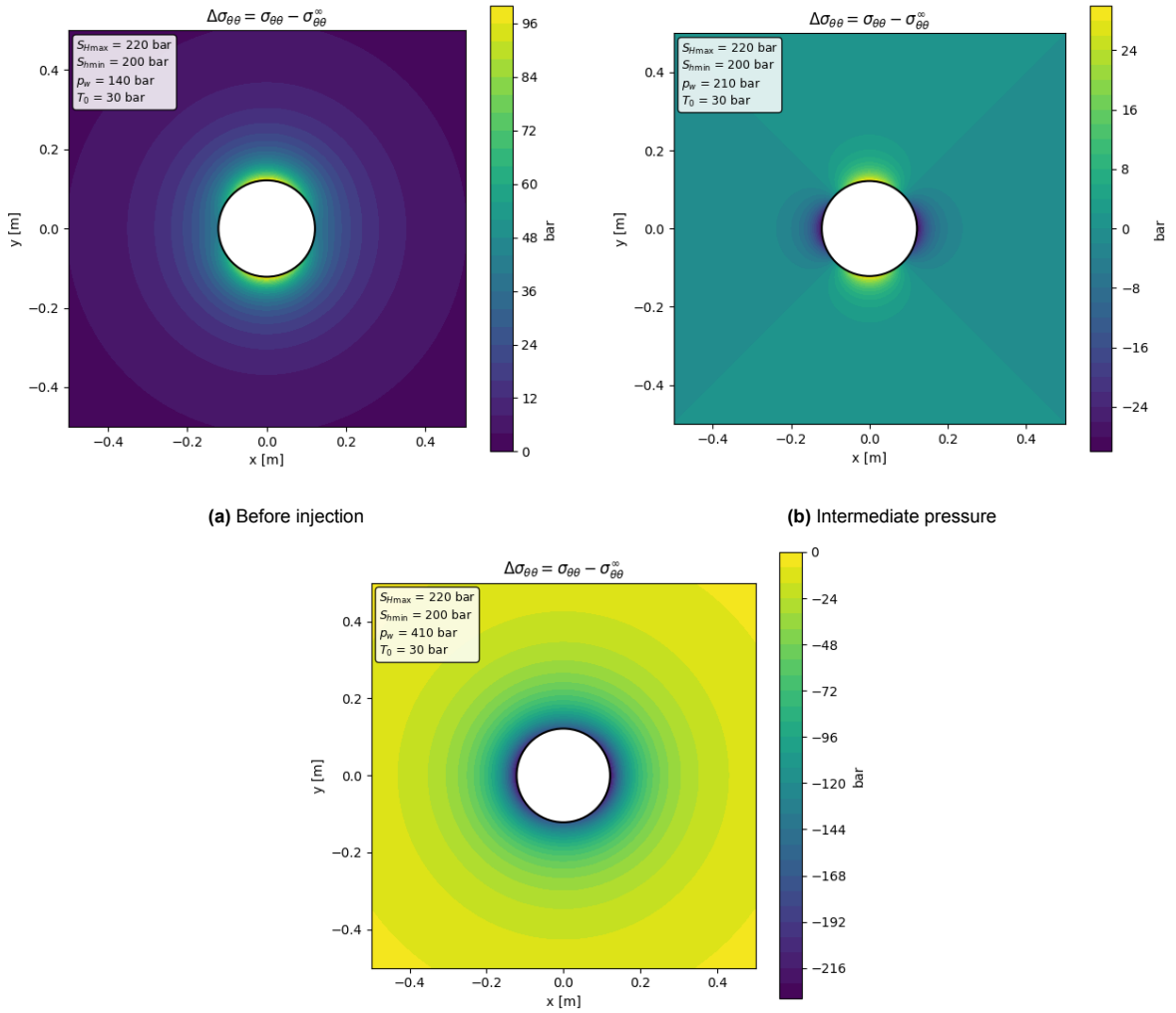

(a) Before injection

(b) Intermediate pressure

(c) At fracture initiation

Figure 2.10: Evolution of tangential (hoop) stress around the wellbore for increasing wellbore pressure.

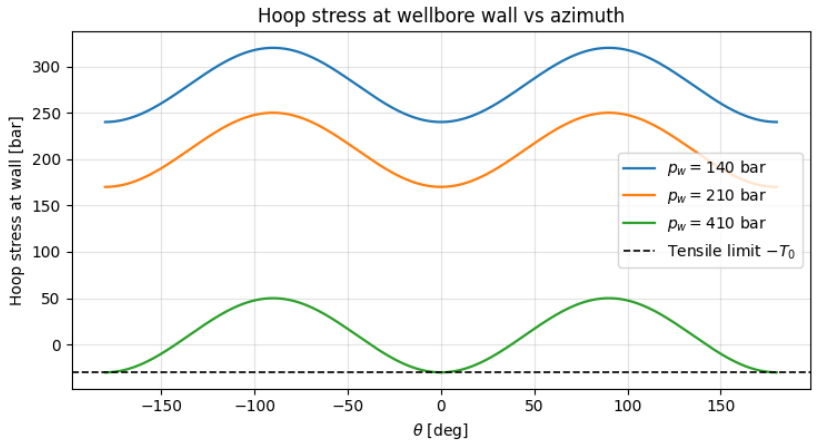

Figure 2.11: Tangential (hoop) stress at the wellbore wall as a function of azimuth for increasing wellbore pressure. The angular variation reflects the far-field horizontal stress anisotropy, while higher wellbore pressure shifts the stress state toward tension. Fracture initiation in the Kirsch framework occurs when the minimum hoop stress equals the tensile strength of the rock, which is the case at $p_w = 410$ bar.

The minimum tangential (hoop) effective stress at the borehole wall is then obtained from the principal stress solution of the in-plane stress tensor:

$$\sigma_{\theta\theta,\min} = \sigma_{11} + \sigma_{22} - 2\sqrt{\left(\frac{\sigma_{11} - \sigma_{22}}{2}\right)^2 + (\sigma_{12})^2} - P_w,$$

where P_w is the wellbore pressure acting as an internal boundary traction.

The square-root term represents the maximum principal stress difference in the borehole cross-sectional plane. The expression therefore corresponds to the most tensile circumferential stress around the wellbore, obtained by selecting the critical angular orientation θ.

Unlike the vertical-well case, the shear stress component σ_{12} is generally non-zero for deviated wells. This introduces coupling between principal stress magnitudes, well inclination, and azimuth, and makes the fracture initiation pressure orientation-dependent.

Fracture initiation occurs when the minimum effective tangential stress equals the tensile strength T_0:

$$\sigma_{\theta\theta} = -T_0.$$

Solving this condition for wellbore pressure yields the initiation pressure for a deviated well.

In deviated wells, fracture initiation pressure therefore depends not only on $S_{h\,\min}$ and $S_{H\,\max}$, but also on:

- well inclination I,
- $S_{H\,\max}$ direction $\theta_{H\,\max}$,
- well azimuth θ_w,
- stress anisotropy ratio $S_{H\,\max}/S_{h\,\min}$,
- vertical stress S_v
- pore pressure P_p,
- Biot coefficient α.

Because deviated wells introduce shear stress at the borehole wall, the relationship between fracture initiation pressure and far-field stresses becomes nonlinear and orientation-dependent.

Key implications are:

- In highly deviated wells, breakdown pressure may significantly fall below $S_{h\,\min}$ even when tensile strength is negligible.
- Initiation pressure is sensitive to stress orientation.
- Translation of FIT or LOT pressures to $S_{h\,\min}$ requires explicit specification of stress ratio and stress azimuth.

This orientation dependence forms the basis for stress inversion approaches, in which measured initiation pressures are used to solve for $S_{h\,\min}$ under assumed values of $S_{H\,\max}$ and stress direction. For the full derivation of the Kirsch solution for deviated wells, see Appendix C.

2.3.3. LEFM model

Linear Elastic Fracture Mechanics (LEFM) describes fracture initiation and propagation from an existing crack or flaw by characterising the singular stress field at the crack tip. For Mode-I loading, the near-tip stress field is given by (Van Eekelen, 1982):

$$\sigma_{ij}(r,\theta) = \frac{K_I}{\sqrt{2\pi r}} f_{ij}(\theta), \tag{2.14}$$

where K_I is the Mode-I stress intensity factor and r is the distance from the crack tip.

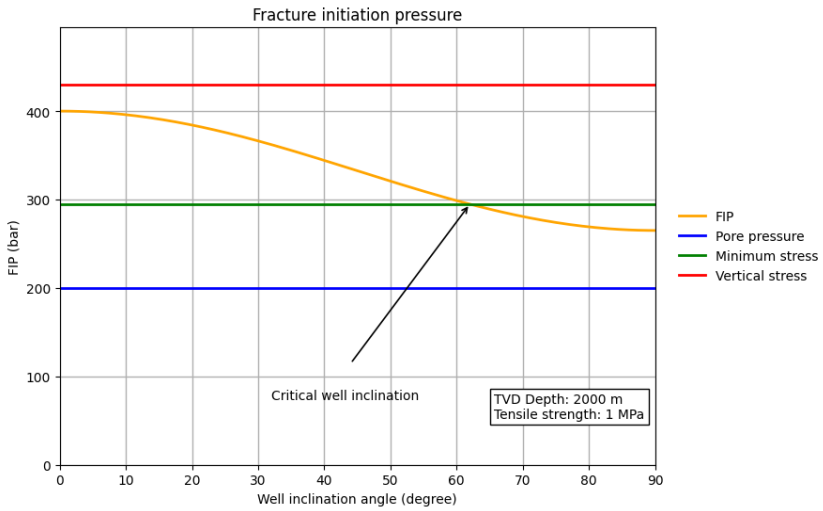

Figure 2.12: Visualization of how the well inclination can lead to lower fracture initiation pressure.

Crack propagation occurs when the stress intensity factor reaches the fracture toughness:

$$K_I = K_{IC}, \tag{2.15}$$

where K_{IC} is the plane-strain fracture toughness of the rock.

For a hydraulically driven crack, the stress intensity factor can be expressed as:

$$K_I = Y\,\sigma_{\text{net}}\sqrt{\pi a}, \tag{2.16}$$

where a is a characteristic crack length, Y is a geometry factor, and the net stress is defined as:

$$\sigma_{\text{net}} = P_f - S_n, \tag{2.17}$$

with P_f the fracture fluid pressure and S_n the normal stress acting on the fracture plane.

For a vertical fracture in a normal faulting stress regime, the normal stress acting on the fracture plane is commonly approximated as:

$$S_n \approx S_{h\,\min}. \tag{2.18}$$

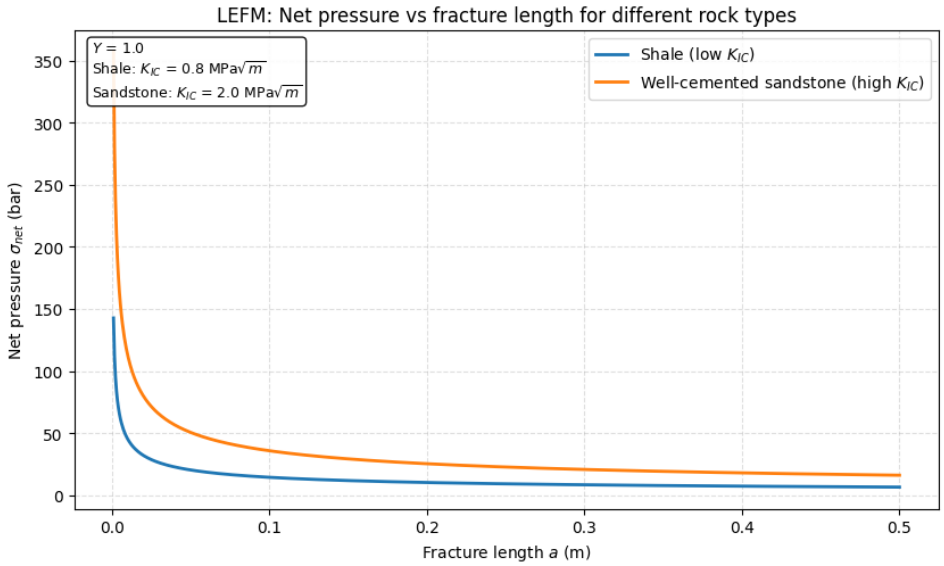

Figure 2.13: LEFM-based relationship between net fracture pressure and fracture half-length for different rock types. The figure illustrates the decrease in required net pressure σ_{net} with increasing fracture length a for shale (low fracture toughness, K_{IC} = 0.8 MPa$\sqrt{\text{m}}$) and well-cemented sandstone (high fracture toughness, K_{IC} = 2.0 MPa$\sqrt{\text{m}}$), assuming a geometry factor γ = 1.0. The higher K_{IC} of sandstone results in substantially larger net pressures, particularly during fracture initiation and early propagation, highlighting the strong control of rock toughness on hydraulic fracture behaviour.

2.4. Diffusion and poro-elasticity

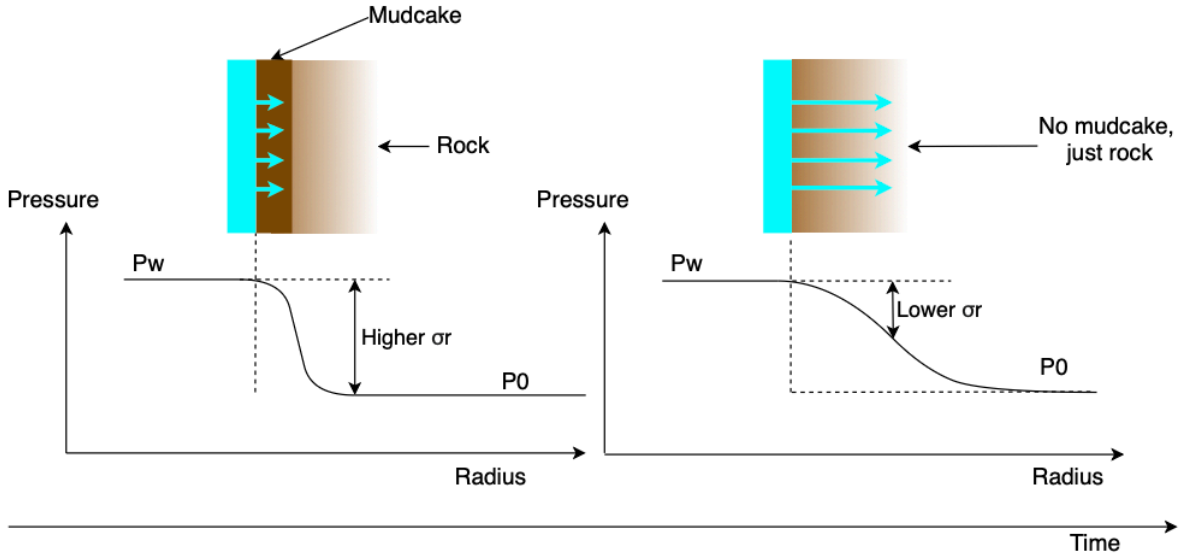

Figure 2.14: Schematic illustration of near-wellbore pore-pressure distribution during injection with (left) and without (right) mudcake formation. When an effective mudcake develops, fluid penetration into the formation is restricted, resulting in a sharp pressure drop across the mudcake and a relatively steep radial pressure gradient in the rock. This leads to a larger effective pressure differential $(P_w - P_0)$ acting on the rock skeleton near the borehole wall and therefore higher effective stress concentration. In the absence of mudcake, fluid penetrates more deeply into the formation, producing a smoother radial pressure gradient and reducing the effective pressure differential at the borehole wall. Consequently, poro-elastic stress redistribution is stronger and the observed fracture initiation pressure may be lower.

Fluid loss from a hydraulic fracture into the surrounding formation is governed primarily by pressure diffusion within the porous rock matrix. This diffusion process controls the rate at which fluid leaks off from the fracture faces and influences the evolution of pore pressure in the near-fracture region. Through effective-stress coupling, changes in pore pressure may also modify the local mechanical stress state around the fracture and wellbore.

2.4.1. Pore-pressure diffusion

In its simplest form, pore-pressure diffusion in a porous medium normal to a fracture face is described by the one-dimensional diffusion equation:

$$\frac{\partial P}{\partial t} = D\frac{\partial^2 P}{\partial x^2}, \qquad D = \frac{k}{\phi \mu c_t}, \tag{2.19}$$

where D is the hydraulic diffusivity, k is permeability, ϕ porosity, μ fluid viscosity, and c_t total compressibility of the fluid–rock system. This equation describes pressure diffusion normal to a fracture face or planar boundary and forms the theoretical basis for the Carter leak-off model.

Under the assumption of a semi-infinite medium subjected to a step increase in boundary pressure, the solution exhibits a $\sqrt{t}$ scaling behaviour, which directly leads to the characteristic $1/\sqrt{t}$ leak-off rate.

Around a wellbore, assuming axisymmetry, pore-pressure evolution follows:

$$\frac{\partial P_p}{\partial t} = D\left(\frac{1}{r}\frac{\partial}{\partial r}\left(r\frac{\partial P_p}{\partial r}\right)\right), \qquad D = \frac{k}{\phi \mu c_t}, \tag{2.20}$$

where k is permeability, ϕ porosity, μ fluid viscosity, and c_t total compressibility. This diffusion process governs fluid penetration away from the fracture surface during injection and shut-in.

2.4.2. Leak-off behaviour

The Carter leak-off model represents the near-fracture solution to the diffusion equation (Carter, 1957; Economides & Nolte, 2000). The instantaneous leak-off velocity at a point on the fracture face exposed for time $t - \tau$ is

$$q_\ell(t;\tau) = \frac{C_L}{\sqrt{t-\tau}}. \tag{2.21}$$

For slightly compressible fluids in a homogeneous porous medium, the Carter leak-off coefficient can be related to formation properties through diffusion theory. In simplified form,

$$C_L = \sqrt{\frac{k\phi c_t}{\pi \mu}}. \tag{2.22}$$

although the precise value depends on assumptions regarding compressibility, boundary conditions, and fracture pressure history. For a planar fracture with area A_f, the total leak-off rate after shut-in is

$$Q_\ell(t) = \frac{2A_f C_L}{\sqrt{t - t_{\text{shut}}}}. \tag{2.23}$$

Thus, Carter leak-off represents the practical fracture-scale manifestation of pore-pressure diffusion.

2.4.3. Poro-elastic stress coupling

Mechanical deformation in porous rocks is governed by effective stress, which relates the total stress acting on the rock to the pore pressure within the pore space:

$$\sigma = S - \alpha P_p, \tag{2.24}$$

where S is the total stress, P_p the pore pressure, and α the Biot coefficient.

An increase in pore pressure reduces the effective stress acting on the rock skeleton:

$$\Delta\sigma = -\alpha \Delta P_p. \tag{2.25}$$

Consequently, fluid penetration during injection modifies the effective stresses acting near the fracture faces and borehole wall. Changes in pore pressure therefore alter the mechanical loading conditions controlling fracture initiation and early fracture growth.

At the borehole wall or fracture surface, the mechanical loading acting on the rock skeleton depends on the difference between the internal fluid pressure and the local pore pressure. The effective pressure differential therefore becomes

$$\Delta P(t) = P_w(t) - P_p(r = R, t), \tag{2.26}$$

where $P_w(t)$ is the wellbore pressure and $P_p(r = R, t)$ is the pore pressure at the borehole wall.

If fluid penetration raises the local pore pressure near the boundary, the effective pressure difference acting across the rock skeleton decreases. As a result, a higher measured wellbore pressure may be required to reach the tensile failure condition at the borehole wall.

The magnitude of these effects depends strongly on formation permeability and injection rate.

In relatively high-permeability formations, fluid penetrates rapidly into the formation and pore pressure near the borehole wall approaches the wellbore pressure. This reduces the effective pressure differential acting on the rock skeleton and may increase the observed wellbore pressure required for tensile failure.

In low-permeability formations, pressure diffusion is limited over the timescale of the test. The pore pressure near the borehole wall remains close to its initial value, and the behaviour approaches the impermeable elastic solution described by the Kirsch model.

Analytical solutions incorporating poro-elastic coupling show that pore-pressure diffusion can modify the apparent breakdown pressure. For example, under idealised conditions (vertical well, isotropic poro-elastic medium, uniform pore pressure), the breakdown pressure can be written as

$$P_b = \frac{3S_{h\,\min} - S_{H\,\max} + T - \alpha\left(\frac{1-2\nu}{1-\nu}\right) P_p}{1 - \alpha\left(\frac{1-2\nu}{1-\nu}\right)}. \tag{2.27}$$

This expression illustrates how pore-pressure diffusion and poro-elastic coupling may influence the observed breakdown pressure under simplified conditions (Haimson & Fairhurst, 1967; Schmitt & Zoback, 1989).

Diffusion, leak-off, and poro-elastic stress redistribution therefore form a coupled process that primarily influences fracture initiation and early-time pressure behaviour. These mechanisms contribute to the system-dependent nature of parameters such as leak-off pressure and breakdown pressure. In contrast, once injection ceases and transient hydraulic effects dissipate, fracture closure is governed primarily by the far-field stress state.

2.5. Fracture closure

Following shut-in, fracture pressure declines as fluid leaks off into the surrounding formation and viscous pressure gradients within the fracture dissipate.

2.5.1. Pressure decline and system compliance

As a first-order approximation for an open fracture, fracture volume can be related to net pressure through an effective fracture compliance:

$$V_f = C_f \left(P_f - S_{h\,\min}\right), \tag{2.28}$$

where C_f is fracture compliance (the inverse of fracture stiffness) and P_f is the average fluid pressure within the fracture.

The total system compliance consists of fracture compliance and wellbore/storage compliance:

$$C_t = C_f + C_w. \tag{2.29}$$

Pressure evolution during fall-off is therefore governed by the relationship between pressure and fracture volume change:

$$\frac{dP}{dt} = \frac{1}{C_t}\frac{dV_f}{dt}. \tag{2.30}$$

After shut-in, fluid leaves the fracture only through leak-off into the surrounding formation. Under this idealised condition, the rate of fracture volume reduction equals the leak-off rate:

$$\frac{dV_f}{dt} = -Q_\ell(t). \tag{2.31}$$

Substituting into Eq. 2.30 yields

$$\frac{dP}{dt} = -\frac{1}{C_t}Q_\ell(t). \tag{2.32}$$

Mechanical fracture closure occurs when the fracture pressure declines to approximately the minimum horizontal stress acting normal to the fracture plane:

$$P_f \approx S_{h\,\min}. \tag{2.33}$$

In practice, closure occurs over a finite pressure interval because fracture surfaces are rough and contact develops progressively between asperities. Once the fracture has propagated beyond the near-wellbore stress concentration zone, equilibrium between fracture pressure and the far-field normal stress governs closure, such that

$$P_{\mathrm{FCP}} \approx S_{h\,\min}.$$

This relationship underpins the use of fracture closure pressure as the most reliable estimator of $S_{h\,\min}$ in XLOT and micro-fracture analysis McClure and Horne (2014), Nolte (1979), and Zoback (2010).

2.5.2. Progressive fracture closure

Fracture closure is not instantaneous. Natural and induced fractures exhibit surface roughness and asperities, such that mechanical contact between opposing fracture surfaces develops progressively as fracture aperture decreases. Contact typically initiates at isolated asperities and expands as pressure declines, producing a gradual increase in fracture stiffness rather than an abrupt loss of aperture (McClure et al., 2016; Wang & Sharma, 2017).

As a result, fracture compliance C_f decreases progressively during shut-in. The reduction in compliance produces a measurable increase in system stiffness:

$$C_f \downarrow \implies C_t \downarrow \implies \frac{1}{C_t} \uparrow .$$

This progressive compliance reduction generates the diagnostic slope change commonly observed in pressure fall-off plots.

In G-function coordinates, the governing relation becomes

$$\frac{dP}{dG} = \frac{1}{C_t}\frac{dV_f}{dG}, \tag{2.34}$$

showing explicitly that the pressure derivative reflects the evolving compliance of the fracture–wellbore system during closure (Nolte, 1979; Raaen et al., 2001). Closure-picking methods based on stiffness evolution therefore aim to identify this transition.

2.5.3. Hydraulic versus mechanical closure

It is useful to distinguish between hydraulic and mechanical closure. Hydraulic closure refers to the loss of efficient fluid transport within the fracture as aperture decreases. Mechanical closure corresponds to load-bearing contact between opposing fracture faces. Diagnostic interpretation methods based on pressure derivatives and stiffness evolution primarily detect mechanical closure, which represents the relevant condition for stress estimation (McClure et al., 2016).

2.5.4. Influence of poro-elastic effects

Poro-elastic diffusion may influence the early-time pressure decline by modifying pore pressure near the fracture faces and altering local effective stresses. These effects can smooth or delay the pressure-derivative response immediately after shut-in. However, once transient hydraulic effects dissipate and fracture pressure approaches the far-field stress level, the stress governing closure is determined primarily by the far-field minimum horizontal stress (Detournay & Cheng, 1988).

2.5.5. Conditions for reliable stress estimation

The equivalence between closure pressure and $S_{h\,\min}$ requires that:

- the fracture extends beyond the near-wellbore stress concentration region,
- pressure interpretation occurs after wellbore storage and viscous pressure gradients dissipate,
- significant stress contrasts due to layering or fracture height growth are absent.

When these conditions are approximately satisfied, closure pressure provides a mechanically robust and reproducible estimate of the minimum horizontal stress. Deviations may occur in very high-permeability formations, short fractures, or mechanically layered sequences, but closure pressure remains the most defensible stress indicator obtainable from hydraulic stress testing.

2.6. Integrated physical framework for hydraulic stress tests

The preceding sections introduced the governing mechanical and hydraulic processes individually. In practice, however, hydraulic stress tests involve the interaction of these processes throughout the fracture lifecycle. The pressure response recorded during injection and shut-in reflects the relative dominance of five coupled mechanisms: (i) stress concentration and tensile failure at the borehole wall, (ii) fracture-mechanics-controlled propagation, (iii) viscous flow within the fracture, (iv) pore-pressure diffusion and leak-off into the formation, and (v) mechanical fracture closure under far-field stresses.

During the initial stage of pressurisation, the response is governed primarily by elastic stress redistribution around the wellbore. Within the Kirsch framework, fracture initiation occurs when the minimum effective tangential stress at the borehole wall reaches the tensile strength of the rock. This stage is controlled by far-field stresses, pore pressure, wellbore geometry, and rock strength, and therefore represents a local borehole-scale process.

Once a fracture has initiated, the dominant mechanism transitions from stress concentration at the borehole wall to fracture-tip mechanics. In a Linear Elastic Fracture Mechanics (LEFM) description, fracture propagation is governed by the stress intensity factor at the crack tip and the fracture toughness of the rock (Eqs. 2.16–2.15). At this stage, the required pressure depends not only on the in-situ stresses but also on fracture geometry and material toughness. Viscous pressure losses within the fracture further contribute to the measured propagation pressure.

Simultaneously, fluid leak-off into the surrounding formation modifies both the hydraulic and mechanical response. Diffusion-driven leak-off reduces fracture pressure during injection and controls the early-time pressure decline after shut-in. Through poro-elastic coupling, increases in pore pressure locally reduce effective stresses, thereby influencing apparent fracture initiation behaviour and early pressure evolution.

After shut-in, the governing mechanism transitions again. As viscous pressure gradients dissipate and leak-off continues, the fracture progressively loses aperture. Mechanical closure occurs when fracture pressure equilibrates with the far-field normal stress acting on the fracture plane. Provided that the fracture has propagated beyond the near-wellbore stress concentration zone, late-time pressure behaviour is governed primarily by far-field stresses rather than by borehole-scale effects. Under these conditions, the fracture closure pressure reflects the minimum horizontal stress $S_{h\,\min}$.

Hydraulic stress tests therefore sample different stages of this coupled mechanical–hydraulic system. Operational tests such as FITs and LOTs primarily interrogate near-wellbore initiation behaviour, whereas diagnostic tests such as XLOTs and micro-fracture tests are designed to capture propagation and closure stages. Differences between test types arise not from fundamentally different physics, but from which stage of the fracture lifecycle is observed and which mechanisms dominate the recorded pressure response.

2.7. Assumptions and Model Idealisation

The physical models presented in this chapter describe hydraulic stress testing within an idealised mechanical framework. These models are necessary to interpret pressure data in terms of far-field stresses, but they rely on simplifying assumptions that are not strictly satisfied in natural formations.

2.7.1. Elastic, homogeneous, isotropic behaviour

The Kirsch solution, LEFM formulation, poro-elastic diffusion model, and fracture compliance relations all assume:

- Linear elastic rock behaviour,
- Homogeneous material properties,
- Isotropic mechanical response,
- A continuous, intact medium without pre-existing discontinuities,
- Plane strain conditions around the wellbore,
- No temperature change during test.

Under these assumptions, stresses are smoothly distributed, fracture initiation occurs in intact rock, and fracture propagation can be described using continuum mechanics. The fracture closure pressure is then interpreted as reflecting equilibrium between fracture pressure and the far-field minimum horizontal stress $S_{h\,\min}$.

2.7.2. Real formation behaviour

In reality, subsurface formations are rarely homogeneous or isotropic. Mechanical stratigraphy, bedding anisotropy, cementation contrasts, natural fractures, stress heterogeneity, and near-wellbore damage can significantly perturb the stress field and hydraulic response.

Layered formations introduce stiffness and stress contrasts that influence fracture height growth and containment. Natural fractures may provide preferential leak-off pathways, altering pressure decline behaviour. Perforations, tortuosity, and drilling-induced damage modify near-wellbore stress concentrations and can affect observed initiation pressures. Thermal effects and time-dependent deformation may further complicate the mechanical response.

As a result, the measured pressures during hydraulic stress tests do not represent purely idealised model behaviour, but rather the combined response of the ideal continuum mechanics framework and local geological complexities.

2.7.3. Implications for interpretation

Interpretation uncertainty arises when real conditions deviate from these idealisations.

For example:

- Breakdown or leak-off pressure may reflect near-wellbore damage or perforation effects rather than intact-rock tensile failure.

- Propagation pressure may be influenced by fracture geometry and viscous losses rather than directly by $S_{h\,\min}$.
- Early-time pressure decline may be dominated by wellbore storage or heterogeneous leak-off rather than fracture mechanics.
- Closure may occur progressively in rough fractures, producing ambiguity in closure-picking methods.

The reliability of stress estimation therefore depends on how closely the field conditions approximate the idealised assumptions underlying the mechanical models. When fractures propagate beyond the near-wellbore stress concentration zone and pressure interpretation is performed after transient storage effects dissipate, closure pressure provides the most mechanically robust estimate of $S_{h\,\min}$. Deviations from these conditions introduce uncertainty that must be evaluated during interpretation.

This study adopts the idealised mechanical framework presented in this chapter as the theoretical basis for stress estimation, while explicitly recognising that differences between test types, formations, and interpretation methods arise from departures from these assumptions. The magnitude and consequences of these departures form a central theme in the analysis of subsequent chapters.

Table 2.3: Overview of key factors influencing hydraulic stress test response and interpretation.

Factor	Type	Primary parameters affected	Key influence / remarks
Porosity / permeability	Formation	LOP, FPP, falloff, FCP	Controls leak-off rate and pressure decline shape; high permeability can mask fracture initiation.
Mechanical properties (tensile strength, toughness, stiffness)	Formation	FIP, FBP, FRP, FPP	Lower tensile strength in sands/limestones than shales; affects breakdown and re-opening pressures.
Stress contrast / layering	Formation	FPP, FCP	Limits fracture height growth; improves closure interpretability when contrasts are strong.
Natural fractures / fissures	Formation	LOP, FPP, falloff	Cause pressure-dependent leak-off and non-ideal falloff; may be drilling-induced or stress-controlled.
Wellbore geometry / inclination	System	LOP, FBP, FRP	Alters hoop stress distribution; inclined wells reduce breakdown pressure; limited influence on FCP.
Cased vs uncased interval	System	LOP, FBP, FRP, storage	Perforations and cement introduce tortuosity; open-hole LOTs unreliable if interval is long.
Fluid properties (viscosity, density)	System	FPP, ISIP, falloff	Viscosity increases viscous losses; affects fluid efficiency and G-function interpretation.
Injection rate	System	FPP, ISIP	Higher rates increase frictional losses and poroelastic effects; closure unaffected if falloff is clean.
Injected volume	System	FRP, FCP	Larger volumes reduce near-wellbore bias and improve far-field stress resolution.
Temperature change	System	LOP, FBP, ISIP	Thermal contraction may reduce effective stress locally; usually secondary in short tests.
Near-wellbore tortuosity	System	FPP, ISIP	Causes pressure-dependent losses; more pronounced in cased and perforated wells.

3

Methodology

The previous chapter elaborated on the background theory needed to understand the topic of this study. This chapter describes the methodology used to answer the research questions.

3.1. Research design and approach

This thesis adopts a structured, field-data-driven workflow to constrain the minimum horizontal stress $S_{h\,\min}$ from hydraulic stress tests. The methodology separates data preparation, pressure interpretation, stress inference, and regional validation into sequential stages. An overview of the interpretation workflow is provided in Figure 3.11.

The first stage comprises compilation, harmonisation, and quality control of hydraulic stress test data (FIT, LOT, XLOT, and micro-fracture tests). Measurements are standardised through unit conversion, hydrostatic depth referencing to the fracture interval true vertical depth (TVD), time alignment of surface and downhole gauges, and resampling where required. Injection cycles are identified, and pre-fracture system compliance is estimated from early-time pressure–volume behaviour. Particular attention is given to density assumptions, gauge offsets, and rate–pressure synchronisation, as preprocessing errors directly propagate into initiation and closure estimates.

In the second stage, characteristic pressures are identified for each cycle, including leak-off pressure (LOP), fracture breakdown pressure (FBP), fracture reopening pressure (FRP), and, where applicable, instantaneous shut-in pressure (ISIP). Picks are supported by pressure–volume trends, compliance evolution, and flow-normalised diagnostics. Internal consistency checks (cycle-to-cycle plausibility, diagnostic agreement, and ambiguity screening) are applied, and tests that fail predefined criteria are interpreted conservatively.

The third stage addresses fracture closure interpretation for XLOT and micro-fracture tests. Multiple closure picking methodologies are applied, including diagnostic time-transform, derivative-based, semilogarithmic, and stiffness-based approaches. The system stiffness method is treated as the primary estimator when data quality permits, while alternative methods quantify method-dependent uncertainty. Reported fracture closure pressures (FCP) therefore include an uncertainty range reflecting inter-method and inter-cycle variability.

In the fourth stage, interpreted pressures are translated into stress constraints. Closure-derived FCP values are taken as the primary proxy for $S_{h\,\min}$ once fracture propagation is assumed to extend beyond the near-wellbore stress concentration zone. FIT and LOT initiation pressures are converted into conditional bounds on $S_{h\,\min}$ using the Kirsch solution for vertical wells and the rotated-stress formulation for deviated wells. The inversion incorporates parameterisation of the stress ratio $k = S_{H\,\max}/S_{h\,\min}$ and tensile strength T_0, and sensitivity analyses are performed to evaluate the impact of these assumptions.

Finally, an offset-data case study assesses whether $S_{h\,\min}$ at a target well can be predicted from nearby FIT/LOT measurements combined with deviated-well Kirsch modelling. Predicted values are compared against closure-derived reference estimates to evaluate reliability and identify systematic deviations.

Overall, the research design prioritises transparency, reproducibility, and explicit treatment of uncertainty. By combining analytical stress solutions with systematic interpretation diagnostics, the workflow enables consistent cross-well comparison while clearly distinguishing measurement-derived constraints from assumption-dependent bounds.

1. **Data and preprocessing**
   (a) Collect and curate data.
   (b) Clean, reference, and harmonise data.
2. **Interpretation to characteristic pressures**
   (a) Pick characteristic pressures per cycle (LOP, FBP, FRP, ISIP where applicable).
   (b) Perform quality control and internal consistency checks.
3. **Closure methodology comparison and uncertainty**
   (a) Closure pressure estimation and method comparison:
      - Apply multiple closure interpretation methods.
      - Select a primary estimator.
      - Quantify uncertainty using inter-method and inter-cycle spread.
      - Define closure time consistently, where applicable.
4. **Stress inference and regional/offset evaluation**
   (a) Translate interpreted pressures into $S_{h\,\min}$ constraints:
      - Initiation-derived bounds from FIT/LOT using the Kirsch solution and rotated-stress generalisation.
      - Sensitivity analysis for $k = S_{H\,\max}/S_{h\,\min}$, tensile strength T_0, pore pressure p_p, and thermal stress (if applicable).
   (b) Offset-data prediction case study:
      - Construct predictor using offset FIT/LOT data and deviated-well Kirsch modelling.
      - Compare predicted and closure-derived reference $S_{h\,\min}$ values.
      - Evaluate prediction performance using defined error metrics and analyse failure cases.

3.2. Data sources and preprocessing

3.2.1. Dataset description

This study is based on a compilation of hydraulic stress test data acquired in geothermal and subsurface exploration wells across the Netherlands. A substantial part of the dataset originates from the *Seismische Campagne Aardwarmte Nederland* (SCAN) programme, coordinated by Energie Beheer Nederland (EBN), complemented by data from the Delft and Middenmeer geothermal projects. The combined dataset covers multiple geological settings, depths, and operational contexts (Figure 3.1; Table 3.1).

The database includes FITs, LOTs, XLOTs, and micro-fracture tests conducted in both open-hole and cased-and-perforated intervals. For each test, available measurements typically comprise surface injection pressure, downhole pressure (where available), injection rate, cumulative injected volume, shut-in timing, fluid density, and basic well geometry (true vertical depth of test interval, casing configuration, lithology). High-resolution downhole gauge data were available for a subset of the SCAN wells, enabling detailed analysis of pressurisation and fall-off behaviour. Where downhole data were unavailable, surface pressures were corrected for hydrostatic head to estimate pressure at the fracture depth.

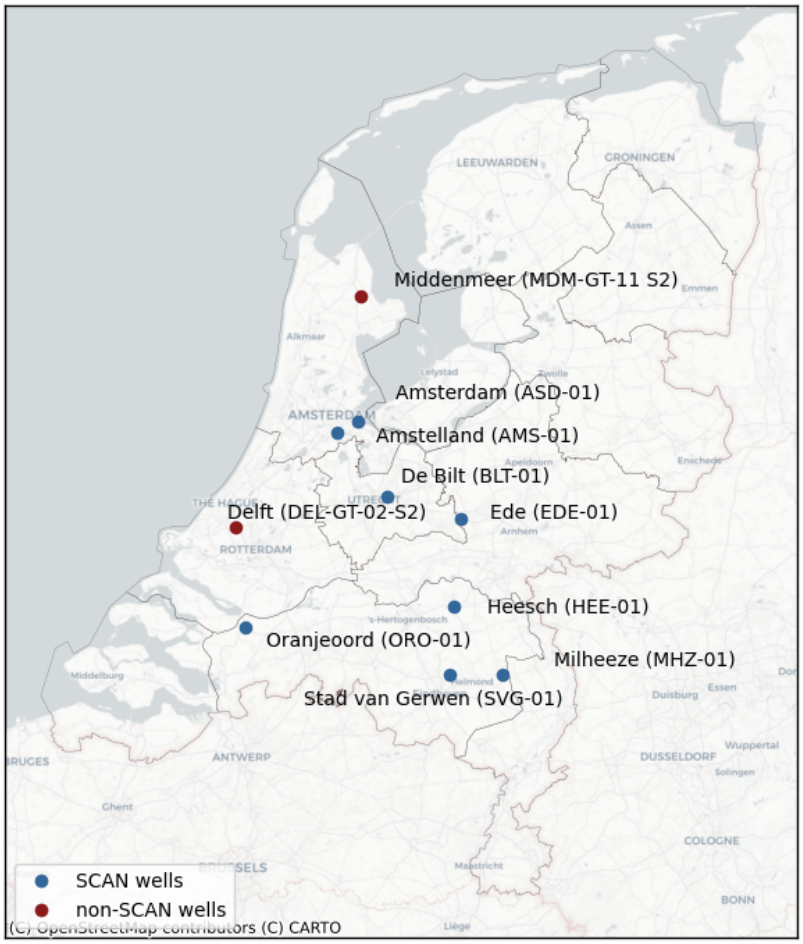

Figure 3.1: Hydraulic stress test locations considered for this study.

3.2.2. Depth referencing and hydrostatic correction

All pressures are referenced to the true vertical depth (TVD) of the fracture interval to ensure comparability between tests. When downhole pressure measurements at or near the test interval are available, these are used directly. When only surface pressures are available, hydrostatic correction is applied according to:

$$p_{\mathrm{TVD}} = p_{\mathrm{surface}} + \rho_f g \left(z_{\mathrm{TVD}} - z_{\mathrm{surface}} \right), \tag{3.1}$$

where ρ_f is the test fluid density, g is gravitational acceleration, and z_{TVD} is the fracture interval depth. Fluid density is taken from reported mud or brine properties during the test.

When both surface and downhole data are available, independently corrected pressures are cross-checked. Discrepancies exceeding approximately 1 bar are treated as indicators of inconsistent density assumptions, gauge depth uncertainties, or pressure losses during pumping, and are resolved prior to interpretation.

Table 3.1: Overview of hydraulic stress tests included in this study, showing well location, test type, and fracture depth.

Well ID	Location	Test number	Test type	Fracture type	Fracture depth TVD [m]
AMS-01	Amstelland	1	XLOT	cased, perforation	1865.3
AMS-01	Amstelland	2	XLOT	cased, perforation	1323.5
AMS-01	Amstelland	3	XLOT	cased, perforation	655.5
AMS-01	Amstelland	1	LOT	open-hole	706.0
AMS-01	Amstelland	2	FIT	open-hole	1798.5
ASD-01	Amsterdam	1	XLOT	cased, perforation	1543.75
ASD-01	Amsterdam	2	XLOT	cased, perforation	833.0
ASD-01	Amsterdam	1	FIT	open-hole	964.0
BLT-01	De Bilt	1	XLOT	cased, perforation	1732.0
BLT-01	De Bilt	2	XLOT	cased, perforation	1325.5
BLT-01	De Bilt	3	XLOT	cased, perforation	1104.7
BLT-01	De Bilt	1	LOT	open-hole	580.0
BLT-01	De Bilt	2	FIT	open-hole	1575.0
DEL-GT-02	Delft	1	Micro-frac	cased, perforation	1973.88
DEL-GT-02	Delft	2	Micro-frac	cased, perforation	2147.14
DEL-GT-02	Delft	3	Micro-frac	cased, perforation	2047.14
DEL-GT-02	Delft	1	FIT	open-hole	841.0
DEL-GT-02	Delft	2	FIT	open-hole	1935.0
EDE-01	Ede	1	XLOT	cased, perforation	1031.25
EDE-01	Ede	1	LOT	open-hole	826.5
HEE-01	Heesch	1	XLOT	cased, perforation	2070.2
HEE-01	Heesch	2	XLOT	cased, perforation	1479.2
HEE-01	Heesch	3	XLOT	cased, perforation	390.2
HEE-01	Heesch	1	LOT	open-hole	486.3
HEE-01	Heesch	2	LOT	open-hole	1915.0
MDM-GT-02	Middenmeer	1	Micro-frac	open-hole	2417.74
MDM-GT-02	Middenmeer	2	Micro-frac	open-hole	2367.24
MDM-GT-02	Middenmeer	3	Micro-frac	open-hole	2252.986
MHZ-01	Milheeze	1	XLOT	cased, perforation	1209.75
MHZ-01	Milheeze	2	XLOT	cased, perforation	485.75
MHZ-01	Milheeze	1	FIT	open-hole	1041.0
MHZ-01	Milheeze	1	LOT	open-hole	542.0
ORO-01	Oranjeoord	1	XLOT	cased, perforation	341.5
ORO-01	Oranjeoord	2	XLOT	cased, perforation	578.5
ORO-01	Oranjeoord	1	FIT	open-hole	624.0
SVG-01	Stad van Gerwen	1	XLOT	cased, perforation	1227.47
SVG-01	Stad van Gerwen	1	LOT	open-hole	1227.0

3.2.3. Time alignment and data harmonisation

Hydraulic stress test interpretation is highly sensitive to time synchronisation between pressure, rate, and volume data. Surface and downhole clocks are therefore inspected and, where necessary, minor time shifts are applied to align pressure and rate responses.

All datasets are converted to consistent units and resampled where required to ensure uniform temporal resolution. Pressure, injection rate, and cumulative volume are synchronised so that pressure derivatives and rate-normalised diagnostics can be computed consistently.

An initial visual inspection of surface and downhole pressure together with injection rate is performed for each test to verify the test sequence and to identify injection cycles. An example of pressure data is shown in Figure 3.2.

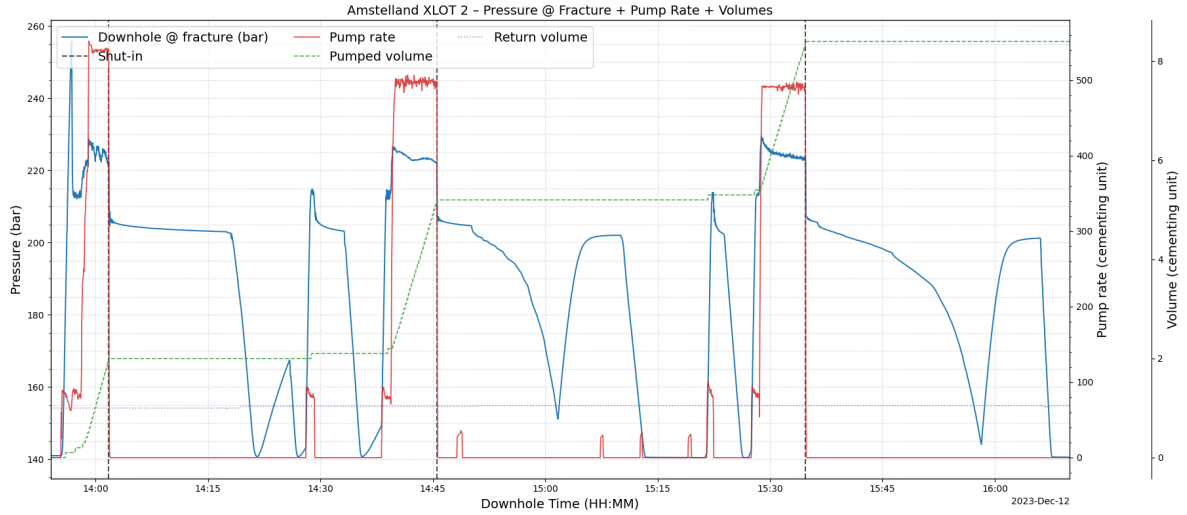

Figure 3.2: Example of downhole and surface pressure data against time after hydrostatic correction and time alignment.

3.2.4. Cycle definition

Injection cycles are defined as the interval between the onset of pressurisation and the end of the subsequent shut-in period. The start of a cycle is identified by a concurrent increase in injection rate and pressure. Shut-in is defined as the time at which injection rate approaches zero and pressure transitions from increasing to decreasing behaviour.

Where multiple cycles are present (e.g. in XLOTs and micro-fracture tests), each cycle is analysed separately. This cycle-based approach enables identification of fracture reopening pressures and assessment of closure pressure.

3.3. Characteristic pressure identification

This section defines how the principal characteristic pressures—leak-off pressure (LOP), fracture breakdown pressure (FBP), and fracture reopening pressure (FRP)—are identified from preprocessed pressure–rate–volume data. The objective is to apply a consistent and reproducible picking strategy across wells and test types.

3.3.1. Compliance estimation

Pre-fracture system compliance is determined for each injection cycle from the early-time pressure–volume response. Under elastic conditions, pressure increases linearly with injected volume prior to fracture initiation. The slope of this linear segment defines the effective wellbore system compliance:

$$C_{\text{well}} = \left(\frac{\Delta V}{\Delta p} \right)_{\text{pre-breakdown}} . \tag{3.2}$$

In practice, compliance is estimated by linear regression of pressure versus injected volume from the start of injection until the first systematic deviation from linearity. The resulting compliance is then used to compute the effective perforation flow rate,

$$q_{\mathrm{perf}} = q_{\mathrm{pump}} - C\,\frac{dp}{dt}, \tag{3.3}$$

where q_{pump} is the measured injection rate and $\frac{dp}{dt}$ is the pressure increase rate. Example pressure build-up behaviour and the corresponding compliance estimate are shown in Figure 3.3.

3.3.2. Picking strategy and supporting diagnostics

Characteristic pressures are identified using a combination of (i) changes in pressure–volume behaviour, (ii) compliance evolution, and (iii) flow-normalised diagnostics. The primary flow-normalised diagnostic used in this study is the effective perforation flow rate q_{perf} (Equation 3.3), which highlights departures from purely elastic behaviour and is less sensitive to variations in pump rate.

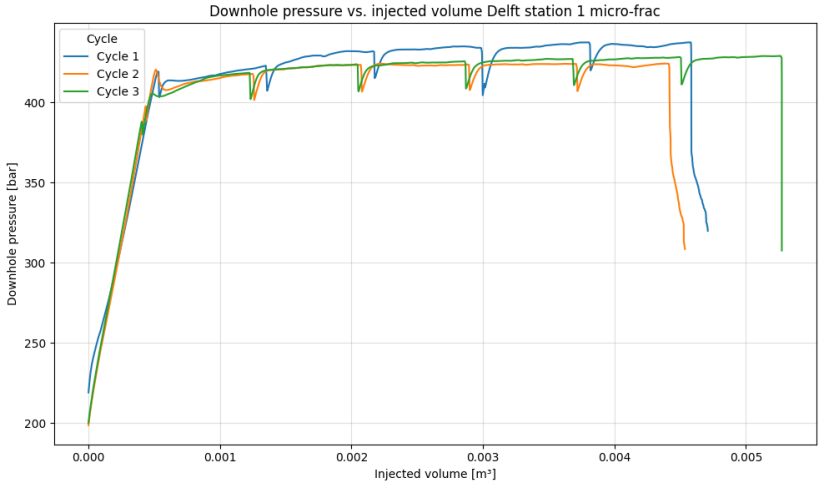

(a) Pressure build-up during injection for several cycles.

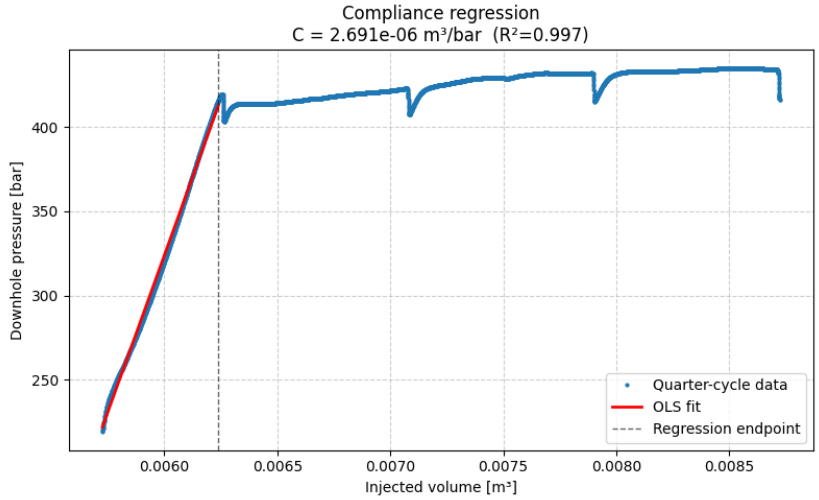

(b) Compliance calculation based on the build-up slope and resulting q_{perf}.

Figure 3.3: Example of pressure build-up and compliance response for the Delft station 1 micro-frac.

3.3.3. Leak-off pressure (LOP)

The leak-off pressure is defined as the first systematic deviation from linear elastic pressurisation during injection. Operationally, LOP is identified at the onset of sustained non-elastic behaviour, supported by:

- deviation from the linear pressure–volume trend used for compliance estimation;
- a sustained increase in q_{perf} indicating fluid entry into the formation and/or a newly initiated fracture;
- a change in the build-up slope relative to earlier elastic behaviour.

An example LOP pick is shown in Figure 3.4.

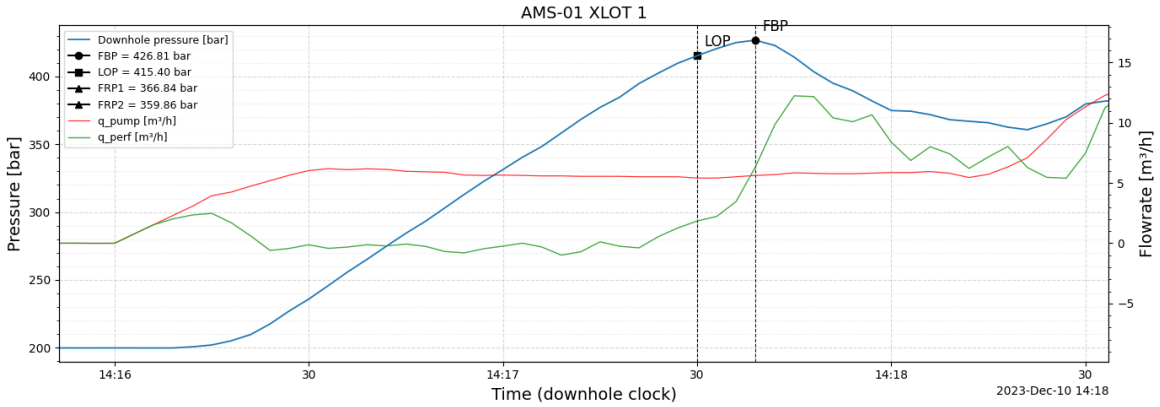

Figure 3.4: Example of leak-off pressure pick for AMS-01 XLOT 1 based on deviation from elastic build-up and increased q_{perf}.

3.3.4. Fracture breakdown pressure (FBP)

The fracture breakdown pressure is defined as the maximum pressure reached during an injection cycle prior to shut-in. In the first cycle, FBP represents the highest pressure required to initiate and begin propagating a fracture in intact rock, reflecting near-wellbore stress concentration and tensile strength effects. In subsequent cycles, the maximum pressure may be influenced by operational limits and does not necessarily correspond to breakdown in intact rock.

3.3.5. Fracture reopening pressure (FRP)

In repeated injection cycles, previously created fractures may reopen at pressures lower than the first-cycle breakdown pressure. The FRP is identified using the same diagnostic criteria as LOP, i.e. renewed deviation from elastic pressurisation and an increase in q_{perf}.

In theory, reopening occurs along an existing fracture such that the tensile strength contribution is reduced. Under ideal elastic conditions, the difference between FIP (first-cycle initiation) and FRP (reopening) provides an approximate constraint on tensile strength (White et al., 2002):

$$p_{\mathrm{FIP}} - p_{\mathrm{FRP}} = T_0, \tag{3.4}$$

with the caveat that perforation friction, near-wellbore damage, and poroelastic effects may bias this relation.

3.3.6. Repeatability and internal consistency

To improve reproducibility and minimise interpreter bias, pressure picks are checked for internal consistency across cycles and diagnostics. Tests that show ambiguous behaviour (e.g. no clear deviation from elastic build-up, or strong rate artefacts) are flagged and interpreted conservatively (meaning that LOP should be near FBP).

A full-cycle overview showing LOP, FBP, and FRPs is provided in Figure 3.5.

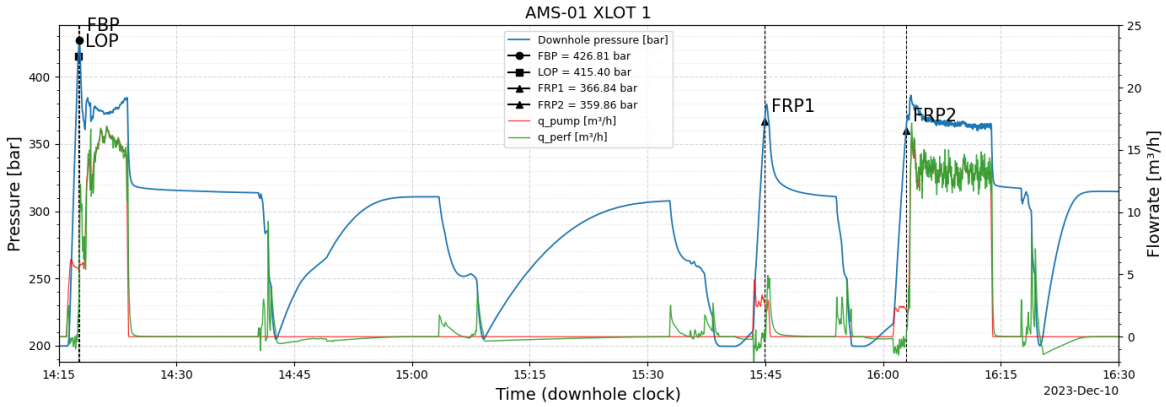

Figure 3.5: Full test overview showing the picked LOP, FBP, and FRPs for AMS-01 XLOT 1.

3.4. Fracture closure interpretation

The most robust estimate of the minimum horizontal stress $S_{h\,\min}$ is obtained from the FCP, which reflects the pressure at which an induced hydraulic fracture can no longer be mechanically sustained against the far-field least principal stress (Economides & Nolte, 2000). Once a fracture has propagated sufficiently far from the wellbore, the influence of near-wellbore stress concentrations, borehole imperfections, and tensile strength diminishes, and fracture behaviour becomes dominated by the in-situ stress state. When the distance from the centre of the wellbore is larger than 4.2 the radius of the wellbore, the tangential stress is smaller than 1% of the $S_{h\,\min}$, see also subsection 2.3.1. Under these conditions, the closure pressure provides a physically defensible proxy for $S_{h\,\min}$.

Fracture closure analysis is therefore a key element of the interpretation workflow for XLOTs and micro-fracture tests, which include a shut-in period during which pressure decline can be observed and analysed. In contrast, FITs and conventional LOTs are typically terminated during injection and do not capture a meaningful pressure fall-off phase. As a result, closure-based stress estimation is not applicable for FIT/LOT data, and the present section is restricted to XLOT and micro-fracture tests.

Fracture closure is not instantaneous but gradual. During fall-off, pressure decline reflects both fluid leak-off to the formation and elastic volume reduction of the fracture–wellbore system. As fracture faces progressively come into contact, the effective compliance decreases (stiffness increases), producing diagnostic changes in the pressure decline response (see section 2.5). Consequently, the inferred FCP is inherently method-dependent and sensitive to data quality, wellbore storage, and deviations from ideal leak-off behaviour.

In this study, multiple closure interpretation methods are applied and compared: (i) pre-holistic deviation methods (Castillo), (ii) derivative-based bilinear fitting (Haimson), (iii) holistic/tangent-based interpretation (Barree), (iv) semilog max picking (algorithmic analogue of Barree), and (v) a mechanically based system stiffness (compliance) method, which is treated as the primary estimator. Method-to-method spread is used to quantify interpretation uncertainty and to flag tests where closure is not sufficiently resolved.

3.4.1. Time transformations

3.4.2. Pre-holistic (Castillo) closure method

The pre-holistic closure method (Castillo, 1987) identifies FCP as the first continuous deviation from an assumed linear pressure decline trend in a diagnostic time transformation (commonly P–G or P–$\sqrt{t}$ space). The underlying assumption is that pre-closure fall-off follows Carter-type leak-off behaviour and that mechanical closure induces a detectable change in slope.

In practice, the Castillo method is implemented by selecting the early-time linear segment of the diagnostic plot and marking the first clear departure from that trend as the closure pressure. The method is attractive because it is simple and can be applied to short shut-ins; however, it is inherently subjective and particularly sensitive to wellbore storage dissipation immediately after shut-in. Early-time

deviations may therefore reflect the transition from storage-dominated to fracture-dominated behaviour rather than true mechanical closure, leading to a systematic tendency to pick an upper bound on $S_{h\,\min}$.

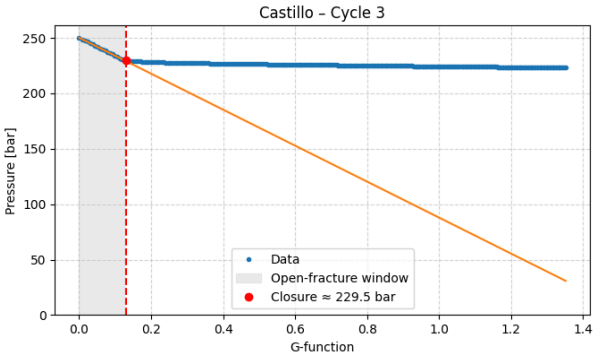

Figure 3.6: Example of closure picking using the Castillo method (ASD XLOT 1, Cycle 3).

3.4.3. Haimson bilinear closure method

The Haimson bilinear method (Lee & Haimson, 1989) identifies closure from a breakpoint between two approximately linear regimes in $\mathrm{d}P/\mathrm{d}t$–P space during shut-in. The conceptual basis is that pressure decline is governed by different effective flow behaviour before and after closure (linear flow vs radial flow), producing two separable derivative trends.

Implementation consists of selecting two fitting windows (early-time and late-time), and determining the intersection pressure of the two linear regressions. When derivative estimates are stable and both regimes are well populated, the method provides an objective and repeatable closure estimate. Its main limitations are the sensitivity of numerical derivatives to noise and the fact that gradual closure may not produce a sharp bilinear transition. In such cases, the inferred intersection can be non-unique and tends to bias toward a lower bound on $S_{h\,\min}$.

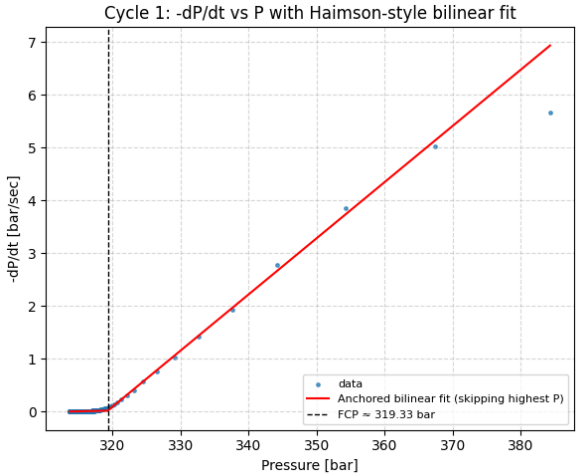

Figure 3.7: Example of closure picking using the Haimson bilinear method (AMS-01 XLOT 1, Cycle 1).

3.4.4. Barree tangent (holistic) closure method

The Barree tangent (holistic) method (Barree et al., 2009) infers closure from the departure of the semilog pressure derivative from an early-time reference trend that is interpreted to represent Carter-type leak-off prior to closure. Compared to pre-holistic methods, it is intended to be more robust to smooth, gradual transitions by focusing on derivative behaviour rather than direct slope changes in pressure–time plots.

In practice, a tangent is defined over an early-time derivative window and closure is picked at the

pressure where the observed derivative departs systematically from this tangent. The key methodological sensitivity lies in the choice of the early-time window: if early-time data are still influenced by wellbore storage or operational transients, the tangent is biased and closure is shifted. Moreover, derivative departures can be produced by processes other than mechanical closure, including evolving fracture surface area (tip extension/height recession) or pressure-dependent leak-off (Economides & Nolte, 2000). At last, early fall-off is suppressed, as the G-function is still small here. This could also wrongly suppress rapid closure, leading to the wrong closure pick.

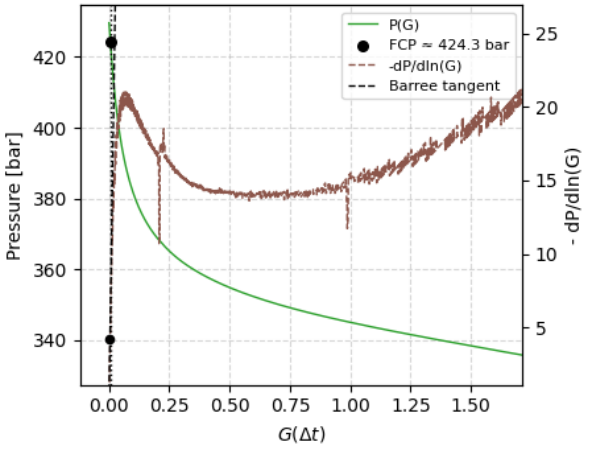

Figure 3.8: Example of closure picking using the Barree tangent method (Delft station 2, Cycle 1). It showcases how hard it is to numerically define deviation from linearity.

3.4.5. Semilog max method

The semilog max method defines closure as the pressure corresponding to the maximum value of the semilogarithmic pressure derivative during fall-off. This method is used by service companies like BakerHughes and Schlumberger. Using a diagnostic variable x (e.g. Δt, $\sqrt{\Delta t}$, or G-time), the semilog derivative is defined as

$$\frac{\mathrm{d}P}{\mathrm{d}\ln x} = x\,\frac{\mathrm{d}P}{\mathrm{d}x}, \tag{3.5}$$

and closure is picked at

$$P_{\mathrm{cl}} = P(x_{\max}), \qquad x_{\max} = \arg\max\left(-\frac{\mathrm{d}P}{\mathrm{d}\ln x}\right). \tag{3.6}$$

This method is conceptually related to the tangent approach but removes the subjective step of constructing a tangent line. It is therefore attractive for automated and consistent processing across many tests. Its main drawback is strong sensitivity to derivative noise, smoothing choices, and sampling resolution. In addition, the maximum in $-\mathrm{d}P/\mathrm{d}\ln x$ is not uniquely diagnostic of mechanical closure and can be triggered by wellbore storage dissipation or other hydraulic artefacts. In this study, semilog-max picks are used primarily as an objective comparator to Barree-based picks.

3.4.6. System stiffness (compliance) method

The system stiffness (compliance) method (McClure et al., 2019) interprets closure as a mechanical transition in the coupled fracture–wellbore system. During fall-off, pressure decline is driven by leak-off and elastic contraction of the fracture volume. While the fracture remains open, the system behaves compliantly; as fracture faces progressively contact, additional pressure decline requires a stiffer mechanical response, leading to a measurable increase in stiffness (decrease in compliance). See also Equation 2.30.

Operationally, the method estimates an effective system compliance during fall-off,

$$C_{\mathrm{sys}} = \frac{\mathrm{d}V}{\mathrm{d}P}, \tag{3.7}$$

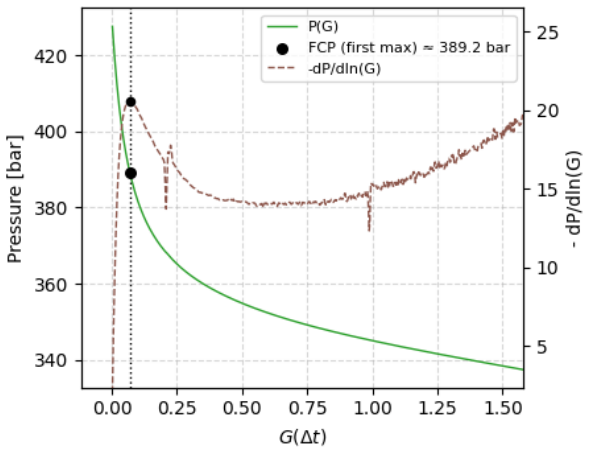

Figure 3.9: Example of closure picking using the semilog max method (Delft station 2, Cycle 1).

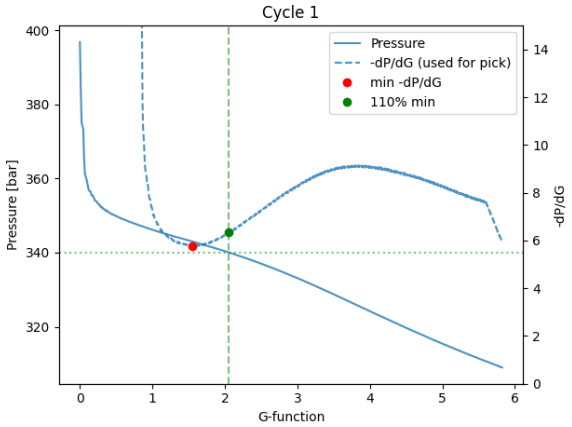

Figure 3.10: Example of closure picking using the system stiffness method (Heesch 01 cycle 1).

where $\mathrm{d}V$ represents the effective volume change associated with leak-off and elastic contraction over a pressure interval. Closure is identified at the onset of a sustained stiffness increase (i.e. a marked reduction in C_{sys}) consistent with progressive fracture contact. 10% is added to the derivative based on empirical results, as fracture contact does not precisely yet represent the $S_{h\,\mathrm{min}}$ (Guglielmi et al., 2022). Relative to purely diagnostic time-transform methods, this approach is more directly tied to fracture mechanics and is less dependent on assuming ideal Carter leak-off.

The stiffness method has higher data-quality demands: it requires sufficiently long shut-in to resolve the transition, and careful handling of wellbore storage and compliance estimation. In complex cases multiple stiffness transitions may occur (e.g. rough fractures, partial closure, or evolving contact area), and closure is interpreted conservatively as the earliest pressure at which a sustained stiffness increase is observed across a meaningful pressure interval.

3.4.7. Method comparison strategy and quality control

Closure pressure picks are generated for each cycle using all applicable interpretation methods and compared to assess sensitivity and internal consistency. Although multiple diagnostic approaches are evaluated — including the system stiffness method, Castillo, Haimson, and Barree techniques — the semilog-maximum method is adopted as the primary estimate for determining $S_{h\,\mathrm{min}}$ in this study. Cycles which had no propagation phase were not considered.

The semilog-maximum method is selected because it provides a robust and consistently identifiable diagnostic feature across the majority of tests, even in cases where pressure resolution, shut-in dura-

tion, or data quality limit the applicability of stiffness-based analysis. In practice, it often yields a clear and reproducible estimate of fracture closure pressure, allowing consistent comparison between wells and test types. For this reason, semilog-max closure picks are used as the primary $S_{h\,\mathrm{min}}$ estimate in subsequent analyses. Alternative closure methods are retained to quantify method-dependent variability and to evaluate epistemic uncertainty in closure interpretation. The spread between methods and between cycles is used to define an uncertainty range for each test.

Table 3.2: Overview of fracture closure pressure interpretation methods used for estimating $S_{h\,\mathrm{min}}$, including their governing principle, strengths, limitations, and typical bias relative to the far-field stress.

Method	Core principle	Strengths	Limitations / pitfalls	Typical bias
Pre-holistic (Castillo, 1987)	FCP from first deviation from linearity in diagnostic time (e.g. P–G or P–$\sqrt{t}$).	Simple; minimal data requirements; highlights early-time behaviour.	Subjective; sensitive to wellbore storage and flow-regime changes; may confuse ISIP dissipation with closure.	Upper bound
Haimson bilinear (Lee & Haimson, 1989)	Two linear regimes fitted in $\mathrm{d}P/\mathrm{d}t$ versus P; closure at intersection.	Objective and repeatable; amenable to automation; robust when regimes are clear.	Requires stable derivatives and sufficient data; gradual closure yields ambiguous fits; breakpoint may be hydraulic rather than mechanical.	Lower bound
Barree tangent (holistic) (Barree et al., 2009)	Closure where semilog derivative departs from an early-time tangent (Carter-type assumption).	Widely used; handles gradual transitions better than pre-holistic picks.	Sensitive to human interpretation and noise; deviations may reflect geometry evolution or storage rather than closure.	Variable
Semilog-maximum	Closure at maximum of $-\,\mathrm{d}P/\mathrm{d}\ln x$ (algorithmic analogue of tangent method).	Objective; easily automatable; useful for consistent batch processing.	Highly sensitive to smoothing and sampling; maxima may reflect artefacts (storage / rate changes) rather than closure.	Variable
System stiffness (compliance) (McClure et al., 2019)	Closure from increase in fracture–wellbore stiffness as fracture faces progressively contact.	Strong physical basis; directly tied to mechanical transition; less dependent on diagnostic time choices.	Potentially requires long fall-off duration; storage/-compliance estimation affects results; multiple stiffness transitions possible.	Lower bound

Notes: "Typical bias" refers to the tendency of each method to overestimate or underestimate the far-field minimum horizontal stress $S_{h\,\mathrm{min}}$ for idealised datasets. In practice, all methods are sensitive to data quality, wellbore storage, fracture geometry evolution, and shut-in duration.

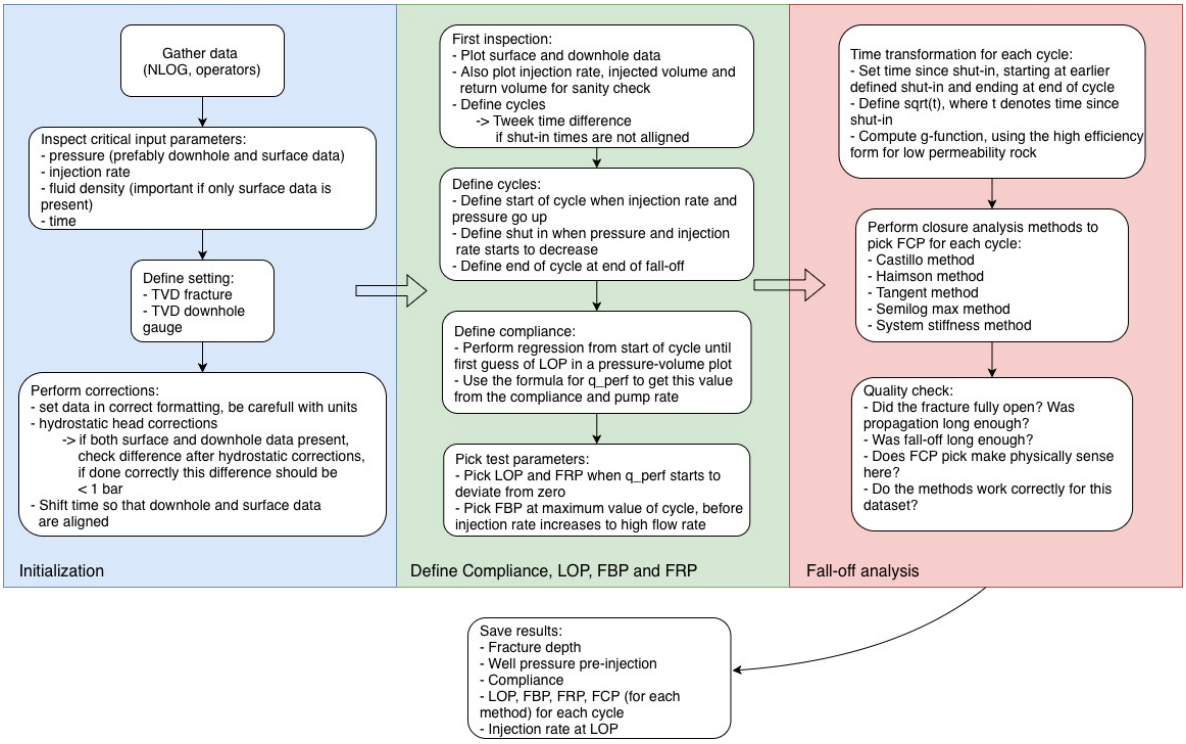

Figure 3.11: Workflow for the interpretation of the XLOTs and micro-fracs.

3.5. Stress inference and regional/offset evaluation

Note that the values used below are assumed based on literature. In reality these values depend on location, depth, lithology, etc. More in depth studies should be performed regarding the input for the proposed model, if one want to get the most accurate results.

3.5.1. Translate interpreted pressures into $S_{h\,\min}$ constraints

Closure-derived pressures from XLOT and micro-fracture tests are treated as primary estimates of $S_{h\,\min}$. For closure-based tests, the fracture closure pressure is assumed to approximate the least principal stress such that

$$S_{h\,\min} \approx P_{\text{closure}}. \tag{3.8}$$

FIT and LOT data are interpreted as initiation-based stress constraints derived from the pressurisation phase of the test. Because these tests do not resolve fracture closure, they do not provide a direct estimate of $S_{h\,\min}$, but can be translated into lower or upper bounds using elastic fracture initiation theory as outlined in subsection 2.3.1 and subsection 2.3.2.

The far-field stress state is defined by the principal stresses S_v, $S_{H\,\max}$, and $S_{h\,\min}$. The orientation of $S_{H\,\max}$ is taken as 135° (clockwise from north), consistent with regional stress compilations and borehole image analyses in the Netherlands (Mechelse, 2017). This orientation is assumed uniform across the study area, while in reality there is some variance.

The vertical stress S_v is approximated using a constant lithostatic gradient of

$$S_v = 225 \text{ bar/km} \times z, \tag{3.9}$$

which corresponds to a representative bulk density of approximately 2300–2350 kg/m^3 for the Dutch sedimentary sequence. This gradient is similar to the gradient found by Verweij (2015). Local deviations due to lithological variations (e.g. salt or low-density sediments) are not explicitly modelled.

The maximum horizontal stress is parameterised as

$$S_{H\,\max} = 1.15\, S_{h\,\min}. \tag{3.10}$$

This value reflects a predominantly normal-faulting stress regime. In reality, $S_{H\,\max}/S_{h\,\min}$ exhibits variance that generally increases with depth due to increased density and structural complexity.

For vertical wells, fracture initiation at the borehole wall is evaluated using the classical Kirsch solution. Tensile failure is assumed to occur when the minimum effective hoop stress equals the tensile strength:

$$\sigma_{\theta\theta,\min} = -T_0. \tag{3.11}$$

Evaluation of the Kirsch solution at the azimuth of minimum hoop stress yields:

$$p_{\mathrm{LOP}} = 3S_{h,\min} - S_{H,\max} - P_p + T_0 + \sigma_T, \tag{3.12}$$

where P_p is pore pressure, T_0 is tensile strength, and σ_T represents thermal stress where applicable.

FIT constraints During a formation integrity test (FIT), injection is terminated prior to fracture initiation. Consequently, the maximum pressure recorded during the test remains below the true leak-off pressure:

$$P_{\mathrm{FIT}} < P_{\mathrm{LOP}}. \tag{3.13}$$

Substituting the observed FIT pressure into Equation 3.12 therefore yields a conservative lower-bound estimate of $S_{h\,\min}$. Because fracture initiation is not reached during a FIT, the recorded maximum pressure cannot be interpreted as an upper bound on $S_{h\,\min}$.

The resulting constraint can be expressed as

$$S_{h\,\min}^{\mathrm{Kirsch,lower}} < S_{h\,\min} < P_{\mathrm{LOP}}. \tag{3.14}$$

LOT constraints For leak-off tests (LOT), injection continues until fracture initiation occurs and the leak-off pressure is observed. Equation 3.12 can therefore be inverted to estimate $S_{h\,\min}$ using the measured P_{LOP}. Because the inversion requires assumptions regarding $S_{H\,\max}$ and tensile strength, the resulting value is interpreted as an upper-bound estimate of $S_{h\,\min}$.

For deviated wells, the far-field stress tensor is constructed and rotated into the wellbore coordinate system. The detailed derivation is not repeated here.

Effective stresses in the plane normal to the borehole are expressed as:

$$\sigma_{11} = S_{11} - P_p, \quad \sigma_{22} = S_{22} - P_p, \quad \sigma_{12} = S_{12}. \tag{3.15}$$

The minimum effective hoop stress is given by the generalised Kirsch formulation:

$$\sigma_{\theta\theta,\min} = \sigma_{11} + \sigma_{22} - 2\sqrt{(\sigma_{11} - \sigma_{22})^2 + (2\sigma_{12})^2} - (P_f - P_p). \tag{3.16}$$

Fracture initiation is assumed when

$$\sigma_{\theta\theta,\min} = -T_0. \tag{3.17}$$

Equation 3.16 forms a nonlinear system in $S_{h\,\min}$ and is solved numerically for each deviated-well LOT.

The stress inversion requires the following input parameters:

- Vertical stress S_v (assumed gradient of 225 bar/km),
- Stress ratio $S_{H\,\max}/S_{h\,\min} = 1.15$,
- Pore pressure p_p assumed hydrostatic,
- Tensile strength T_0 assumed 0,
- Thermal stress σ_T assumed 0,
- Well inclination and azimuth.

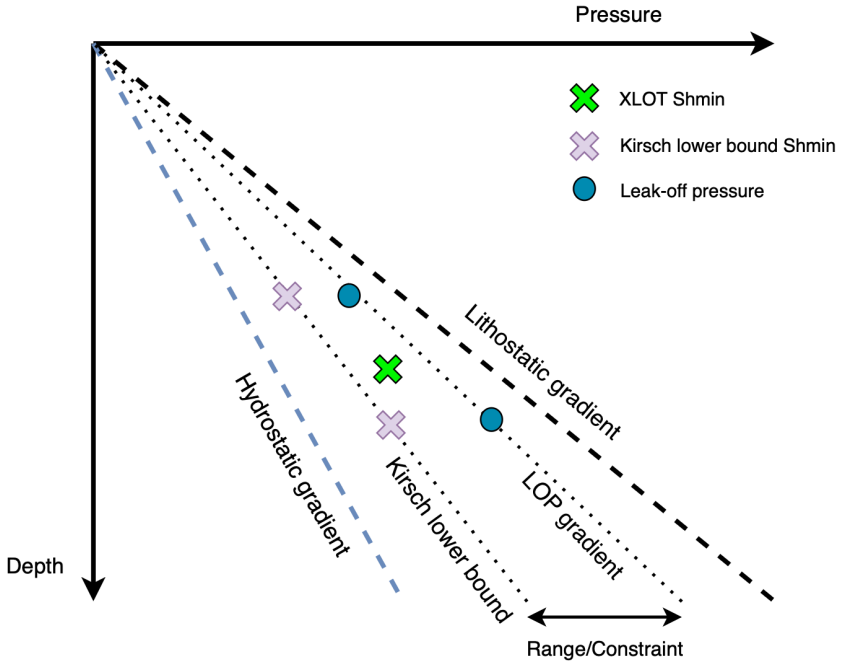

Figure 3.12: Schematic illustration of how formation tests constrain the minimum horizontal stress. LOT leak-off pressures represent fracture initiation and provide an upper bound and a lower bound when inverted using Kirsch. Closure-based tests provide the primary estimate $S_{h\,\min} \approx P_{\text{closure}}$.

3.5.2. Offset-data prediction case study

To assess whether initiation-based constraints can be used predictively at field scale, an offset-data workflow is applied. The objective is to estimate $S_{h\,\min}$ prior to drilling, using only information available from nearby wells.

FIT and LOT data from surrounding wells are interpreted following the methodology described in the previous sections. Where the leak-off pressure had already been evaluated by the operator and the supporting data quality was considered adequate, that interpretation was retained. The DEL-GT-02 well in Delft is selected as the target well for this case study.

For the target location, the far-field stress tensor is constructed based on the regional stress model and subsequently transformed into the wellbore coordinate system. The deviated-well fracture initiation criterion (Equation 3.16) is then inverted to obtain an estimate of $S_{h\,\min}$, without incorporating any local fracture-closure measurements.

The predicted $S_{h\,\min}$ values are compared against closure-derived estimates from micro-fracture tests, which are treated as mechanically representative reference values.

3.6. Summary

This chapter was written to document, in a transparent and reproducible way, how the hydraulic stress test dataset is processed and interpreted to address the central research objective: constraining the minimum horizontal stress $S_{h\,\min}$ and evaluating how reliably it can be inferred and transferred between wells.

The methodology is organised as a sequential workflow. First, FIT, LOT, XLOT, and micro-fracture datasets are compiled, harmonised, and quality controlled through unit standardisation, depth referencing to fracture-interval TVD, hydrostatic correction, and time alignment of pressure–rate–volume records. Second, cycle-level characteristic pressures (LOP, FBP, FRP, and ISIP where applicable) are identified using pressure–volume behaviour, compliance evolution, and rate-normalised diagnostics, with internal consistency checks used to flag ambiguous cycles.

Third, fracture closure pressures are interpreted for XLOT and micro-fracture tests using multiple established techniques. Method-to-method and cycle-to-cycle variability is retained as an explicit uncertainty measure, while a primary closure estimator is selected to ensure consistent cross-well comparison.

Finally, interpreted pressures are translated into stress constraints. Closure-derived pressures provide the mechanically grounded estimates of $S_{h\,\min}$, whereas FIT/LOT initiation pressures are converted into conditional bounds using Kirsch-based initiation criteria for vertical and deviated wells. The stress inversion is performed under explicit assumptions for S_v, $S_{H\,\max}/S_{h\,\min}$, pore pressure, tensile strength, and thermal stress, and sensitivity to these parameters is evaluated. An offset-data case study then tests regional applicability by predicting $S_{h\,\min}$ at a target well from nearby initiation data and comparing the prediction to closure-derived reference values.

Overall, the chapter establishes the full chain from raw measurements to stress constraints, clearly separating measurement-based estimates from assumption-dependent bounds and providing a consistent basis for the results and discussion chapters.

4

Results

This chapter presents the interpreted hydraulic stress test results and the derived stress constraints. The structure follows the research questions. Closure-derived $S_{h\,\min}$ values obtained using the semilog max method are treated as the primary stress estimates. Initiation-based constraints (FIT/LOT) are presented separately and subsequently evaluated relative to the closure-derived values.

4.1. Test diagnostics

4.1.1. Leak-off pressure and $S_{h\,\min}$

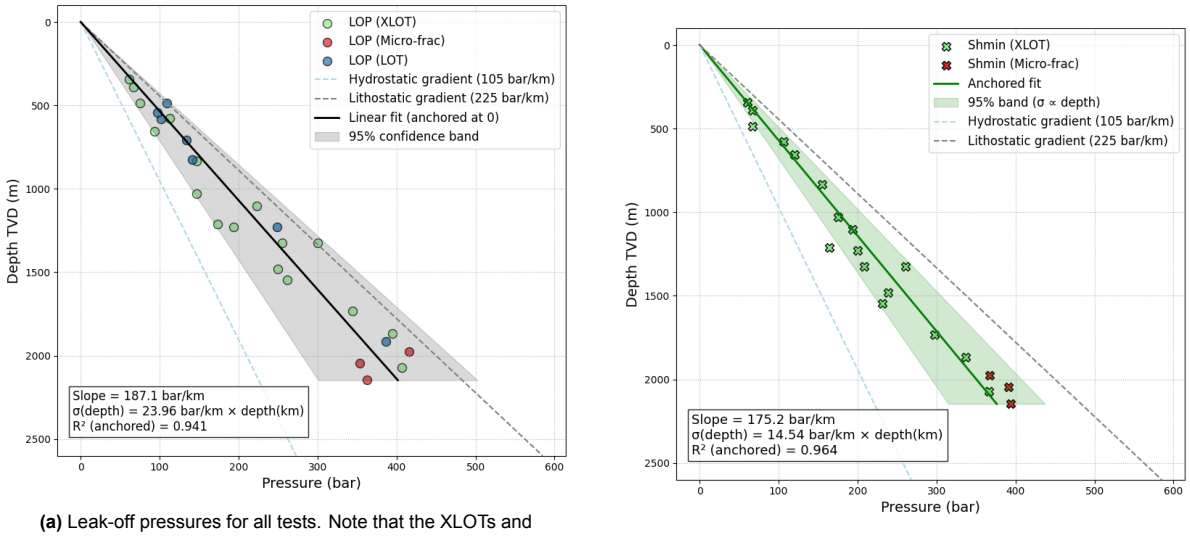

(a) Leak-off pressures for all tests. Note that the XLOTs and Micro-frac were performed in perforations, and the LOTs in open-hole.

(b) $S_{h\,\min}$ (FCP) for all tests.

Figure 4.1: Overview of leak-off pressures (left) and $S_{h\,\min}$ (right) for all analyzed tests. Note that the Middenmeer data has been removed, as these $S_{h\,\min}$ values were significantly lower than the rest, due to cooling.

Figure 4.1a shows leak-off pressure as a function of depth. A clear linear increase with depth is observed, consistent with first-order control by the regional stress gradient. No systematic separation between LOT and XLOT LOP values is evident: both datasets overlap and exhibit comparable scatter around the regression trend. Within this dataset, the operational difference between LOT and XLOT does not translate into a consistent difference in LOP magnitude, although the LOT leak-off pressures seem to be higher on average.

The overall correlation is strong (R^2 = 0.941), indicating that LOP is largely depth-controlled. One can furthermore see that the scatter in LOP is higher than the scatter in $S_{h\,\min}$ in Figure 4.1b, because the R^2 is higher for the latter.

Figure 4.1b compares depth trends of closure-derived $S_{h\,\min}$ (XLOT + micro-frac). Closure-derived $S_{h\,\min}$ shows strong internal consistency (R^2 = 0.967).

4.1.2. Fracture reopening and tensile strength

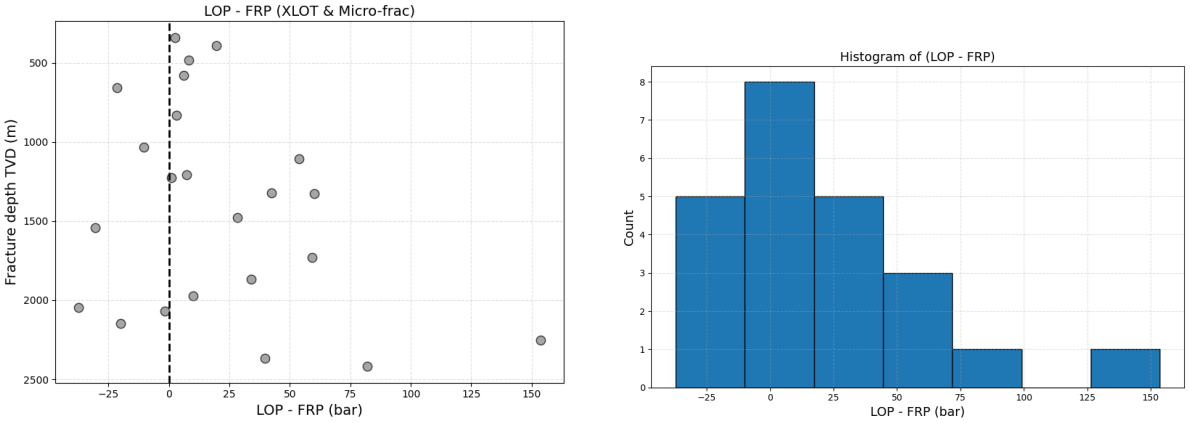

(a) The difference in leak-off pressure and fracture reopening pressure versus depth.

(b) Distribution of the difference in leak-off and fracture reopening pressures.

Figure 4.2: Comparison of leak-off pressure (LOP) and fracture reopening pressure (FRP) for all analyzed tests.

Figure 4.2a compares LOP and fracture reopening pressure (FRP). Under idealized intact-wellbore conditions, the difference between initiation and reopening pressures can be related to tensile strength T_0 and near-wellbore stress concentration, implying LOP $>$ FRP by a physically meaningful margin (see Equation 3.4).

The dataset shows significant variability. While some tests exhibit LOP $>$ FRP, many show small differences and several yield LOP $<$ FRP. The histogram in Figure 4.2b confirms that (LOP $-$ FRP) spans both positive and negative values (26% of the values are negative), implying negative apparent tensile strengths in a subset of cases.

4.2. Closure pressure

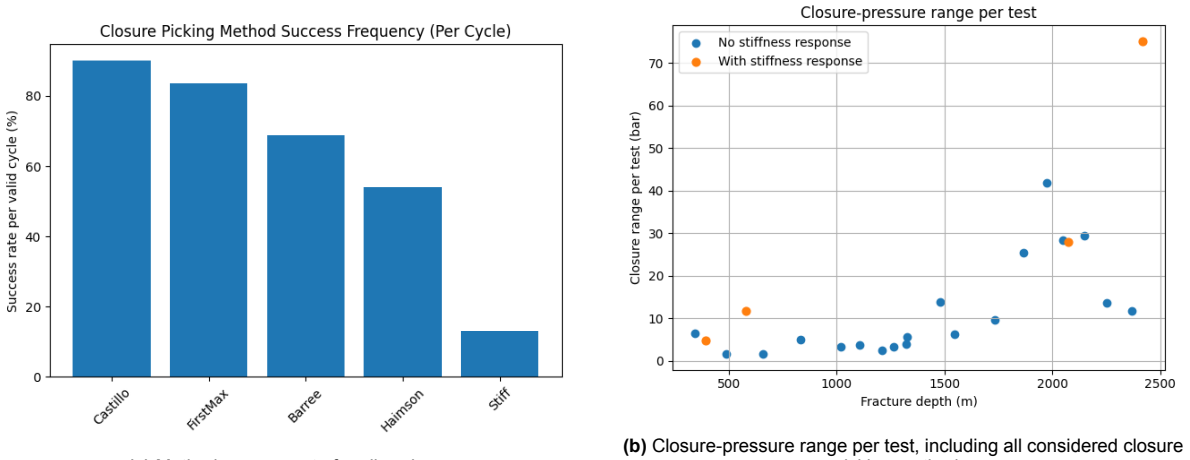

(a) Method success rate for all cycles.

(b) Closure-pressure range per test, including all considered closure picking methods.

Figure 4.3: Operational robustness and associated uncertainty of closure-picking methods.

Figure 4.3a summarises how often each closure-picking method yields a usable closure estimate per cycle. Differences in success rate reflect both method requirements (e.g., derivative stability, identifiable stiffness evolution) and data quality, as well as quality of the algorithm.

Figure 4.3b shows the inter-method spread in closure pressure per test. Up to approximately 1500 m

depth, the closure-pick range is generally limited. At greater depths, the spread increases significantly, indicating higher method sensitivity and/or reduced diagnostic clarity in the fall-off data. Stiffness-based interpretations tend to return lower closure pressures than derivative-based methods when applicable, and therefore often enlarge the overall closure-pressure range.

4.2.1. Example of a fall-off curve

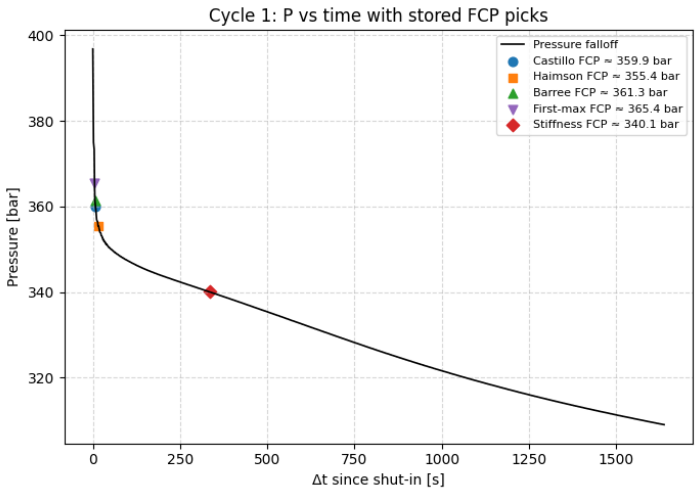

Figure 4.4: Closure picks of multiple methods shown on the pressure fall-off curve for a representative cycle.

Figure 4.4 shows closure picks from different methods on the pressure fall-off curve for Cycle 1. All methods identify closure after shut-in, but a spread between interpreted closure pressures is evident.

Castillo, Haimson and the Barree method cluster within a narrow pressure interval of approximately 355–361 bar, indicating relatively strong internal consistency under this closure definition. The First-Maximum method yields a slightly higher value (approximately 365 bar).

The stiffness-based interpretation yields a substantially lower closure pressure (approximately 340 bar) at a later shut-in time. The resulting inter-method spread of roughly 20–25 bar illustrates that closure pressure is method-dependent and that different diagnostics can reflect different physical aspects of fracture shut-in.

4.2.2. Comparison with EBN/BakerHughes

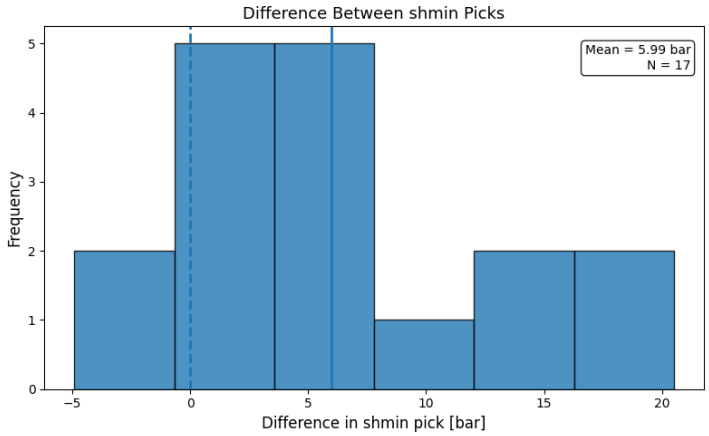

Figure 4.5: Distribution of the difference between the semilog max FCP picks and the FCP values reported by EBN/BakerHughes. Positive values indicate higher picks obtained in this study.

Figure 4.5 shows the difference between closure pressures obtained with the semilog-max method and

closure pressures reported by EBN/BakerHughes. The distribution is shifted toward positive values, indicating that the semilog-max interpretation yields higher closure pressures on average (5.99 bar, or 1.77%, higher). This systematic offset implies that closure picking is method-sensitive and that inter-interpreter variability can introduce a measurable shift in derived $S_{h\,\min}$.

4.2.3. Comparison between closure methods

Different closure diagnostics do not necessarily identify the same stage of the fracture closure process. As discussed in chapter 2, each interpretation method uses a different proxy in the pressure decline behaviour to infer the onset of fracture closure. Consequently, systematic differences between closure pressure estimates obtained using different diagnostics can be expected.

To quantify these differences, closure pressures obtained using the Castillo, Haimson, Barree, and Semilog Max (FirstMax) methods were compared for all cycles in which a valid pick was available for each method. After filtering incomplete rows, 17 cycles remained available for comparison, corresponding to approximately 24% of the dataset. The relatively small fraction reflects the fact that not all interpretation methods produced a valid closure pick in every cycle.

Figure 4.6 shows the mean signed pairwise difference between closure pressures obtained using the different diagnostics. Each value in the matrix represents the average difference between two methods across all considered cycles, with positive values indicating that the method on the vertical axis yields higher closure pressures than the method on the horizontal axis.

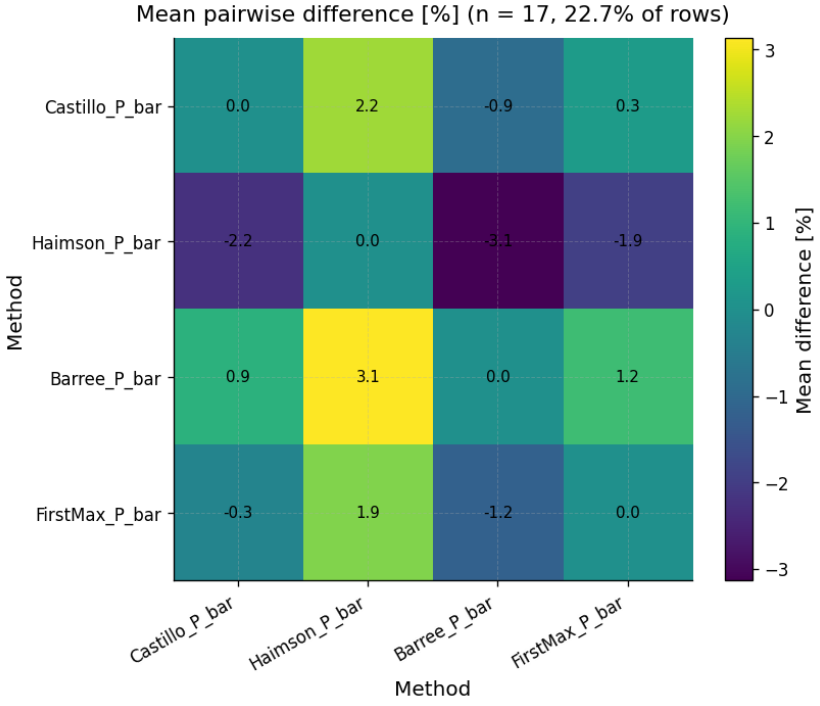

Figure 4.6: Mean signed pairwise difference between closure pressure estimates obtained using different interpretation methods. Values represent the average difference between methods across cycles where all methods produced a valid pick ($n = 17$ cycles, corresponding to 23.9% of the dataset). Positive values indicate that the method on the vertical axis yields higher closure pressures than the method on the horizontal axis.

Several systematic trends can be observed. The Barree method generally produces higher closure pressure estimates than the other diagnostics, exceeding the Haimson picks by approximately 10 bar on average. In contrast, the Haimson method tends to yield the lowest closure pressures among the considered diagnostics. The Semilog Max method produces intermediate values, typically several bar higher than Haimson but lower than Barree. The Castillo method also lies between these two extremes, although its relative position varies depending on the specific comparison.

These differences are consistent with the conceptual basis of the respective diagnostics. Methods such

as Haimson's approach tend to identify closure earlier in the pressure decline, whereas stiffness-based or derivative-based approaches may identify closure later in the progressive fracture closure process. As a result, different diagnostics may correspond to different physical stages of fracture closure rather than representing identical definitions of the same event.

Although the observed offsets are systematic, the limited number of cycles available for direct comparison should be considered when interpreting these results. The purpose of this analysis is therefore not to establish a definitive ranking between methods, but rather to illustrate the magnitude of interpretation variability that can arise when different closure diagnostics are applied to the same dataset.

These findings highlight that the choice of interpretation method can introduce differences in inferred closure pressure on the order of several bar to more than 10 bar. Such differences are comparable to, or larger than, the repeatability variability observed between repeated injection cycles. Consequently, methodological consistency is important when comparing stress estimates derived from different hydraulic stress tests or when combining results interpreted using different closure diagnostics.

4.3. Results per well

4.3.1. Well locations

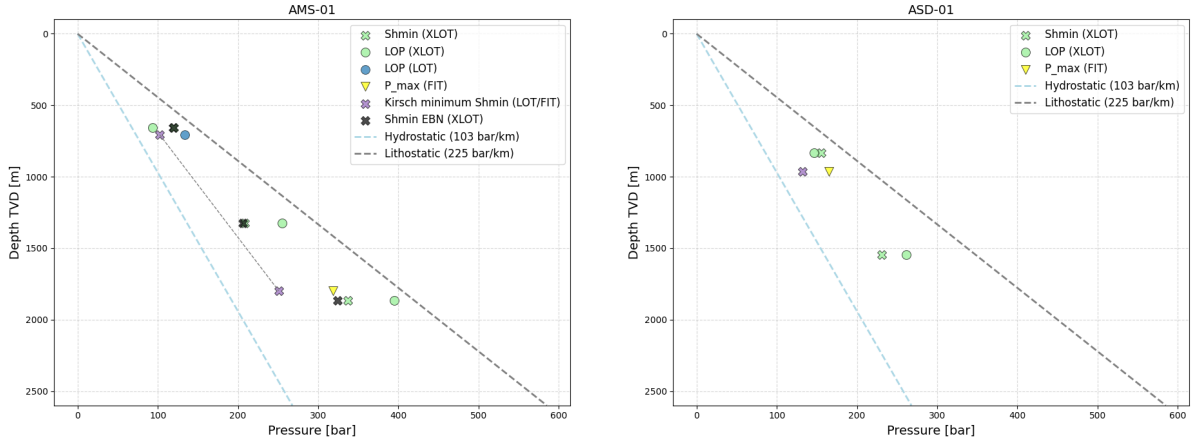

(a) AMS-01 test results.

(b) ASD-01 test results.

Figure 4.7

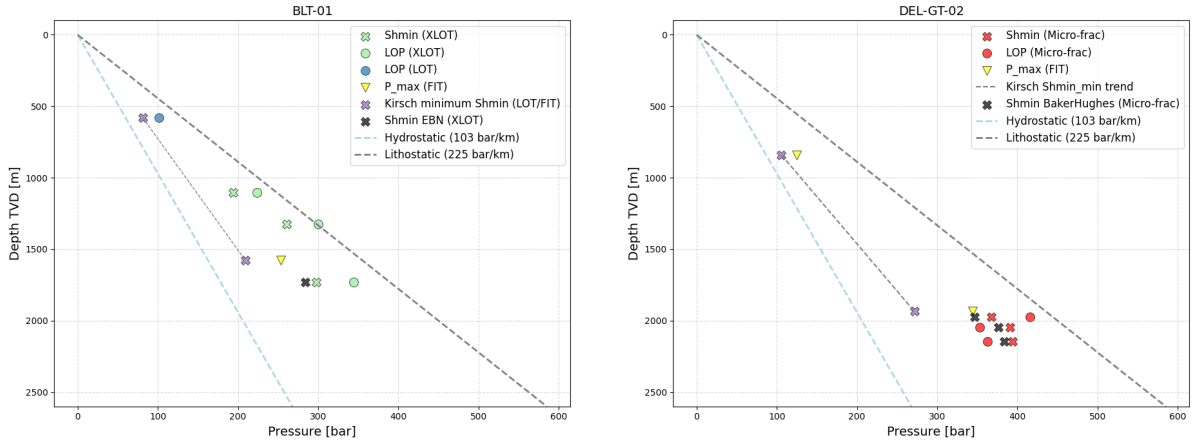

(a) BLT-01 test results.

(b) DEL-GT-02 test results.

Figure 4.8

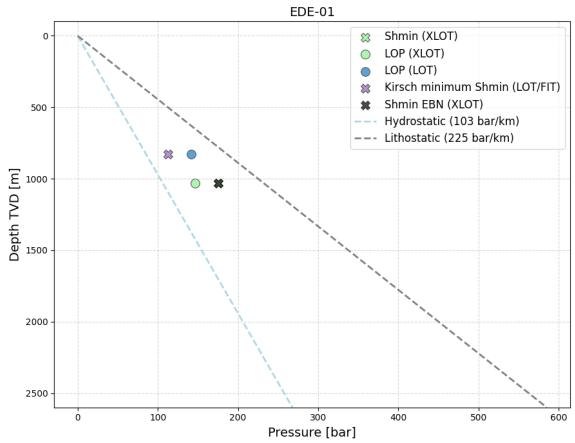

(a) EDE-01 test results (same own $S_{h\,\min}$ estimate as EBN).

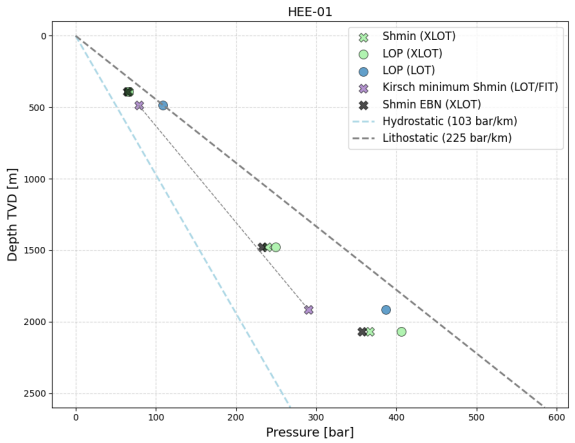

(b) HEE-01 test results.

Figure 4.9

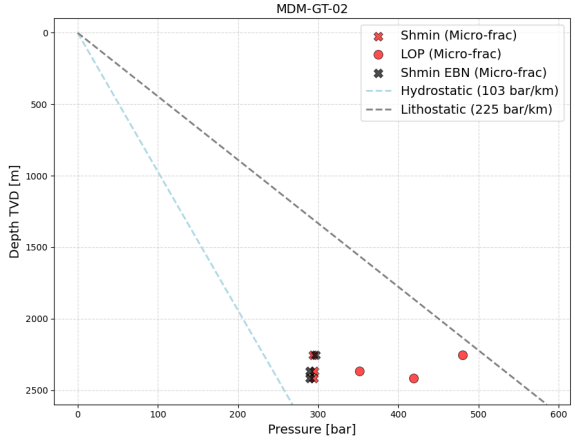

(a) MDM-GT-02 test results.

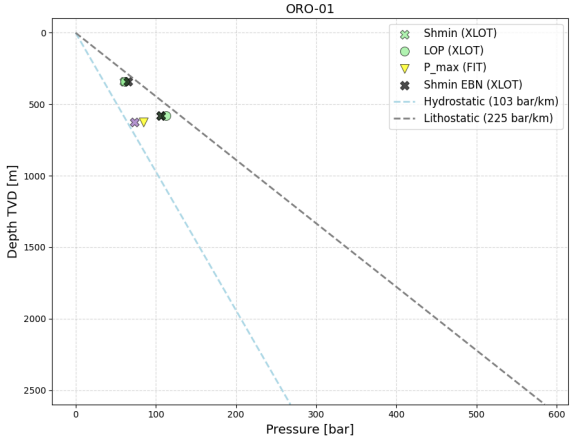

(b) ORO-01 test results. Deepest $S_{h\,\min}$ estimate same as EBN.

Figure 4.10

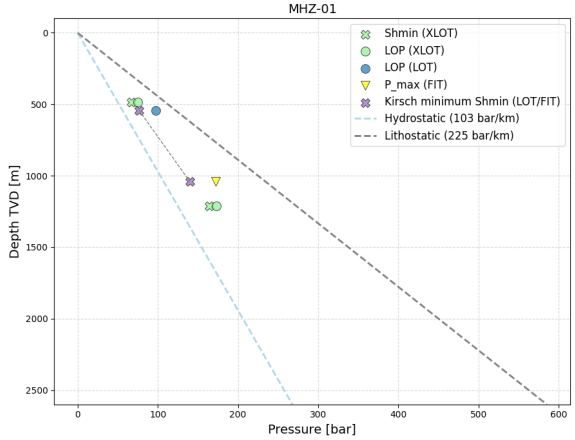

(a) MHZ-01 test results.

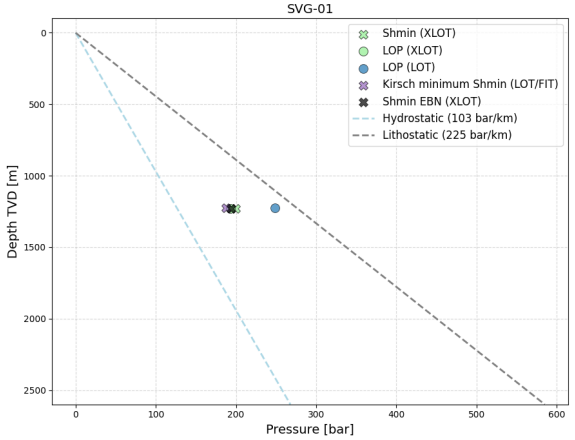

(b) SVG-01 test results.

Figure 4.11

Figure 4.7 shows the Amstelland (AMS-01) and Amsterdam (ASD-01) results. For AMS-01, most measurements fall within the interpreted envelope, while one shallow XLOT LOP at approximately

650 m deviates from the overall trend.

For ASD-01, closure-derived $S_{h\,\min}$ values remain above the Kirsch-based minimum bound. Two XLOT-derived $S_{h\,\min}$ estimates indicate a change in gradient with depth.

Figure 4.8 shows that BLT-01 includes an intermediate $S_{h\,\min}$ value elevated relative to neighbouring depth trends, while all measurements remain above the Kirsch-based lower bound. For DEL-GT-02, closure-derived values and initiation-based bounds follow a consistent ordering.

Figure 4.9 shows closure-derived $S_{h\,\min}$ values that generally fall within the initiation-based bounds. In EDE-01, one XLOT-derived LOP is lower than the corresponding closure-derived $S_{h\,\min}$. HEE-01 displays a consistent distribution of measurements without clear outliers.

Figure 4.10 shows relatively low $S_{h\,\min}$ values in MDM-GT-02 compared to the other wells. In ORO-01, closure-derived values align with the overall trend defined by the regional envelope.

Figure 4.11 shows that the Kirsch-based minimum trend lies close to the closure-derived $S_{h\,\min}$ gradient for MHZ-01. In SVG-01, a LOT and XLOT occur at similar depth, and the closure-derived $S_{h\,\min}$ lies between the Kirsch-based minimum and the LOP-derived upper bound.

4.3.2. Summary statistic

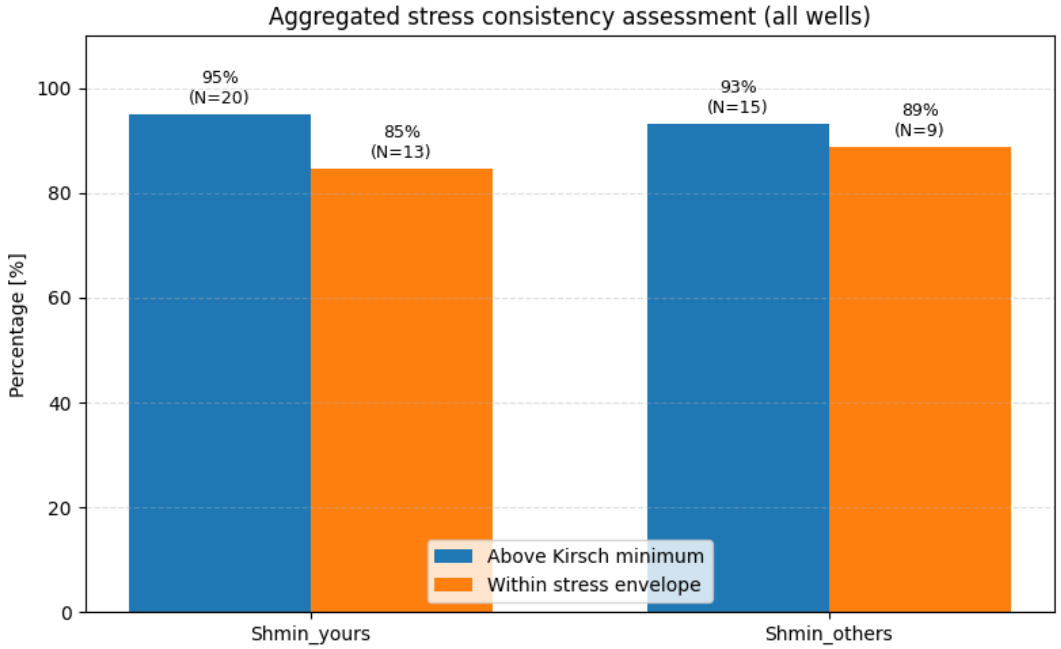

Figure 4.12: Summary of initiation-based bounds and closure-derived $S_{h\,\min}$ values across the dataset.

Figure 4.12 summarises the dataset-wide relationship between initiation-based bounds and closure-derived $S_{h\,\min}$. Across most wells, closure-derived values fall within the envelope defined by the Kirsch-based minimum bound and the LOT-derived upper trend. 95% of the closure picks from this study are located above the lower boundary, and 93% of the closure picks by other interpreters are above the lower boundary. Respectively 85% and 89% of the closure picks are located between the lower boundary and leak-off pressure values (if these are present).

4.4. Case study: Constraining $S_{h\,\min}$ using offset data

4.4.1. Regional structural context

Figure 4.13 presents the regional $S_{h\,\min}$ gradient map, as well as the locations of the offset wells around the DEL-GT-02 well location, including depth to top Delft sandstone and the spatial distribution of stress-related gradients. The map indicates that DEL-GT-02 is located in the central Delft Graben, in an area

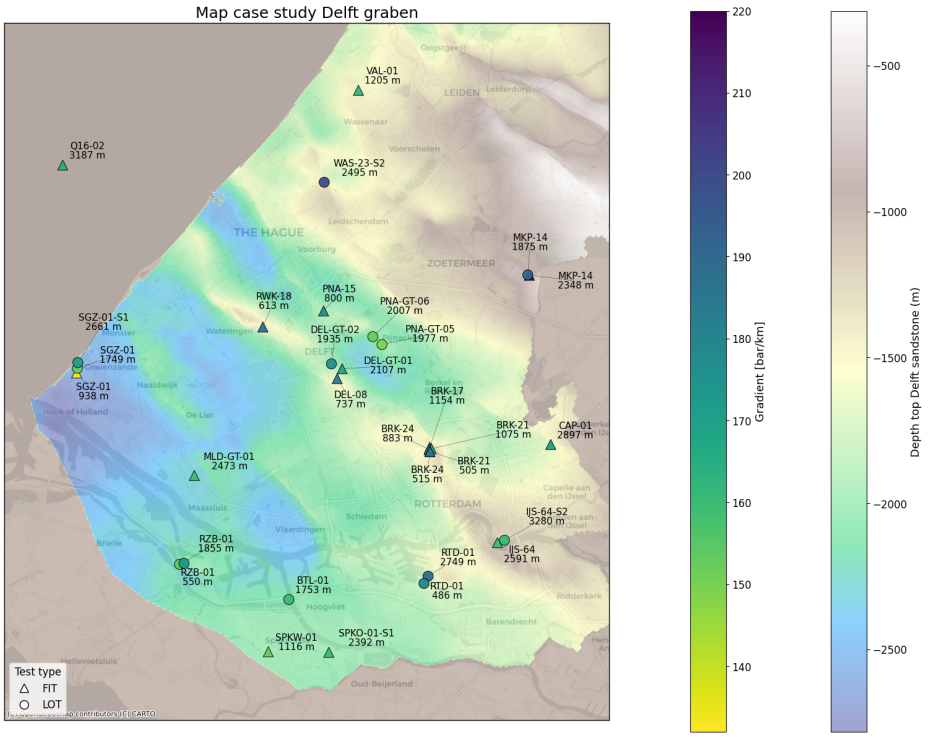

Figure 4.13: Spatial distribution of gradient and depth to top Delft sandstone in the Delft Graben. Circles denote LOTs, triangles FITs.

characterised by intermediate depth and gradients relative to surrounding structural highs and deeper graben segments.

4.4.2. Offset LOT and FIT trends

Measured LOT (LOP) and FIT ($P_{\max}$) data from the offset wells are shown in Figure 4.14. Both datasets increase approximately linearly with depth, consistent with increasing vertical stress and depth-dependent stress concentration requirements for initiation. Datapoints located in the Delt Graben are highlighted in green. It can be found that the maximum pressures of the FIT data, and the leak-off pressure of the LOT data generally have a lower gradient than that of the $S_{h\,\min}$, which would mean that you can't predict the $S_{h\,\min}$ based on offset LOT and FIT data, as the $S_{h\,\min}$ should fall in between the lower bound $S_{h\,\min}$ and leak-off pressures.

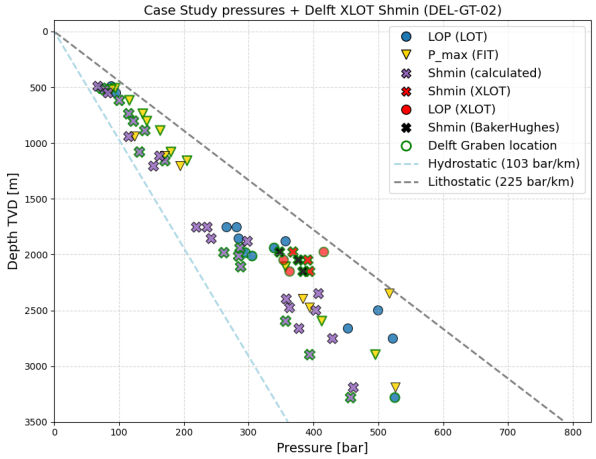

Figure 4.14: Regional pressure–depth envelope derived from offset LOT/FIT data compared with measured XLOT-derived $S_{h\,\min}$ in DEL-GT-02.

4.4.3. Correction for deviation

After correcting for deviation, the leak-off pressure are changed to the values these wells would have if the well was vertical. This makes it easier to compare the leak-off values with the closure pressures of DEL-GT-02 (for closure pressure, no correction has to be made for deviation). One can observe in Figure 4.15 that the leak-off pressure gradients are actually lower than that of the $S_{h\,\min}$. If one were to apply a constrain, the $S_{h\,\min}$ would fall further out of the bound within Figure 4.15 than in Figure 4.14.

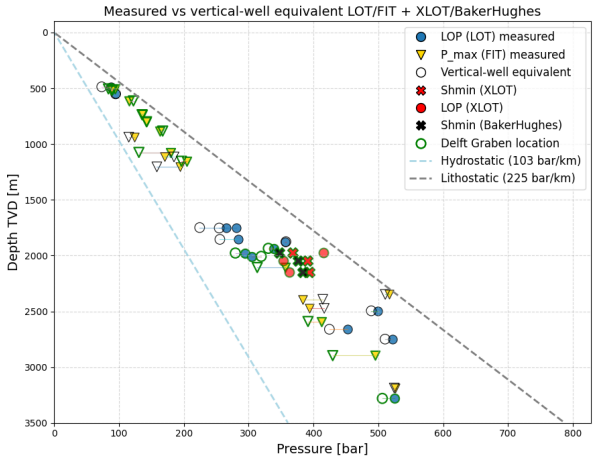

Figure 4.15: Measured LOT and FIT data from offset wells as a function of depth, corrected for deviation.

4.5. Summary

This chapter presented the interpreted hydraulic stress test results and the derived stress constraints across the analysed wells. Closure-derived $S_{h\,\min}$ values obtained using the semilog max method show strong internal consistency and a clear depth-dependent trend. Leak-off pressures also increase approximately linearly with depth, although they exhibit larger scatter compared to closure-derived stresses.

The comparison between leak-off pressure (LOP) and fracture reopening pressure (FRP) reveals substantial variability. Differences between LOP and FRP span both positive and negative values, indicating that the classical tensile-strength relation is not consistently observed in the dataset.

Closure-pressure interpretation shows method sensitivity. While most methods identify closure within a relatively narrow pressure interval for individual cycles, systematic differences occur between derivative-based and stiffness-based interpretations. The semilog-max method generally yields slightly higher closure pressures compared to values reported by external interpreters.

Across the analysed wells, closure-derived $S_{h\,\min}$ values are generally located within the envelope defined by the Kirsch-based lower bound and initiation-based upper bounds derived from leak-off pressures. The majority of closure picks fall within this mechanically consistent range.

The offset-well case study around DEL-GT-02 shows that regional LOT and FIT data follow a clear depth trend but exhibit gradients that are lower than the measured $S_{h\,\min}$ gradient. After correcting for well deviation, the initiation-based gradients remain lower, indicating that offset LOT and FIT data alone do not reliably constrain $S_{h\,\min}$ at the study location using methodology presented in this study.

5

Discussion

This chapter interprets the results presented in the previous chapter within a broader mechanical and methodological context. It reflects on how the research focus developed during the study, discusses the main findings in relation to the literature, and evaluates the reliability and limitations of the applied interpretation workflow. Particular attention is given to the method dependence of fracture closure pressure, the limited interpretability of initiation-based pressures from FIT and LOT tests, and the implications for estimating the minimum horizontal stress $S_{h\,\min}$. The chapter concludes by discussing uncertainty, repeatability, applicability of offset data, and the implications of the results for future hydraulic stress test interpretation.

5.1. Reflection on the research process

The initial objective of this research was to investigate whether formation integrity tests and leak-off tests from offset wells could be used to estimate the minimum horizontal stress $S_{h\,\min}$. During the early stages of the study it became clear that extended leak-off tests and micro-fracture tests provide a more direct estimate of $S_{h\,\min}$ because fracture closure can be identified during the pressure fall-off phase. These tests therefore provided a reference against which initiation-based pressures from FIT and LOT tests could be evaluated. As a result, the scope of the study expanded to include the interpretation of closure pressures from XLOT and micro-fracture data.

While analysing the closure behaviour of these tests, it became apparent that fracture closure pressure cannot be determined uniquely from the pressure fall-off curve. Instead, closure must be inferred from diagnostic features such as changes in derivative behaviour or stiffness evolution. Different interpretation methods therefore identify different proxies for the closure process, leading to systematic differences between closure estimates. Because the determination of $S_{h\,\min}$ was central to the objectives of this study, additional effort was devoted to evaluating multiple closure picking methods and comparing their results. Among the tested approaches, the semilogarithmic maximum derivative method proved to be the most operationally robust within the analysed dataset. This robustness arises from the relatively clear diagnostic feature used by the method, namely the maximum in the semilog derivative during early fall-off. However, this does not imply that the semilog-max method represents a uniquely correct definition of fracture closure, but rather that it provides a consistent operational estimator within the available data.

Once closure-derived estimates of $S_{h\,\min}$ had been obtained, the relationship between these stresses and the characteristic pressures measured during FIT and LOT tests was investigated. To compare these pressures meaningfully, it was necessary to examine how leak-off pressure and fracture initiation relate to the in-situ stress state. Analytical models such as the Kirsch wellbore stress solution and concepts from linear elastic fracture mechanics provide theoretical frameworks for this relationship. The Kirsch solution describes the stress concentration around a cylindrical wellbore and provides a first-order estimate of fracture initiation pressure under idealized conditions. In practice, fracture initiation is often influenced by imperfections, microfractures, and perforation geometry, which are better described

by fracture mechanics concepts. However, the geometry and size of such imperfections are typically unknown in field applications. For this reason, the Kirsch-based initiation criterion was used in this study to construct conservative stress bounds, while recognizing that the underlying assumptions introduce uncertainty.

Additional processes, such as permeability-controlled leak-off and poroelastic stress changes during injection, may also influence fracture initiation behaviour. These effects were not explicitly modelled in this study. Because most analysed tests were conducted in relatively low-permeability formations, the interpretation focused on the elastic initiation framework as a first-order approximation.

Finally, a case study was conducted to evaluate whether $S_{h\,\min}$ derived from micro-fracture tests could be predicted using offset FIT and LOT data. The DEL-GT-02 well was selected for this analysis because a micro-fracture test had been performed at this location, providing a closure-derived estimate of $S_{h\,\min}$ that could be compared with offset test data. This case study served as a practical test of the initial research hypothesis and provided insight into the limitations of using initiation-based pressures for stress prediction.

5.2. Overview of findings

This study analysed hydraulic stress test data from multiple wells to evaluate how reliably the minimum horizontal stress $S_{h\,\min}$ can be inferred from field measurements and how initiation-based tests (FIT/LOT) compare with closure-based tests (XLOT/micro-frac). The results show that the closure pressure depends on which method one uses, whereas initiation-based pressures primarily act as constraints rather than direct stress measurements.

Across the analysed wells, closure pressures derived from XLOT and micro-fracture tests show a coherent depth-dependent trend and generally fall within the mechanically expected envelope defined by a Kirsch-based lower bound and initiation-based upper bounds derived from leak-off pressures. This indicates internal consistency between the interpreted closure pressures and the adopted mechanical framework.

Initiation-based pressures from FIT and LOT tests exhibit different behaviour. Leak-off pressures generally increase with depth and typically exceed closure-derived $S_{h\,\min}$, reflecting fracture initiation rather than far-field stress equilibrium. In the XLOT and micro-fracture dataset, the difference between LOP and fracture reopening pressure (FRP), sometimes interpreted as an apparent tensile strength, frequently yielded non-physical results: approximately 26% of the values were negative. This suggests that LOP–FRP differences cannot be reliably interpreted as intact-rock tensile strength, likely due to near-wellbore damage, perforation effects, and other non-ideal test conditions. Maximum FIT pressures also cannot be interpreted directly as lower bounds on $S_{h\,\min}$ because near-wellbore stress concentrations and tensile-strength effects can elevate the initiation pressure. When interpreted through a fracture initiation model, however, FIT measurements can still provide conservative lower-bound constraints under explicit assumptions.

A key observation is that the inferred fracture closure pressure—and therefore $S_{h\,\min}$—depends on the closure interpretation method. Closure cannot be observed directly and must instead be inferred from diagnostic signatures such as derivative behaviour, tangent intersections, or stiffness evolution. As a result, different diagnostics identify slightly different stages of the fracture shut-in process. In individual cycles, the spread between closure interpretations can reach approximately 20–25 bar, illustrating that method selection introduces systematic interpretation variability.

Despite this variability, the semilog max method yielded the most internally consistent results across wells and cycles and was therefore adopted as the primary estimator of $S_{h\,\min}$. Compared with closure pressures reported by external interpreters, the semilog-max picks are on average about 5.99 bar (1.77%) higher, demonstrating that closure interpretation can introduce measurable systematic offsets.

Initiation-based pressures from FIT and LOT tests exhibit different behaviour. Leak-off pressures generally increase with depth and typically exceed closure-derived $S_{h\,\min}$, reflecting fracture initiation rather than far-field stress equilibrium. Maximum FIT pressures cannot be interpreted directly as lower bounds on $S_{h\,\min}$ because near-wellbore stress concentrations and tensile strength effects can elevate the initiation pressure. In addition, the commonly used Kirsch-based initiation criterion assumes a vertical

wellbore. When wells are deviated, the stress concentration around the borehole depends on the orientation of the well relative to the principal stress directions, which modifies the pressure required for fracture initiation. As a result, initiation pressures measured in deviated wells do not directly constrain the magnitude of the fracture closure pressure or $S_{h\,\mathrm{min}}$. When interpreted through a fracture initiation model under explicit geometric and mechanical assumptions, however, FIT measurements can still provide conservative lower-bound constraints. The fracture closure pressure is not influenced by deviation of a wellbore.

Finally, the offset-data case study using initiation-based pressures unsuccessfully predicted the $S_{h\,\mathrm{min}}$ at a target well. The resulting gradients from the LOT and FIT tests remained lower than the closure-derived stress gradient at the study location. This indicates that initiation pressures are strongly influenced by other properties, like local formation properties, interpretation and/or test configuration, limiting their predictive capability.

Overall, the results support a hierarchical interpretation framework in which closure-derived pressures from XLOT and micro-fracture tests provide the most reliable estimates of $S_{h\,\mathrm{min}}$, while FIT and LOT measurements should be interpreted as bounds rather than direct stress measurements.

5.3. Positioning within the literature

Determining the magnitude of the least principal stress $S_{h\,\mathrm{min}}$ is a central objective of hydraulic stress testing because it controls fracture gradients, drilling windows, and the mechanical stability of the subsurface during fluid injection or production (Fjær et al., 2008; Zoback, 2010). Reliable estimates of $S_{h\,\mathrm{min}}$ are therefore essential not only for drilling operations but also for assessing risks associated with induced seismicity in geo-energy systems such as geothermal production or CO_2 storage (Ge et al., 2022; Verdon, 2021). In practice, stress magnitudes are inferred from borehole observations and hydraulic tests, each providing partial constraints on the in-situ stress state (Han & van der Baan, 2024; Zoback et al., 2003).

The literature relevant to hydraulic stress testing spans several topics, including fracture initiation mechanics, closure pressure diagnostics, hydraulic fracture simulation, and regional stress analysis.

5.3.1. Analytical fracture initiation models

Analytical models for fracture initiation provide a theoretical framework for relating the pressure applied in a wellbore to the onset of rock failure. These models aim to predict the breakdown pressure p_f required to initiate a hydraulic fracture as a function of the far-field stress state, pore pressure, and rock mechanical properties. Because fracture initiation occurs in the highly stressed region surrounding the wellbore, most analytical approaches build upon the elastic stress solution for a cylindrical cavity in an infinite medium originally derived by Kirsch (1898). By combining the Kirsch stress distribution with different rock failure criteria, several classes of fracture initiation models have been proposed.

Historically, the earliest analytical approaches assumed that fracture initiation occurs when the circumferential effective stress at the wellbore wall reaches the tensile strength of the rock. This concept forms the basis of the classical Hubbert–Willis breakdown pressure relation (Hubbert & Willis, 1957). In this model the rock is assumed to be intact and impermeable, such that pore pressure does not diffuse into the formation during pressurization. Later extensions relaxed this assumption by incorporating poroelastic effects and formation permeability. For example, the Haimson–Fairhurst formulation accounts for fluid penetration into the rock matrix and modifies the effective stress distribution accordingly (Haimson & Fairhurst, 1967; Schmitt & Zoback, 1989). These tensile-strength–based models remain widely used because of their simplicity and their direct connection to measurable parameters such as tensile strength and far-field stresses.

Recognizing that fracture initiation may not occur exactly at the wellbore wall, subsequent work introduced the so-called point stress criterion. In this approach, fracture initiation is assumed to occur at a finite distance from the wellbore wall where the circumferential stress first reaches the tensile strength of the rock. The distance from the wall is related to the fracture toughness and tensile strength, thereby introducing a link between classical stress-based criteria and fracture mechanics concepts (Ito, 2008; Ito & Hayashi, 1991). This modification partially accounts for the presence of microcracks and stress concentrations near the borehole.

Alternative analytical approaches assume that failure is controlled by shear rather than tensile stresses. In such models, fracture initiation occurs when the effective stress state satisfies the Mohr–Coulomb failure criterion. These shear-based models are particularly relevant in highly permeable formations where pore pressure diffusion significantly alters the effective stresses around the wellbore (Morgenstern, 1962).

More advanced formulations treat fracture initiation explicitly within the framework of linear elastic fracture mechanics (LEFM), which was already introduced in chapter 2. In these models, small pre-existing flaws or microcracks near the wellbore act as fracture nucleation sites. Fracture propagation begins when the Mode I stress intensity factor K_I reaches the fracture toughness K_{IC} of the rock. This approach provides a more physically rigorous description of crack initiation and propagation, particularly in heterogeneous rock where imperfections control fracture nucleation (Abou-Sayed et al., 1978; Hardy, 1973; Van Eekelen, 1982). Closely related are energy-based approaches derived from Griffith's fracture criterion, which states that fracture growth occurs when the released strain energy exceeds the surface energy required to create new fracture surfaces (Griffith, 1921).

Although these analytical models differ in their assumptions and complexity, they all attempt to relate fracture initiation pressure to the underlying stress state and rock properties. In practice, the applicability of each model depends on formation characteristics such as permeability, heterogeneity, and the presence of natural fractures. An overview of the main analytical fracture initiation models, their governing criteria, assumptions, and references is provided in Table 5.1. In future research, all these initiation models should be integrated into the frameworks which extract the far-field stresses from leak-off pressures and fall-off curves.

Table 5.1: Overview of breakdown pressure models, their governing criteria, assumptions, and crack criteria, from Wu et al. (2020).

Breakdown pressure model		Criteria formula	Rock property hypothesis	Crack criterion	References
Tensile strength-based models	H–W model	$p_f = 3\sigma_h - \sigma_H - \alpha p + \sigma_t$	intact and impermeable	When the circumferential effective stress on the wellbore wall reaches the rock tensile strength.	Hubbert and Willis (1957); Bredehoeft et al. (1976)
	H–F model	$p_f = \frac{3\sigma_h - \sigma_H - 2\eta p + \sigma_t}{2(1-2\eta)}$	intact and permeable	Same tensile failure criterion applied to permeable formations.	Haimson and Fairhurst (1967); Schmitt and Zoback (1989)
	Point stress model	$\sigma_\theta(r_w + d_c,\ \theta = 0^\circ,\ p_w = p_f) = \sigma_t$ $d_c = \frac{1}{\pi}\left(\frac{K_{IC}}{\sigma_t}\right)^2$		When the circumferential effective stress at a point located a constant distance from the wellbore wall reaches the rock tensile strength.	Ito and Hayashi (1991); Ito (2008)
Shear failure-based models		$\tau = c + \sigma_n \tan\phi$ $\sigma_n = S_n - (1-\alpha_a)p$	intact, highly permeable	When the effective stress circle first touches the failure envelope (Mohr–Coulomb) at the wellbore wall.	Morgenstern (1962)
Fracture mechanic-based models		$K_I(r_w + a,\ \sigma_\theta,\ p_a,\ p_f) = K_{IC}$	Intact except for an initial symmetrical double microcrack extending from the borehole.	When the stress intensity factor for Mode I fracture propagation reaches the fracture toughness of the rock.	Van Eekelen (1982); Hardy (1973); Abou-Sayed et al. (1978); Zhang et al. (2017)
Energy release rate-based approaches		$\frac{dU_s}{dc} \geq \frac{dU_\gamma}{dc}$		The released strain energy during initial crack propagation must be greater than or equal to the required surface energy.	Griffith (1921)

5.3.2. Closure pressure determination

The determination of fracture closure pressure from fall-off analysis of hydraulic stress tests remains a topic of active discussion in the literature, and no single interpretation method has been universally accepted. Closure pressure cannot be observed directly in the pressure record and must instead be

inferred from diagnostic features in the pressure decline curve. As a result, several interpretation approaches have been proposed, each relying on different assumptions about the hydraulic and mechanical processes controlling fracture closure.

In recent years, several studies have argued that the system stiffness (or fracture compliance) method provides the most reliable estimate of fracture closure pressure (Dutler et al., 2020; McClure et al., 2019; Wang & Sharma, 2019). This method identifies closure from changes in the combined stiffness of the fracture and wellbore system during pressure decline. When the fracture closes, the system compliance decreases, which produces a characteristic change in the pressure derivative behaviour. These studies conclude that stiffness-based approaches provide a physically consistent interpretation of the closure process.

Fracture closure, however, is increasingly understood as a progressive mechanical process rather than a single instantaneous event. As pressure declines after shut-in, opposing fracture surfaces begin to contact at asperities while other portions of the fracture remain open. This progressive contact leads to a gradual increase in fracture stiffness and a nonlinear reduction in fracture aperture during pressure decline (Barton et al., 1985; Sneddon, 1946). Direct deformation measurements obtained during fracture injection experiments confirm this behaviour. Observations using downhole displacement sensors show that fracture aperture decreases asymptotically as pressure declines and that mechanical contact between fracture surfaces may occur while the fracture still retains measurable aperture, as can be seen in Figure 5.1 (Guglielmi et al., 2022). Because different closure diagnostics respond to different signatures of this evolving stiffness behaviour, interpretation methods may identify closure at different stages of the progressive closure process.

However, most of this work focuses on diagnostic fracture injection tests (DFITs) conducted in very low-permeability shale reservoirs. In such settings, pressure fall-off may last for several hours or even days, allowing detailed derivative diagnostics to be applied. The pressure response of these tests therefore differs significantly from that of extended leak-off tests or micro-fracture tests, which are commonly performed in more permeable formations and exhibit much more rapid pressure decline.

Within the DFIT literature, the commonly used Barree tangent method has been criticised for lacking a clear physical definition of fracture closure and for potentially identifying closure at pressures that are too low (Dutler et al., 2020; McClure et al., 2019). Because the method relies on geometric construction rather than a direct physical criterion, the interpreted closure pressure may not correspond to the actual mechanical closure of the fracture.

For hydraulic stress tests with rapid fall-off behaviour, such as XLOT and micro-fracture tests, alternative interpretation approaches are often recommended. In particular, the statistical method introduced by Lee and Haimson (1989), referred to as the Haimson method in this study, has been applied to identify closure pressure from the pressure decline curve.

Overall, the literature suggests that the most appropriate closure picking method depends strongly on the type of hydraulic test, the permeability of the formation, and the duration of the fall-off period. Consequently, interpretation methods developed for DFIT analysis cannot always be applied directly to XLOT or micro-fracture tests, and the choice of closure diagnostic should reflect the hydraulic behaviour of the specific test configuration. This is the reason why several closure methods were applied in this study. Further research is required to determine which interpretation methods are most appropriate under different geological and hydraulic conditions. Fracture closure simulation, as described below, could help address this question.

5.3.3. Hydraulic fracture simulation

A potential extension of this study is the use of hydraulic fracture simulation. Numerical models can provide insight into the physical processes governing hydraulic stress tests and the pressure signatures observed during injection and shut-in. By explicitly modelling fracture initiation, propagation, fluid flow within the fracture, and leak-off into the surrounding formation, simulation tools can help interpret the pressure response recorded during hydraulic fracturing tests.

Hydraulic fracture simulators typically couple several physical processes, including elastic rock deformation, fluid flow within the fracture, pore-pressure diffusion in the surrounding formation, and fracture

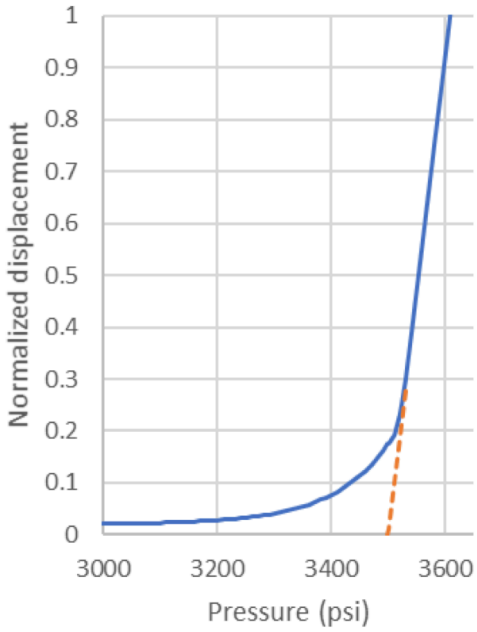

Figure 5.1: Conceptual relationship between fracture aperture (or displacement) and fluid pressure during fracture closure. When the fracture is mechanically open, displacement increases approximately linearly with pressure. As pressure declines, contact between fracture asperities causes a progressive increase in stiffness and a nonlinear reduction in aperture. Extrapolation of the linear "open fracture" behaviour to zero displacement provides an estimate of the minimum horizontal stress $S_{h\,\min}$. From (Guglielmi et al., 2022).

propagation governed by tensile failure or fracture mechanics criteria. In many numerical approaches, fracture growth occurs when the tensile stress at the fracture tip exceeds the tensile strength of the rock, while fluid flow within the fracture is commonly described using lubrication theory and Poiseuille-type flow relations (Bakhshi et al., 2020). The fracture geometry therefore evolves dynamically as pressure is injected into the formation.

A variety of numerical methods have been developed to simulate hydraulic fracture propagation. These include finite element and extended finite element methods (Boone & Ingraffea, 1990), discrete element methods (Cundall & Hart, 1985), and phase-field approaches capable of representing complex fracture growth without explicit crack tracking (Borden et al., 2012). More advanced models also incorporate fully coupled hydro-mechanical formulations that simulate interactions between hydraulic fractures and pre-existing natural fractures (Dahi-Taleghani & Olson, 2011).

Such simulations can reproduce the pressure behaviour observed during hydraulic stress tests. During injection, pressure evolution reflects wellbore pressurisation and fracture initiation, while the shut-in pressure decline is controlled by fluid leak-off and progressive mechanical closure of the fracture. Numerical modelling therefore provides a useful framework for understanding how characteristic pressures such as initiation pressure and fracture closure pressure emerge from the underlying hydraulic and mechanical processes.

Although hydraulic fracture simulation was beyond the scope of this study, such modelling frameworks could ultimately be integrated with the workflow developed here to evaluate the sensitivity of closure interpretations to different hydraulic and mechanical conditions.

5.3.4. Local studies

As illustrated in Figure 5.2, the scope of this thesis does not focus on large-scale data-driven analysis. Instead, the emphasis is placed on understanding the physical mechanisms governing hydraulic stress tests before attempting to analyse large databases such as the Pressure SNS database described by Verweij (2015). A detailed understanding of the processes controlling fracture initiation and closure is essential for interpreting stress measurements reliably, particularly when individual tests may be influenced by operational or geological factors.

Regional compilations of leak-off pressure data in the Dutch subsurface demonstrate substantial variability at comparable depths, indicating that leak-off pressures are affected by local geological conditions and testing procedures. Nevertheless, the lower bound of the observed pressures tends to follow the expected gradient of the minimum horizontal stress, suggesting that leak-off tests can provide useful constraints on $S_{h\,\mathrm{min}}$ when interpreted carefully (Verweij, 2015).

Further regional analyses confirm that leak-off pressures often exceed the true minimum horizontal stress due to near-wellbore stress perturbations and other operational effects. For this reason, the lower bound of LOT measurements is commonly interpreted as representative of the regional $S_{h\,\mathrm{min}}$ gradient. In the Netherlands, this gradient averages approximately $14\,\mathrm{MPa/km}$, although variations occur as a function of lithology, tectonic region, and depth (Bakx et al., 2022).

Studies of the regional stress field further indicate that the present-day maximum horizontal stress in the Netherlands is predominantly oriented NW–SE and that the subsurface is generally characterized by a normal faulting stress regime. However, reliable estimates of stress magnitudes remain limited due to the scarcity of direct measurements and the reliance on interpreted well data (Mechelse, 2017).

While large databases provide valuable regional constraints on stress magnitudes, their interpretation ultimately depends on how individual hydraulic stress tests are analysed. Variability in leak-off and closure pressures may arise not only from geological differences but also from interpretation choices and test conditions. The present study therefore focuses on the consistent interpretation of individual hydraulic stress tests, with the aim of clarifying how methodological choices influence the inferred value of $S_{h\,\mathrm{min}}$. By establishing a transparent interpretation workflow, the results of this study can contribute to improving the reliability of stress estimates used in larger regional datasets.

5.3.5. Contribution of this thesis

The primary contribution of this thesis lies in the systematic interpretation of hydraulic stress test data within a consistent methodological framework. While previous studies have focused on regional compilations of stress measurements or large-scale databases, this study concentrates on the interpretation of individual hydraulic tests and the uncertainties associated with deriving $S_{h\,\mathrm{min}}$ from such measurements.

First, multiple closure interpretation methods are applied to the same dataset in order to assess their consistency and repeatability. By comparing the resulting closure pressures, the study evaluates the sensitivity of $S_{h\,\mathrm{min}}$ estimates to the interpretation method used. This provides insight into the degree to which methodological choices influence the inferred stress magnitude.

Second, the study explicitly distinguishes between closure-derived stress estimates and initiation-based pressure measurements such as formation integrity tests and leak-off tests. Instead of treating these measurements interchangeably, they are interpreted within a mechanical framework that clarifies how each test constrains the stress state. Closure pressures are treated as primary estimates of $S_{h\,\mathrm{min}}$, while initiation pressures are interpreted as bounds on the stress magnitude.

Third, the study investigates the applicability of offset data by comparing measurements from different wells and test configurations. This analysis addresses a practical question frequently encountered during well planning: whether stress estimates derived from nearby wells can be used as reliable constraints at a new location.

Taken together, these elements provide a transparent interpretation workflow that connects the physical processes governing hydraulic stress tests with practical stress estimation. In this way, the thesis occupies an intermediate position between detailed mechanistic modelling and large-scale data-driven analyses, aiming to improve the robustness and reproducibility of stress interpretations derived from hydraulic fracturing tests.

5.4. Interpretation of fracture closure diagnostics

The theoretical background of fracture closure diagnostics and their physical interpretation was discussed in section 5.3. The present section focuses on how these diagnostics behave when applied to the analysed dataset and highlights practical limitations encountered during closure interpretation.

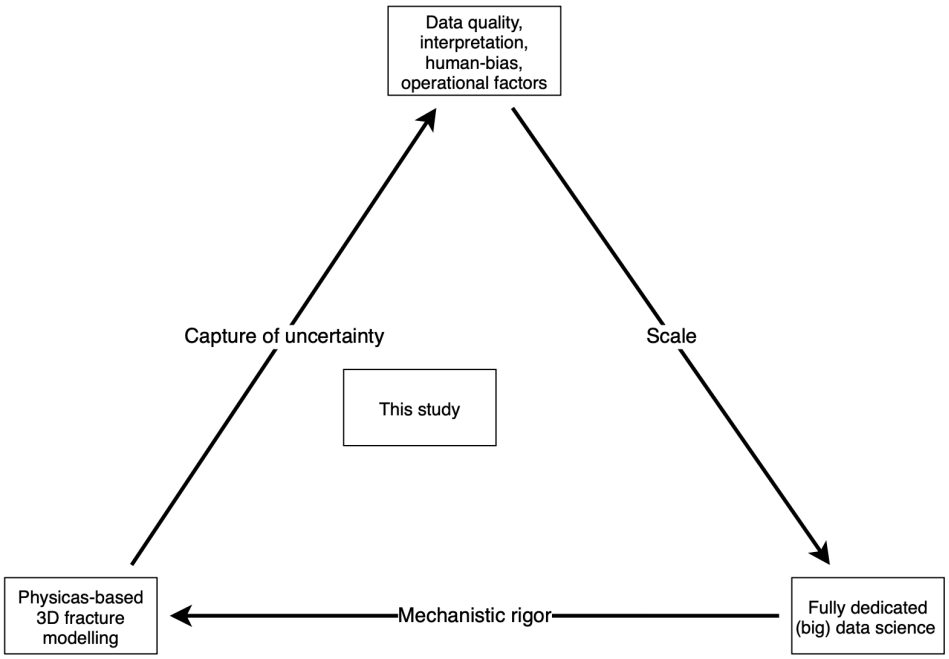

Figure 5.2: Conceptual framework illustrating the trade-off between mechanistic modelling and data-driven approaches in stress analysis. Physics-based fracture modelling provides high mechanistic rigor but is computationally demanding, whereas large-scale data-driven approaches enable analysis of extensive datasets but may incorporate uncertainties related to data quality, interpretation choices, and operational factors. The workflow applied in this study occupies an intermediate position, aiming to capture key uncertainties while maintaining physical interpretability.

Fracture closure pressure is widely used as a proxy for the least principal stress $S_{h\,\min}$ because closure occurs when an induced hydraulic fracture can no longer be mechanically sustained against the far-field stress field (Zoback, 2010). However, fracture closure cannot be observed directly in the pressure record and must instead be inferred from diagnostic features in the pressure decline during shut-in. As a result, closure pressure is inherently method-dependent, and different interpretation techniques effectively operationalize different definitions of the closure process.

In the analysed dataset, this method dependence is not negligible: closure pressures derived from different diagnostics within a single injection cycle can differ by up to approximately 20–25 bar, with typical differences on the order of several bar. This spread is comparable to, or larger than, the variability observed between repeated cycles in the same interval, highlighting that interpretation methodology is a primary source of uncertainty.

As discussed in the literature review, fracture closure is not an instantaneous event but a progressive mechanical process (Jung et al., 2016). During shut-in, pressure within the fracture decreases as fluid leaks off into the formation, causing the fracture aperture to decrease gradually. Contact progressively occurs between asperities along the fracture surfaces, resulting in a continuous evolution of both hydraulic behaviour and mechanical stiffness during the fall-off phase. Because these processes overlap in time, different diagnostics may identify different stages of fracture closure, meaning that closure pressure cannot be uniquely defined from pressure data alone.

Several commonly used closure diagnostics rely on analysing the pressure derivative during the fall-off phase. Methods such as the Castillo, Haimson, Barree, and semilogarithmic maximum derivative approaches identify closure from characteristic changes in derivative behaviour that arise from evolving system compliance and leak-off conditions (Barree et al., 2009; Castillo, 1987; Haimson & Fairhurst, 1967). In practice, however, derivative-based diagnostics are highly sensitive to data quality and preprocessing choices. The pressure derivative depends strongly on the exact shut-in pick, the sampling frequency of the pressure data, and any smoothing or filtering applied during preprocessing. Early-time pressure oscillations such as water-hammer effects can further distort derivative behaviour and obscure diagnostic signatures.

In the analysed dataset, such preprocessing-related effects can shift derivative-based closure picks by several bar, particularly when early-time oscillations dominate the signal. This sensitivity is most pronounced immediately after shut-in, where small differences in filtering or derivative window selection can lead to different interpretations of the diagnostic features.

The following examples illustrate situations in which derivative-based closure diagnostics become difficult to apply due to signal instability during the early fall-off phase.

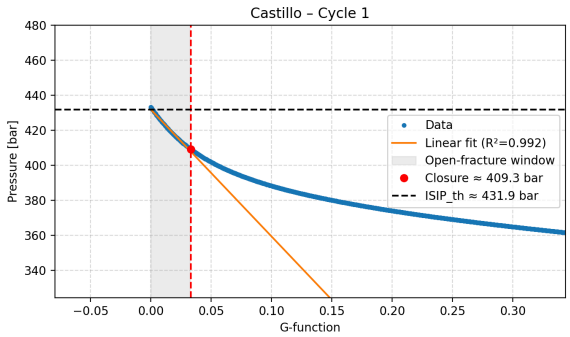

(a) Example where the Castillo diagnostic yields an not so clearly defined closure signature.

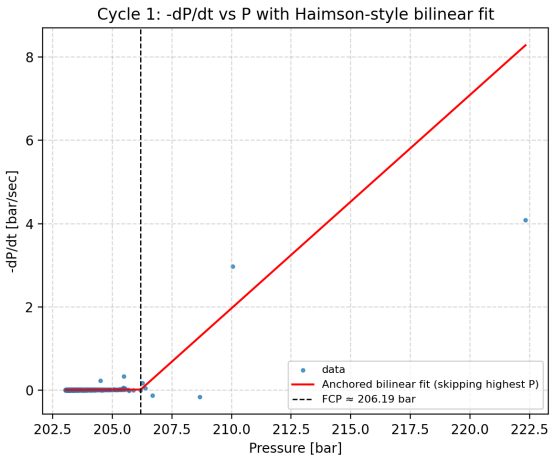

(b) Early-time oscillations affecting derivative-based diagnostics such as the Haimson method.

Figure 5.3: Examples of derivative-based closure diagnostics becoming unreliable due to early-time pressure oscillations and derivative instability.

In these cases, derivative oscillations and early-time noise lead to ambiguous diagnostic features, making closure identification difficult or subjective. Similar issues are illustrated in Figure 5.4, where early-time pressure oscillations or the absence of a clear stiffness transition prevent reliable interpretation using several closure diagnostics. These examples demonstrate that derivative-based methods may fail operationally when the signal-to-noise ratio is low or when the early fall-off response is dominated by waterhammer effects.

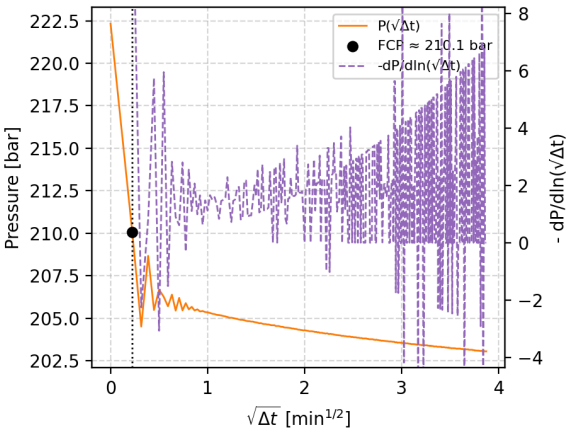

(a) Water-hammer oscillations leading to unstable derivatives and unreliable semilog-based diagnostics.

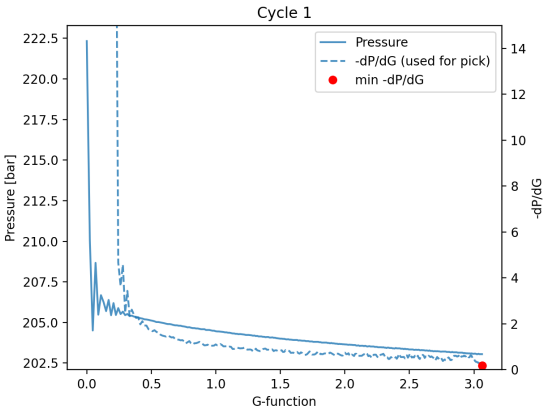

(b) Example where no clear stiffness transition is observed, preventing application of stiffness-based diagnostics.

Figure 5.4: Examples of closure diagnostics failing due to signal distortion or insufficient mechanical response contrast.

An alternative interpretation approach focuses on changes in system stiffness or fracture compliance. These diagnostics aim to detect the transition from a compliant fracture system to a stiffer system once fracture faces begin to contact (McClure et al., 2019; Raaen et al., 2001). Physically, the total system compliance during a hydraulic fracturing test includes contributions from the wellbore, the fluid, and

the fracture itself. While the fracture remains open it contributes significantly to system compliance, but once fracture faces begin to contact the fracture compliance decreases rapidly, increasing overall system stiffness.

The competing hydraulic and mechanical processes governing pressure decline behaviour are illustrated conceptually in Figure 5.5. During fall-off, the slope of the pressure decline is controlled by the ratio between leak-off rate and system compliance. As fracture closure progresses, fracture compliance decreases, which increases system stiffness and tends to steepen the pressure decline. At the same time, the leak-off rate decreases as the pressure difference between fracture and formation diminishes, which tends to reduce the slope. The observed change in slope therefore reflects the balance between these competing processes (Raaen et al., 2001).

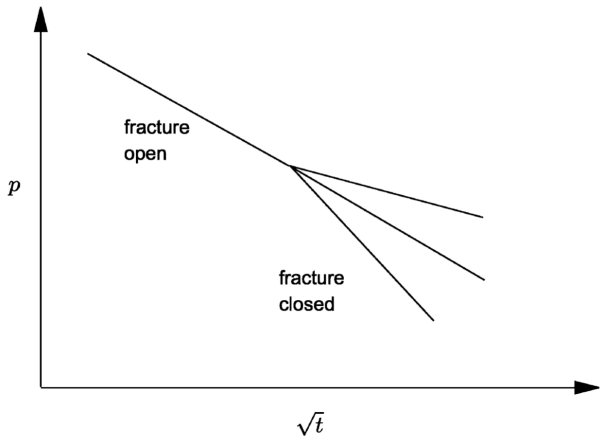

Figure 5.5: Schematic pressure versus square-root-of-time response during fracture closure. The slope change reflects the competing effects of decreasing leak-off rate and increasing system stiffness as fracture compliance decreases. From Raaen et al. (2001).

Within the analysed dataset, the semilogarithmic maximum derivative method produced the most operationally robust closure estimates across wells and cycles. The diagnostic feature—the maximum derivative during early fall-off—is relatively straightforward to identify compared with tangent-based approaches that require subjective selection of linear segments. As a result, this method yielded the most internally consistent closure pressures, with average deviations of approximately 6 bar (about 1.8%) compared to external interpretations. Nevertheless, the method remains sensitive to early-time artefacts and derivative instability immediately after shut-in. Careful data conditioning and appropriate derivative window selection are therefore necessary to avoid biased closure picks.

Not all injection cycles produced interpretable closure diagnostics. In the analysed dataset, several cycles were excluded from closure interpretation because fracture propagation could not be demonstrated. When fracture propagation is limited or absent, the measured pressure response reflects near-wellbore processes rather than far-field stress equilibrium (see Figure 5.6. In such cases, closure pressure cannot be interpreted as $S_{h\,\mathrm{min}}$.

Overall, the comparison of closure diagnostics demonstrates that closure pressure interpretation is inherently sensitive to both the chosen diagnostic method and the quality of the pressure data. In practice, the combined effect of method selection and data preprocessing can introduce variability ranging from several bar to on the order of tens of bar. Closure-derived estimates of $S_{h\,\mathrm{min}}$ should therefore not be interpreted as uniquely defined physical values but rather as operational estimates that depend on the diagnostic used and the interpretation workflow applied. Transparent documentation of interpretation methods, preprocessing steps, and quality criteria is therefore essential when comparing closure-derived stress estimates across wells, datasets, or studies.

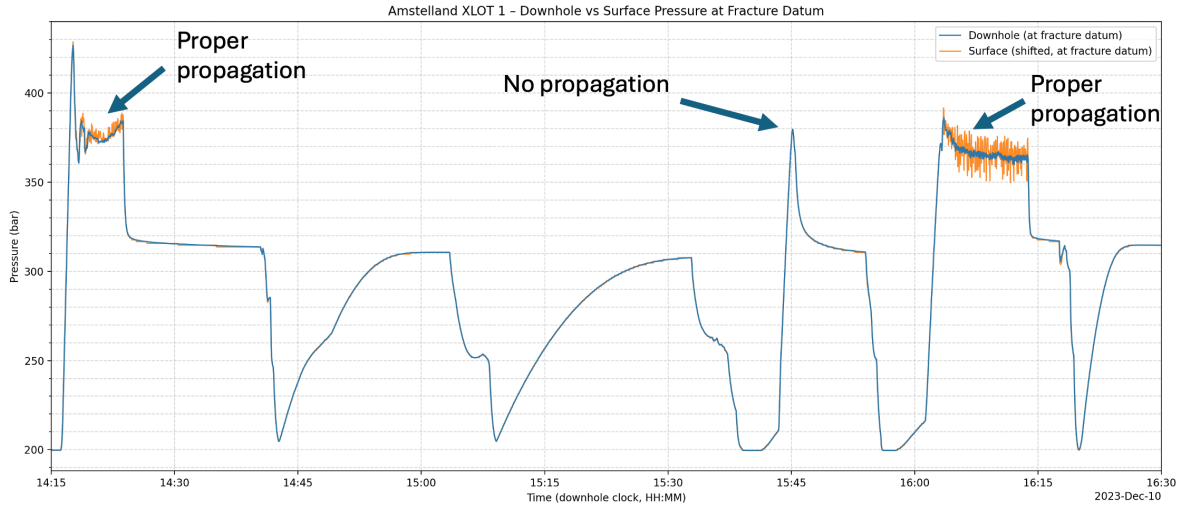

Figure 5.6: An example where the second cycle does not have a proper propagation phase.

5.5. Observability of fracture initiation

Fracture initiation in hydraulic stress testing is theoretically defined as the moment at which the tensile stress at the borehole wall exceeds the tensile strength of the rock, causing a tensile crack to form. For a vertical wellbore in an elastic stress field, this condition is commonly approximated using the Kirsch solution for hoop stress concentration around the wellbore, excluding thermal stress effects (Haimson & Fairhurst, 1967). Under simplified conditions, the initiation pressure can be written as

$$P_{\text{init}} = 3S_{h\,\min} - S_{H\,\max} - P_p + T_0, \tag{5.1}$$

where $S_{h\,\min}$ and $S_{H\,\max}$ are the minimum and maximum horizontal stresses, P_p is pore pressure, and T_0 is the tensile strength of the rock. In theory, this pressure marks the first onset of tensile failure at the borehole wall. In field data, however, that first initiation event is not necessarily observable.

The main reason is that the measured pressure response reflects the behaviour of the entire pressurized system rather than the fracture alone. This system includes the wellbore, tubing, pumps, surface lines, and the near-wellbore formation. If the fracture volume created at the onset of tensile failure is very small relative to the total compressible system volume, the pressure response remains dominated by system compressibility rather than by fracture growth.

This behaviour can be expressed through the relationship between pressure change and system compressibility:

$$\beta_s = \frac{1}{V_s}\frac{dV_s}{dP}, \tag{5.2}$$

where V_s is the effective system volume and β_s is the effective system compressibility. For constant injection rate, the pressure evolution can then be written as

$$\frac{dP}{dt} = \frac{1}{\beta_s V_s}\frac{dV}{dt}. \tag{5.3}$$

A measurable change in pressure behaviour therefore requires a measurable change in effective system volume. If the initial fracture nucleus created during tensile failure is extremely small, its hydraulic volume is negligible relative to the total system volume, and the pressure curve may continue along essentially the same trend as before initiation. In that case, the earliest tensile damage event does not produce a detectable signature in the pressure record.

As a result, the first observable departure from elastic pressurization may correspond not to the first tensile failure event, but to a later stage of fracture growth. The pressure feature commonly interpreted as leak-off pressure may therefore correspond to the point at which fracture growth begins to measurably influence the system response, rather than to the true initiation pressure itself. Depending on the test conditions, this observable feature may reflect stable fracture growth, unstable fracture extension, or a change in filtration behaviour. This interpretation is consistent with previous studies showing that observed leak-off pressures often deviate from theoretical initiation pressures predicted by simple elastic models (Alberty & McLean, 2004; Van Oort & Vargo, 2008).

The observability of fracture initiation also depends strongly on test configuration. Formation integrity tests and leak-off tests are commonly conducted in relatively large pressurized systems with substantial wellbore storage and comparatively high injection rates. Under these conditions, the fracture volume created at first tensile failure may remain too small to influence the measured pressure response. In contrast, micro-fracture and mini-frac tests are designed to reduce system volume and injection rate, making the recorded pressure response more sensitive to fracture growth. Fracture initiation is therefore often more clearly resolved in micro-frac style tests than in conventional FIT or LOT tests.

Additional processes may further obscure the pressure signature of initiation. Fluid filtration into permeable formations can gradually modify the pressure-volume response without producing a distinct initiation feature. Near-wellbore damage, perforation-induced stress concentrations, and fracture tortuosity may also cause fracture growth to develop progressively rather than as a discrete event. Under such conditions, the pressure response may evolve smoothly and the onset of tensile failure cannot be identified unambiguously.

These considerations have important implications for the interpretation of initiation-based pressures. Because the earliest initiation event may not be observable in the pressure data, pressures identified as leak-off or breakdown should not automatically be interpreted as the theoretical initiation pressure. Instead, they are operational indicators of a change in pressurization behaviour whose relationship to fracture mechanics depends on the hydraulic configuration and formation properties. This helps explain why initiation-based pressures from FIT and LOT tests often show substantial scatter when compared with closure-derived estimates of $S_{h\,\min}$.

The Delft micro-fracture examples in Figures 5.7 and 5.8 illustrate this uncertainty. Even when deviation-from-linearity or compliance-based methods identify a distinct pressure feature, that feature does not necessarily correspond to the true moment of fracture initiation. When the fracture volume created at initiation is small relative to the total compressible system volume, the pressure response remains dominated by system compressibility and the earliest tensile damage event may remain undetectable. In such cases, the observed “breakdown” feature may instead correspond to a later stage of fracture growth, such as the onset of unstable propagation. This follows directly from Equation 5.3.

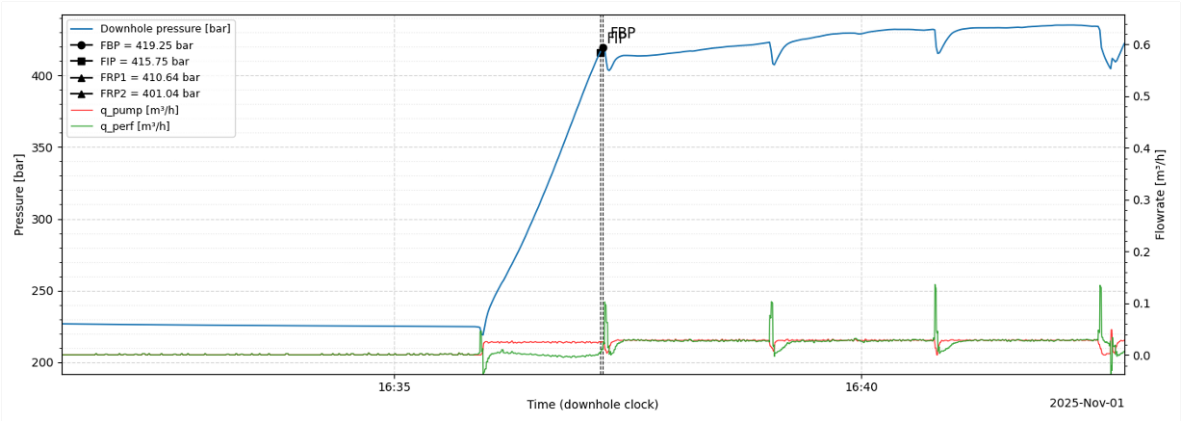

Figure 5.7: Micro-fracture example showing that fracture initiation is located near to formation breakdown pressure.

Overall, the limited observability of fracture initiation highlights a fundamental challenge in interpreting hydraulic stress tests. Although initiation can be defined theoretically through wellbore stress analysis, the measured pressure response does not necessarily resolve the moment of first tensile failure.

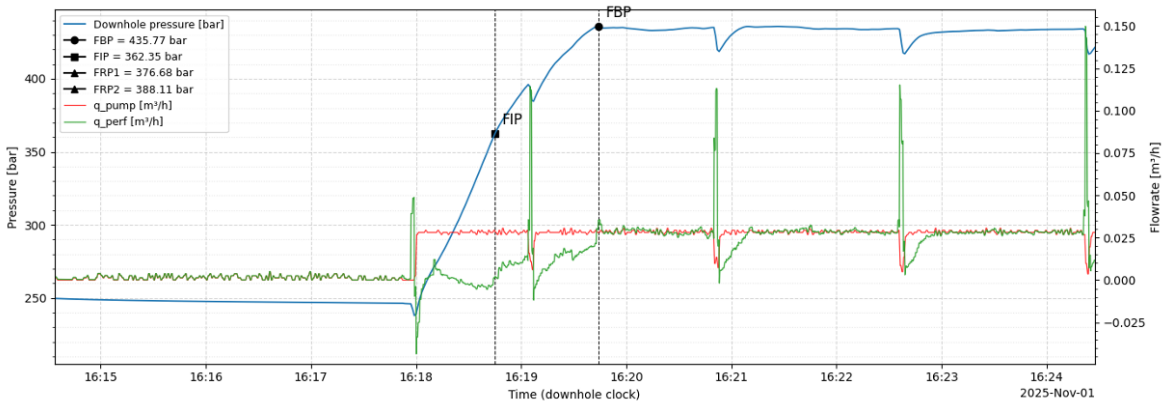

Figure 5.8: Second micro-fracture example illustrating that a picked leak-off is located further away from formation breakdown pressure.

Initiation-based pressures should therefore be interpreted cautiously and used primarily as constraints rather than as direct estimates of the in-situ stress state.

5.6. Sensitivity and interpretation uncertainty

The stress estimates derived in this study are not direct measurements but the result of an interpretation workflow applied to pressure–time data from hydraulic stress tests. Consequently, the inferred values of $S_{h\,\min}$ are sensitive to both data quality and methodological choices. These sensitivities arise from pressure preprocessing, closure diagnostic selection, and the assumptions used to translate initiation-based pressures into stress constraints.

Not all sources of uncertainty contribute equally. Within the analysed dataset, the dominant source of variability is the closure interpretation method, followed by preprocessing-related effects. Uncertainty associated with fracture initiation models primarily affects the interpretation of FIT and LOT data rather than closure-derived estimates. As shown in Appendix D, uncertainty in tensile strength, maximum horizontal stress, and leak-off pressure can propagate into variations of several tens of bar in the inferred $S_{h\,\min}$. In addition, initiation pressure is strongly dependent on well trajectory, demonstrating that initiation-based measurements do not uniquely reflect the far-field stress state even when that stress state remains unchanged.

5.6.1. Data quality and preprocessing

A first source of sensitivity arises from pressure data quality and processing. Closure diagnostics rely on pressure derivatives during fall-off and are therefore highly sensitive to noise and early-time transients. Small oscillations, such as water-hammer effects, can be amplified during derivative calculation and obscure diagnostic features.

Closure picks can therefore depend on filtering, sampling frequency, and the identification of shut-in time. In practice, such preprocessing choices can shift derivative-based closure picks by several bar. Consistent preprocessing is therefore essential when comparing results across tests or wells.

5.6.2. Closure diagnostic selection

A second, and often dominant, source of uncertainty is the closure interpretation method. Because fracture closure cannot be observed directly, different diagnostics identify different proxies for the closure process. Derivative-based methods capture changes in hydraulic behaviour, while stiffness-based approaches target the onset of mechanical contact.

These diagnostics correspond to different stages of a progressive closure process and therefore do not yield identical closure pressures. In the analysed dataset, inter-method differences reach up to approximately 20–25 bar within individual cycles. This spread is comparable to, or larger than, cycle-to-cycle variability, indicating that interpretation methodology can dominate the uncertainty in $S_{h\,\min}$.

5.6.3. Mechanical model assumptions

Additional uncertainty arises when initiation-based pressures are translated into stress constraints. Lower bounds derived from FIT data depend on fracture initiation models, which require assumptions about $S_{H\,\max}$, tensile strength T_0, pore pressure, and stress orientation. These parameters are often poorly constrained and directly influence the inferred stress bounds.

The interpretation of leak-off pressure is also non-unique. Deviations from linear pressurization may reflect fracture initiation, reopening, filtration effects, or the onset of unstable propagation. As discussed earlier, the earliest initiation event may not be observable if the initial fracture volume is small relative to the compressible system volume. In such cases, the observed leak-off pressure represents a later stage of fracture growth.

The sensitivity analysis in Appendix D shows that these uncertainties can produce variations of several tens of bar in inferred stress magnitude, with tensile strength exerting the strongest influence. This strong parameter sensitivity highlights a fundamental limitation of initiation-based stress estimation.

5.6.4. Summary of interpretation sensitivities

The main sources of interpretation uncertainty are summarized in Table 5.2. These uncertainties arise from both the pressure data and the interpretation framework.

Table 5.2: Main sources of uncertainty affecting the interpretation of $S_{h\,\min}$ from hydraulic stress tests.

Source of uncertainty	Mechanism	Typical impact
Pressure data preprocessing	Filtering, smoothing, sampling frequency, and shut-in identification affect derivative behaviour during fall-off.	Closure pick shifts of several bar.
Closure interpretation method	Different diagnostics identify different proxies for progressive fracture closure.	Inter-method spread up to $\sim$20–25 bar.
Pressure data quality	Noise, water-hammer oscillations, and limited fall-off duration obscure diagnostic features.	Reduced interpretability.
Fracture initiation model assumptions	Uncertainty in $S_{H\,\max}$, tensile strength T_0, pore pressure, and stress orientation.	Variations of several tens of bar in inferred stress.

Because these uncertainties interact, closure-derived stress estimates cannot be expressed as a single value with a well-defined error margin. Instead, $S_{h\,\min}$ is better represented as an envelope of plausible values constrained by multiple diagnostics and mechanical considerations.

The interpretation workflow adopted in this study therefore emphasizes consistency and transparency. Applying identical preprocessing and diagnostic criteria across wells reduces systematic bias and ensures that inferred stress estimates remain reproducible and mechanically defensible within the limits of the available data.

5.7. Repeatability vs interpretation uncertainty

Uncertainty in closure-derived estimates of $S_{h\,\min}$ can be separated into two conceptually distinct components: repeatability and interpretation uncertainty. Repeatability refers to the variability observed between repeated injection cycles performed under comparable test conditions within the same interval. Interpretation uncertainty, in contrast, arises from methodological choices made during the analysis of the pressure fall-off data, such as the closure picking method, derivative calculation, or the selection of diagnostic windows.

Repeatability primarily reflects the physical behaviour of the fracture system during repeated injections. In hydraulic stress tests, several factors can influence repeatability, including variations in fracture geometry, leak-off behaviour, local heterogeneity in formation properties, and changes in system com-

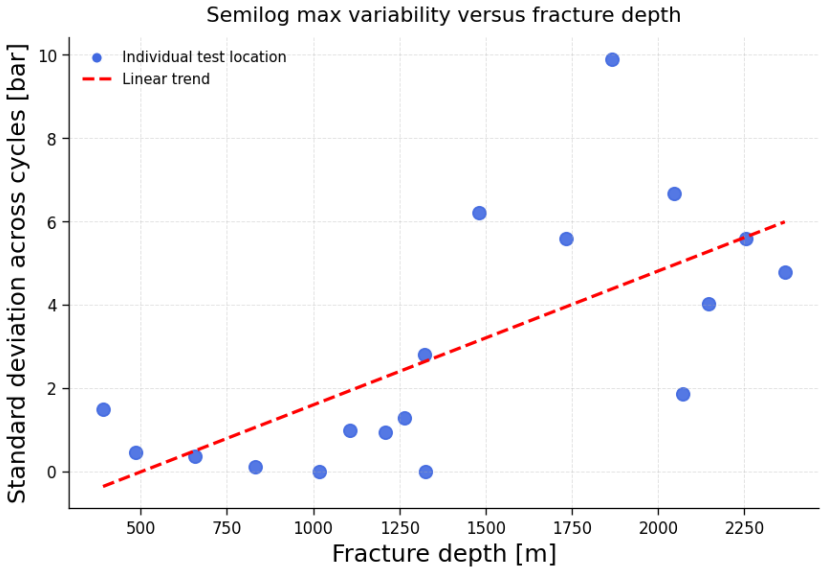

Figure 5.9: Cycle-to-cycle variability of the Semilog Max closure pressure estimate as a function of fracture depth. Each point represents the standard deviation of closure pressures obtained from repeated injection cycles at a single test location. The dashed line indicates a linear trend fitted to all observations. Most locations exhibit variability of only a few bar, although some intervals show larger deviations. The scatter suggests that repeatability is influenced both by depth and by local fracture behaviour.

pliance between injection cycles. Even when injection procedures are similar, fractures may propagate into slightly different parts of the formation during subsequent cycles, leading to small variations in the observed closure pressure. In addition, fracture surface roughness and progressive fracture development may influence how fracture faces come into contact during shut-in.

The repeatability of the Semilog Max closure pressure estimate in the analysed dataset is illustrated in Figure 5.9. The figure shows the standard deviation of closure pressures obtained from repeated injection cycles at each test location. Across all locations, the average cycle-to-cycle standard deviation of the Semilog Max closure pressure is 2.95 bar, indicating generally good repeatability of the method under comparable testing conditions. For most intervals, variability remains within only a few bar, although several locations display larger deviations approaching ~ 10 bar. These larger variations likely reflect differences in local fracture behaviour, such as variations in fracture geometry, leak-off conditions, or mechanical interaction between fracture faces during closure. A weak increase in variability with depth is also suggested by the fitted trend, although the scatter indicates that local conditions remain an important controlling factor.

Interpretation uncertainty arises when different closure diagnostics are applied to the same pressure fall-off curve. Because fracture closure cannot be observed directly, each interpretation method identifies closure based on a specific proxy within the pressure response. Derivative-based methods detect characteristic changes in the pressure decline behaviour, whereas stiffness- or compliance-based approaches attempt to identify the onset of mechanical contact between fracture faces. As discussed earlier, these diagnostics correspond to different stages of the progressive closure process and therefore do not necessarily produce identical closure pressures.

In the analysed dataset, the spread between closure pressures obtained using different diagnostics occasionally reaches several tens of bar within individual cycles, demonstrating that interpretation methodology alone can introduce substantial variability in the inferred stress magnitude. Compared with the cycle-to-cycle repeatability of approximately 2.95 bar observed for the Semilog Max method, this indicates that interpretation choices can represent a comparable or even dominant source of uncertainty in the inferred stress magnitude.

These observations highlight the importance of applying a consistent interpretation workflow when analysing hydraulic stress test data. Using multiple closure diagnostics, documenting preprocessing

choices, and evaluating the spread between interpretation methods provides a more robust basis for stress inference than relying on a single closure pick. Repeatability analysis therefore complements the sensitivity analysis presented in the previous section by helping to distinguish between variability arising from subsurface fracture behaviour and variability introduced by interpretation methodology.

5.8. Case study: thermal effects

The interpretation of hydraulic stress tests commonly assumes that the in-situ stress state remains unchanged during the test. In practice, however, thermal effects associated with fluid injection can locally perturb the stress field. This is particularly relevant when relatively cold fluids are injected into a warmer formation, as thermal contraction of the rock can reduce the effective stress acting normal to the fracture. In such cases, the measured fracture closure pressure may underestimate the true far-field minimum horizontal stress $S_{h\,\mathrm{min}}$.

This effect is illustrated by the Middenmeer test highlighted in Figure 5.10. Compared to other tests, the closure pressure at this location appears anomalously low. To interpret this behaviour, it is necessary to consider the potential influence of thermo-mechanical stress changes during injection.

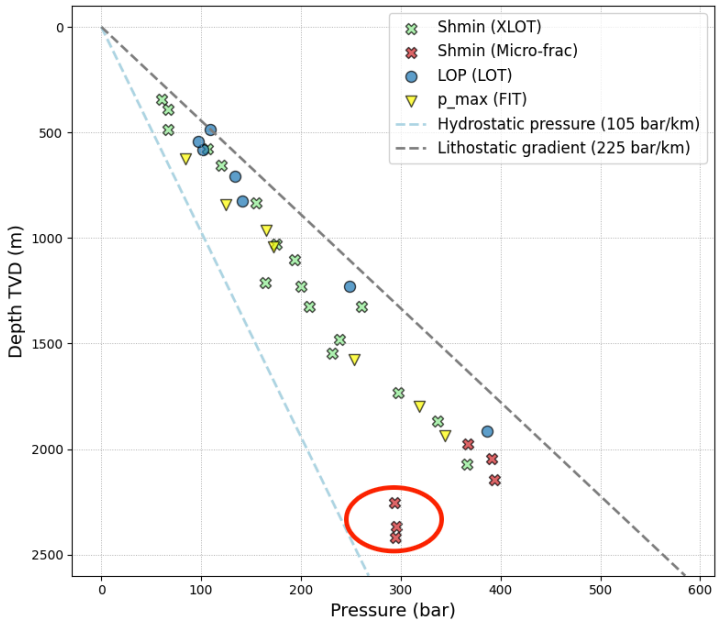

Figure 5.10: Closure pressures of the analysed tests, with the Middenmeer test highlighted. The relatively low closure pressure suggests a local perturbation of the stress field.

Fracture initiation is commonly approximated using the Kirsch-based relation

$$P_{\mathrm{init}} = 3S_{h\,\mathrm{min}} - S_{H\,\mathrm{max}} - P_p + T_0, \tag{5.4}$$

which assumes purely mechanical loading under isothermal conditions. However, when thermal effects are present, an additional stress component must be considered. A temperature change ΔT induces a thermoelastic stress change that can be approximated as

$$\sigma_{\theta\theta}^{\Delta T} = -\frac{E\alpha\Delta T}{1-\nu}, \tag{5.5}$$

where E is Young's modulus, α is the coefficient of thermal expansion, and ν is Poisson's ratio. Cooling of the formation ($\Delta T < 0$) therefore results in a reduction of the minimum horizontal stress.

In the context of hydraulic stress testing, this implies that the effective stress acting normal to the fracture may decrease during injection if the injected fluid is colder than the surrounding formation. As a result,

the fracture can remain open at lower pressures, leading to a reduced apparent closure pressure. In such cases, the measured closure pressure reflects a thermally perturbed stress state rather than the undisturbed far-field $S_{h\,\mathrm{min}}$.

This interpretation is supported by Figure 5.11, which shows that the closure pressure in the Middenmeer test is very close to the well pressure prior to injection. This behaviour indicates that only a small additional pressure was required to keep the fracture open, consistent with a reduced effective stress due to cooling.

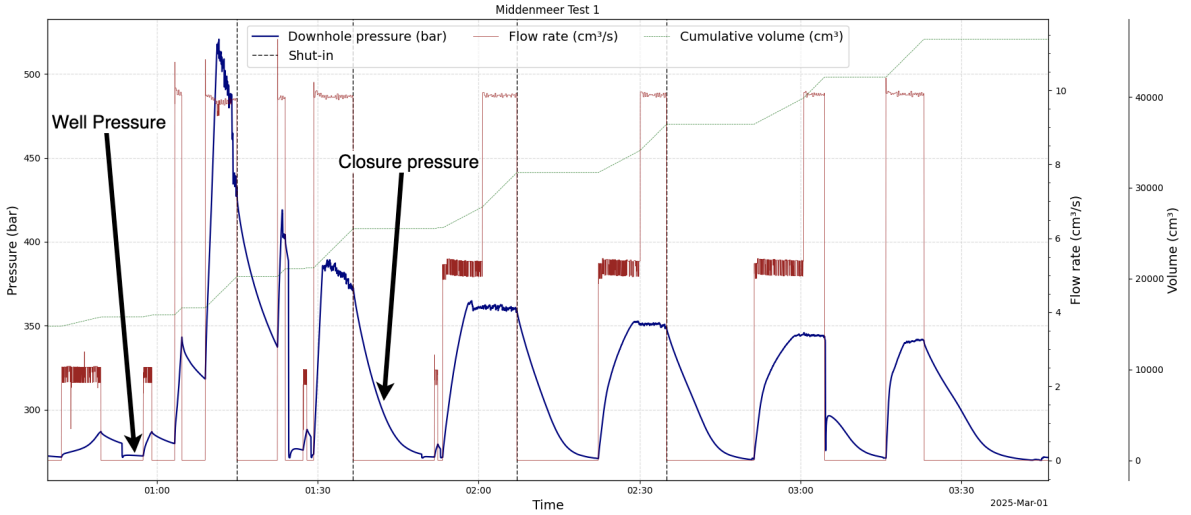

Figure 5.11: Comparison between well pressure prior to injection and interpreted closure pressure for the Middenmeer test. The small difference indicates a reduced effective stress acting on the fracture.

In contrast, Figure 3.5 shows a typical injection cycle in which the difference between the well pressure prior to injection and the interpreted closure pressure is significantly larger. In such cases, a higher pressure is required to maintain fracture opening, which is consistent with closure occurring under the undisturbed far-field stress state. This comparison highlights that the small pressure difference observed in the Middenmeer test is not characteristic of the general dataset, but rather represents an anomalous behaviour.

Taken together, these observations suggest that thermal effects may have influenced the stress measurements in the Middenmeer test. If the formation experienced cooling during injection, the inferred closure pressure would underestimate the true far-field stress magnitude. More generally, this case study demonstrates that deviations in closure pressure should not automatically be interpreted as variations in the regional stress field. Local effects such as thermal cooling, fluid–rock interaction, or changes in system compliance can significantly influence the observed pressure response.

Although thermal effects were not explicitly modelled in this study, their potential influence should be considered in future analyses, particularly in geothermal systems or in tests where significant temperature contrasts exist between injected fluids and the formation.

5.9. Applicability of offset data

A practical question in subsurface operations is whether the minimum horizontal stress $S_{h\,\mathrm{min}}$ can be predicted prior to drilling using information from nearby wells. In many drilling and geothermal projects, formation integrity tests and leak-off tests from offset wells are used to estimate fracture gradients and to anticipate the stress conditions expected during drilling. However, the results of the case study performed in this thesis indicate that the applicability of such offset data for estimating $S_{h\,\mathrm{min}}$ is limited.

The fundamental challenge is that initiation-based pressures recorded during FIT and LOT tests are strongly influenced by geology, near-wellbore conditions and operational factors. Unlike closure-derived measurements from XLOT or micro-fracture tests, these pressures do not directly reflect far-field stress equilibrium. Instead, they depend on factors such as wellbore geometry, mudcake development, drilling-

induced damage, perforation configuration, injection rate, and the compressibility of the pressurized system (Alberty & McLean, 2004; Van Oort & Vargo, 2008; Zoback, 2010). As a result, even if the regional stress field is relatively uniform, initiation-based pressures can vary significantly between wells.

The transferability of offset data is therefore conditional on a high degree of geological and operational similarity between wells. At minimum, the following conditions should be approximately satisfied for meaningful comparison:

1. comparable lithology and mechanical properties,
2. similar depth and burial conditions,
3. comparable pore-pressure regimes,
4. absence of significant facies variations,
5. similar wellbore configuration and test execution.

If these conditions are not satisfied, differences in measured FIT or LOT pressures are more likely to reflect variations in formation properties or near-wellbore effects rather than differences in the regional stress field. Even when geological conditions appear similar, the interpretation of offset initiation pressures remains uncertain because the relationship between LOP and fracture initiation is not uniquely defined.

The case study analysed in this thesis illustrates these limitations. Although offset FIT and LOT data can be used to construct broad envelopes of plausible fracture gradients, they do not provide reliable predictions of $S_{h\,\min}$. In the analysed dataset, the scatter between offset initiation pressures and closure-derived $S_{h\,\min}$ values was substantial, indicating that initiation-based pressures cannot be directly translated into stress magnitude without additional assumptions. In particular, variations in lithology, permeability, and near-wellbore conditions introduce significant variability that is difficult to account for when using offset data alone.

Nevertheless, offset data can still provide useful contextual information when interpreted cautiously. Rather than attempting to predict a single stress value, offset FIT and LOT data can be used to construct conservative bounds on the expected fracture gradient prior to drilling. Such bounds can inform drilling window design and operational planning, especially in areas where no closure-based stress measurements are available. However, these bounds should be interpreted as operational constraints rather than as direct estimates of the in-situ stress state.

Overall, the results of this study suggest that offset initiation-based data should be used primarily as a first-order screening tool rather than as a substitute for closure-based stress measurements. Reliable determination of $S_{h\,\min}$ requires hydraulic tests that explicitly resolve fracture closure, such as XLOT or micro-fracture tests, which directly probe the far-field stress equilibrium.

5.10. Limitations

Several limitations should be considered when interpreting the results of this study. These arise from data quality, interpretation methodology, and simplifying assumptions in the mechanical framework. They do not contribute equally: within the analysed dataset, the dominant source of uncertainty is the closure interpretation method, followed by preprocessing-related effects, while uncertainties in initiation-based mechanical models mainly affect derived stress bounds rather than closure-derived estimates of $S_{h\,\min}$.

A first limitation concerns pressure data quality and resolution. Early-time oscillations, noise, and limited fall-off duration complicated closure interpretation in several tests. Because derivative-based diagnostics amplify noise, small differences in filtering, sampling frequency, or shut-in identification can shift closure picks by several bar. Cycles without clear fracture propagation or diagnostic fall-off behaviour were excluded to avoid misinterpretation, reducing the number of usable observations.

A more fundamental limitation is that fracture closure does not correspond to a single physically well-defined pressure, but to a progressive mechanical process. Different diagnostics therefore identify different stages of closure, making the interpreted closure pressure inherently method-dependent. In

the analysed dataset, the spread between closure interpretations reaches up to approximately 20–25 bar within individual cycles, showing that methodological choices can dominate the uncertainty in $S_{h\,\min}$.

Additional uncertainty arises from initiation-based interpretations. Lower bounds derived from FIT data depend on simplified fracture initiation models based on the Kirsch solution, which require assumptions about $S_{H\,\max}$, tensile strength, pore pressure, and stress orientation. These assumptions directly affect the inferred stress bounds. A first-order sensitivity analysis of this framework is presented in Appendix D.

Another limitation is the observability of fracture initiation. The initial fracture volume may be too small relative to the compressible system volume to produce a detectable pressure signature, so observed leak-off pressures may correspond to a later stage of fracture growth rather than to true initiation.

The applicability of offset data is also limited. Differences in lithology, permeability, wellbore configuration, and operational conditions can introduce substantial variability in measured initiation pressures, even between nearby wells. In addition, several physical processes were not explicitly modelled, including thermo-mechanical effects, poroelastic stress changes, and detailed leak-off behaviour in heterogeneous formations.

Despite these limitations, the main conclusions remain robust. Closure-derived estimates of $S_{h\,\min}$ are strongly method-dependent, initiation-based pressures are influenced by near-wellbore effects, and consistent interpretation workflows are essential for obtaining reproducible stress estimates. The identified limitations therefore define the scope and uncertainty of the results rather than undermining their validity.

5.11. Implications

The findings of this study have several implications for hydraulic stress test interpretation and for subsurface operations that rely on accurate estimates of the minimum horizontal stress $S_{h\,\min}$.

First, initiation-based pressures from formation integrity tests and leak-off tests LOT should not be interpreted as direct measurements of $S_{h\,\min}$ under typical field conditions. These pressures are controlled by near-wellbore stress concentrations, rock strength, system compliance, and operational factors, and therefore reflect fracture initiation rather than far-field stress equilibrium. The observation that approximately 26% of apparent tensile-strength values derived from LOP–FRP differences are negative further shows that initiation-based interpretations cannot be directly linked to intact rock properties.

Instead, the results support a hierarchical interpretation framework. Closure-derived pressures from XLOT and micro-fracture tests provide primary estimates of $S_{h\,\min}$, LOT pressures provide upper-bound constraints, and FIT pressures can only be interpreted as conditional lower bounds when translated through an explicit fracture initiation model.

Second, interpretation methodology matters. Because closure pressure is inherently method-dependent, reported values of $S_{h\,\min}$ are not unique but depend on the diagnostic used. In the analysed dataset, differences between closure methods reach up to 20–25 bar, indicating that interpretation choices can influence stress estimates as much as, or more than, physical variability between tests. This highlights the need for standardized workflows and transparent reporting of preprocessing and picking criteria.

Third, initiation-based pressures from offset wells cannot reliably predict $S_{h\,\min}$ because they are highly sensitive to local geological and operational conditions. In practice, drilling programs relying solely on FIT or LOT data may therefore misestimate the minimum stress and the associated fracture gradient. Offset data can still be used to define broad operational envelopes, but not to determine stress magnitudes.

Finally, future stress estimation workflows should prioritize closure-based measurements and integrate sensitivity analysis and mechanical modelling rather than relying on initiation-based pressures alone. Reliable determination of $S_{h\,\min}$ therefore requires both appropriate test design and a consistent, physically informed interpretation framework.

5.12. Answers to research questions

The research questions posed in Chapter 1 can now be answered based on the results and analysis presented in this thesis.

Research question 1: *What are the physical principles underlying hydraulic stress tests, and how do different test types relate to $S_{h\,\min}$?*

Hydraulic stress tests measure the interaction between fluid pressure, rock deformation, and fracture mechanics. A fundamental distinction exists between drilling tests (FIT/LOT) and diagnostic tests (XLOT/micro-frac). LOT measurements capture the onset of fluid loss or fracture initiation under near-wellbore conditions (FIT stops before fracture initiation), whereas XLOT and micro-fracture tests explicitly create and monitor a hydraulic fracture and allow fracture closure to be identified during fall-off. Because closure reflects mechanical equilibrium with the far-field stress, closure-based measurements provide a direct estimate of $S_{h\,\min}$, while initiation-based pressures reflect local failure conditions and must be interpreted within a mechanical framework.

Research question 2: *Which closure interpretation method is most suitable for estimating $S_{h\,\min}$?*

The comparison of closure diagnostics shows that closure pressure is inherently method-dependent. Within individual cycles, different diagnostics yield spreads of up to approximately 20–25 bar. In contrast, the repeatability of a single method (Semilog Max) is much higher, with an average cycle-to-cycle standard deviation of approximately 2.95 bar.

A direct comparison between methods highlights systematic differences. The Haimson method consistently yields the lowest closure pressures, with average differences of approximately -7.6 bar relative to Castillo and up to -10.4 bar relative to Barree. In contrast, the Barree method produces the highest closure pressures, exceeding Haimson by about 10.4 bar and semilog max by approximately 5.6 bar on average. The semilog max method lies between these extremes, typically giving slightly lower values than Castillo (about -2.8 bar) and Barree (about -5.6 bar), but higher than Haimson (about $+4.8$ bar). Castillo and semilog max are therefore relatively close, while Haimson and Barree form lower and upper bounds, respectively.

In addition to these systematic offsets, the operational applicability of the methods differs significantly. The Castillo and semilog max methods show the highest success rates, being applicable in approximately 90% and 84% of cycles, respectively. Barree performs moderately (about 69%), while Haimson is less frequently applicable (about 54%). The system stiffness (compliance) method shows very limited applicability (approximately 13%), as a clear stiffness transition is often not observable in the analysed XLOT and micro-fracture data. In the limited number of cases where the stiffness method could be applied, it tended to yield relatively low closure pressure estimates compared to other methods. However, the small number of valid applications limits its reliability and prevents robust comparison across the dataset.

This behaviour contrasts with findings from DFIT literature, where stiffness-based methods are often considered more physically representative. The discrepancy highlights that the applicability of such methods strongly depends on test type, fall-off duration, and data quality, and that they are not always suitable for the rapid fall-off behaviour typical of XLOT and micro-fracture tests.

Among the evaluated methods, the semilogarithmic maximum derivative method proved to be the most operationally robust, combining high applicability with consistent closure picks across wells and cycles. Compared to external interpretations, this method shows an average offset of approximately 5.99 bar (1.77%), indicating systematic but relatively small bias compared to inter-method variability.

Taken together, these results demonstrate that method selection is the dominant source of uncertainty in closure-derived $S_{h\,\min}$, with systematic inter-method differences of up to ~ 10 bar and total spreads reaching 20–25 bar within individual cycles. The semilog max method provides the most reliable operational estimate within the analysed dataset.

Research question 3: *How reliable are FIT and LOT measurements relative to closure-derived estimates of $S_{h\,\min}$ within a well?*

FIT and LOT pressures cannot be interpreted as direct measurements of $S_{h\,\min}$. Leak-off pressures

generally exceed closure-derived stresses and increase with depth, consistent with fracture initiation behaviour rather than far-field stress equilibrium. In addition, approximately 26% of apparent tensile-strength values derived from LOP–FRP differences are negative, demonstrating that initiation-based interpretations are frequently non-physical and strongly influenced by near-wellbore effects.

Despite this, initiation-based pressures do provide useful constraints when interpreted in a mechanical framework. A stress consistency analysis shows that the majority of closure-derived $S_{h\,\min}$ values fall within physically expected bounds defined by the Kirsch-based minimum stress and the initiation-based envelope. Specifically, 95% of the semilog-derived $S_{h\,\min}$ values exceed the Kirsch minimum and 85% fall within the expected stress envelope. Comparable results are obtained for external interpretations (93% and 89%, respectively). This indicates that, while initiation-based pressures are not reliable as direct measurements, they are broadly consistent with closure-derived stresses when used as bounds.

However, the uncertainty associated with these bounds remains substantial. FIT pressures are influenced by stress concentrations and tensile-strength effects, meaning that the maximum recorded pressure can lie between $S_{h\,\min}$ and the leak-off pressure. Moreover, sensitivity analysis shows that uncertainties in tensile strength, $S_{H\,\max}$, and leak-off pressure can propagate into variations of several tens of bar in inferred stress magnitude. As a result, FIT and LOT data should be interpreted as qualitative constraints rather than quantitative estimates of $S_{h\,\min}$.

Research question 4: *To what extent can $S_{h\,\min}$ be inferred from offset FIT and LOT data?*

According to the performed case study, the $S_{h\,\min}$ cannot be reliably predicted from offset FIT and LOT data. Differences between offset initiation-based pressures and closure-derived stresses are substantial and cannot be explained by depth trends alone. Variations in lithology, permeability, wellbore configuration, and operational conditions introduce variability that is comparable to, or larger than, the stress signal of interest. As a result, offset data may define broad operational envelopes but do not provide quantitative predictions of $S_{h\,\min}$. Performing more case studies using validated XLOT and micro-frac $S_{h\,\min}$ data could give more insights.

Taken together, these results demonstrate that the most reliable estimation of $S_{h\,\min}$ is obtained from closure-based measurements, with interpretation uncertainty dominated by closure method selection (up to 20–25 bar), while initiation-based methods provide only constraints.

5.13. Recommendations

Based on the results and their mechanical interpretation, the following recommendations are made:

- **Standardize closure interpretation.** Report the closure method, filtering strategy, derivative window selection, operational factors (i.e. perforations, casing, viscosity fluid) and geological setting (i.e. permeability) Without these, closure-derived stress datasets are not directly comparable.
- **Use FIT/LOT as bounds (within one well), not as $S_{h\,\min}$ measurements.** Treat the leak-off pressure as an upper constraint (while taking into account deviation and orientation), and FIT as a potential lower constraint only after explicit model translation and sensitivity analysis on uncertain inputs (pore pressure, stress ratio, tensile strength bounds, wellbore geometry, vertical stress).
- **Investigate initiation observability.** Laboratory and controlled field experiments could give insights to which extent true initiation can be separated from observed macroscopic breakdown as a function of toughness, permeability, porosity, and viscosity. This will give an understanding in how to pick realistic leak-off pressure values.
- **Perform forward modelling to better understand the closure and initiation process.** As many input parameters were uncertain, it makes sense to use a hypothesized physical model to predict initiation and closure pressure, and compare to real data. This gives more insights into these parameters and the physical processes. Leak-off behaviour in natural fractured rock, or in high permeability rock, was not elaborate investigated in this study. Here forward modelling can help, as can be read in subsection 5.3.3.
- **Perform more case studies.** By performing more case studies that try to quantify the $S_{h\,\min}$ based on offset LOT and FIT data, one can get more insights into whether the $S_{h\,\min}$ can be

predicted this way. The Pressure SNS database could help with this (Verweij, 2015).

- **Consider empirical methods** These were not performed in this study, but empirical relations may provide first-order estimates when no closure data exist, but should be used as contextual benchmarks rather than as substitutes for closure-derived $S_{h\,\min}$ (see page 291 in Zoback (2010)).

6

Conclusion

6.1. Summary of conclusions

The main objective of this study was to determine to what extent the minimum horizontal stress $S_{h\,\min}$ can be reliably inferred from hydraulic stress tests, and whether initiation-based tests such as formation integrity tests (FIT) and leak-off tests (LOT) can be used to estimate $S_{h\,\min}$, either directly or through offset data. The research question was:

To what extent can the S_{hmin} be reliably estimated in regions for which only FIT and/or LOT data is available in the Netherlands?

The results demonstrate that $S_{h\,\min}$ cannot be reliably determined from initiation-based pressures under typical field conditions. Instead, closure-derived pressures from extended leak-off tests (XLOT) and micro-fracture tests provide the most reliable estimate of $S_{h\,\min}$, as fracture closure reflects mechanical equilibrium with the far-field stress field. Initiation-based pressures are strongly influenced by near-wellbore stress concentrations, rock strength, poroelastic effects, and operational factors, and should therefore be interpreted as constraints rather than direct stress measurements.

A key finding is that closure pressure is inherently method-dependent. Fracture closure is a progressive process, and different interpretation methods identify different stages of closure. In the analysed dataset, the spread between methods reaches up to approximately 20–25 bar, whereas the repeatability of a single method is much smaller, with an average cycle-to-cycle standard deviation of approximately 2.95 bar. Systematic differences between methods are also significant, with average inter-method offsets reaching up to ~ 10 bar. This demonstrates that interpretation methodology is the dominant source of uncertainty in closure-derived $S_{h\,\min}$.

Among the evaluated methods, the semilog max method proved to be the most operationally robust. It combines high applicability (approximately 84% success rate) with consistent closure picks and relatively small systematic bias (average offset of 5.99 bar or 1.77% compared to external interpretations). Other methods show clear limitations: the Haimson method systematically yields lower closure pressures, the Barree method tends to overestimate closure, and stiffness-based methods are only applicable in a small fraction of cases (approximately 13%), reflecting the absence of clear stiffness transitions in rapid fall-off data.

Initiation-based pressures from FIT and LOT tests exhibit fundamentally different behaviour. Leak-off pressures generally exceed closure-derived $S_{h\,\min}$ and increase with depth, reflecting fracture initiation rather than far-field stress equilibrium. In addition, approximately 26% of apparent tensile-strength values derived from LOP–FRP differences are negative, demonstrating that initiation-based interpretations are frequently non-physical and strongly affected by near-wellbore conditions.

When interpreted within a mechanical framework, initiation-based pressures provide constraints that are broadly consistent with closure-derived stresses, but remain highly uncertain. A stress consistency

analysis shows that 95% of semilog-derived $S_{h\,\min}$ values exceed the Kirsch-based minimum stress and 85% fall within the expected stress envelope. Comparable values are obtained for external interpretations (93% and 89%, respectively). However, sensitivity analysis demonstrates that uncertainties in tensile strength, $S_{H\,\max}$, and leak-off pressure can propagate into variations of several tens of bar in inferred stress magnitude. As a result, FIT and LOT data should be interpreted as qualitative bounds rather than quantitative estimates of $S_{h\,\min}$.

The case study further shows that initiation-based pressures from offset wells do not reliably predict $S_{h\,\min}$ at a target location. Differences between offset initiation pressures and closure-derived stresses are substantial and cannot be explained by depth trends alone. Variability in lithology, permeability, and operational conditions introduces uncertainty that is comparable to, or larger than, the stress signal of interest. While offset data may define broad operational envelopes, they cannot replace closure-based measurements.

Taken together, these findings support a hierarchical interpretation framework: closure-derived pressures from XLOT and micro-fracture tests provide primary estimates of $S_{h\,\min}$, LOT pressures provide upper-bound constraints, and FIT pressures only provide conditional lower bounds when interpreted through an explicit fracture initiation model.

Finally, this study demonstrates that uncertainty in stress estimation is controlled not only by subsurface variability, but also by interpretation methodology. The dominant uncertainty arises from closure method selection, followed by preprocessing-related effects, while uncertainties in mechanical models mainly affect initiation-based constraints.

In conclusion, reliable estimation of $S_{h\,\min}$ requires both appropriate test design and a consistent, physically informed interpretation framework. Closure-based measurements remain essential, while initiation-based pressures must be interpreted cautiously within a mechanical context. The reliability of $S_{h\,\min}$ estimation therefore depends as much on interpretation methodology as on the underlying physics of hydraulic fracturing.

6.1.1. Recommendations

Based on these findings, several recommendations can be made. Closure interpretation should be standardized by consistently reporting the applied method, data processing choices, and relevant operational and geological conditions. FIT and LOT data should be treated as bounds rather than direct measurements of $S_{h\,\min}$, with leak-off pressure providing an upper constraint and FIT a potential lower constraint only after explicit model-based translation and sensitivity analysis. Further research is needed to improve understanding of fracture initiation and its observability under varying conditions. Forward modelling is recommended to better constrain initiation and closure processes, particularly in complex formations. Expanding case studies, for example using the Pressure SNS database, would help assess the predictive value of offset data. Finally, empirical methods may provide first-order estimates where no closure data are available, but should only be used as contextual references rather than substitutes for closure-derived stress measurements.

References

Abou-Sayed, A. S., Brechtel, C. E., & Clifton, R. J. (1978). In situ stress determination by hydrofracturing: A fracture mechanics approach. *Journal of Geophysical Research: Solid Earth*, *83*(B6), 2851–2862. https://doi.org/10.1029/JB083iB06p02851

Addis, M., Hanssen, T., Yassir, N., & Willoughby, D. (1998). A comparison of leak-off test and mini-frac test data for stress estimation. *SPE/ISRM Rock Mechanics in Petroleum Engineering*. https://doi.org/10.2118/47260-MS

Alberty, M. W., & McLean, M. R. (2004). Fracture gradient: Why pressure integrity tests leak off. *SPE Drilling & Completion*, *19*(1), 28–38. https://doi.org/10.2118/77489-PA

Anderson, E. M. (1951). *The Dynamics of Faulting and Dyke Formation with Applications to Britain* (2nd). Oliver and Boyd.

Andrews, J. S., Fintland, T. G., Helstrup, O. A., Horsrud, P., & Raaen, A. M. (2016). Use of unique database of good quality stress data to investigate theories of fracture initiation, fracture propagation and the stress state in the subsurface. *Proceedings of the 50th US Rock Mechanics / Geomechanics Symposium*.

Bakhshi, E., Golsanami, N., & Chen, L. (2020). Numerical modeling and lattice method for characterizing hydraulic fracture propagation: A review of the numerical, experimental, and field studies. *Archives of Computational Methods in Engineering*. https://doi.org/10.1007/s11831-020-09501-6

Bakx, E., Buijze, L., & Wassing, B. e. a. (2022). *Formation, lithology and region-specific minimum horizontal stress field in the netherlands (warmingup theme 4b1 final report)* (tech. rep.). TNO.

Barree, R. D., Barree, V. L., & Craig, D. P. (2009). Diagnostic fracture injection tests: Common mistakes, misfires, and misconceptions. *SPE Production & Operations*, *24*(3), 468–475. https://doi.org/10.2118/107877-PA

Barton, N., Bandis, S., & Bakhtar, K. (1985). Strength, deformation and conductivity coupling of rock joints. *International Journal of Rock Mechanics and Mining Sciences & Geomechanics Abstracts*, *22*(3), 121–140. https://doi.org/10.1016/0148-9062(85)93227-9

Boone, T. J., & Ingraffea, A. R. (1990). A numerical procedure for simulation of hydraulically-driven fracture propagation in poroelastic media. *International Journal for Numerical and Analytical Methods in Geomechanics*, *14*(1), 27–47. https://doi.org/10.1002/nag.1610140103

Borden, M. J., Verhoosel, C. V., Scott, M. A., Hughes, T. J. R., & Landis, C. M. (2012). A phase-field description of dynamic brittle fracture. *Computer Methods in Applied Mechanics and Engineering*, *217–220*, 77–95. https://doi.org/10.1016/j.cma.2012.01.008

Bredehoeft, J. D., Wolff, R. G., Keys, W. S., & Shuter, E. (1976). Hydraulic fracturing to determine the regional in situ stress field, piceance basin, colorado. *Geological Society of America Bulletin*, *87*(2), 250–258. https://doi.org/10.1130/0016-7606(1976)87<250:HFTDTR>2.0.CO;2

Buijze, L., Fokker, P., & Wassing, B. (2021). *Quantification of induced seismicity potential of geothermal operations – analytical and numerical model approaches (warmingup theme 4b final report)* (tech. rep.). TNO.

Carslaw, H. S., & Jaeger, J. C. (1959). *Conduction of heat in solids*. Oxford University Press.

Carter, E. D. (1957). Optimum fluid characteristics for fracture extension. *Drilling and Production Practice*, 261–270.

Castillo, J. L. (1987). Modified fracture pressure decline analysis including pressure-dependent leakoff [Presented May 18–19, 1987]. *Proceedings of the SPE/DOE Low Permeability Reservoirs Symposium*, SPE 16417. https://doi.org/10.2118/16417-MS

Cundall, P. A., & Hart, R. D. (1985). *Development of generalized 2d and 3d distinct element programs for modeling jointed rock* (tech. rep.). Itasca Consulting Group Inc.

Dahi-Taleghani, A., & Olson, J. E. (2011). Numerical modeling of multistranded hydraulic fracture propagation: Accounting for the interaction between induced and natural fractures. *SPE Journal*, *16*(3), 575–581. https://doi.org/10.2118/124884-PA

Detournay, E., & Cheng, A. H.-D. (1988). Poroelastic response of a borehole in a non-hydrostatic stress field. *International Journal of Rock Mechanics and Mining Sciences & Geomechanics Abstracts*, *25*(3).

Dutler, N., Valley, B., Gischig, V., Jalali, M., Brixel, B., Krietsch, H., Roques, C., & Amann, F. (2020). Hydromechanical insight of fracture opening and closure during in-situ hydraulic fracturing in crystalline rock. *International Journal of Rock Mechanics and Mining Sciences*, *135*, 104450. https://doi.org/10.1016/j.ijrmms.2020.104450

Dutta, N. C., Bachrach, R., & Mukerji, T. (2021). *Quantitative analysis of geopressure for geoscientists and engineers*. Cambridge University Press. https://doi.org/10.1017/9781108151726.002

Economides, M. J., & Nolte, K. G. (2000). *Reservoir stimulation* (3rd ed.). John Wiley & Sons.

Fjær, E., Holt, R. M., Horsrud, P., Raaen, A. M., & Risnes, R. (2008). *Petroleum related rock mechanics* (2nd ed.). Elsevier.

Ge, S., Ghassemi, A., & Zhou, X. (2022). Induced seismicity during geoenergy development: A hydromechanical perspective. *Journal of Geophysical Research: Solid Earth*, *127*(8), e2022JB024268. https://doi.org/10.1029/2022JB024268

Griffith, A. A. (1921). The phenomena of rupture and flow in solids. *Philosophical Transactions of the Royal Society of London. Series A, Containing Papers of a Mathematical or Physical Character*, *221*(582–593), 163–198. https://doi.org/10.1098/rsta.1921.0006

Guglielmi, Y., McClure, M., Burghardt, J., Morris, J. P., Doe, T., Fu, P., Knox, H., Vermeul, V., & Kneafsey, T. (2022). Estimating Stress from Fracture Injection Tests: Comparing Pressure Transient Interpretations with in-situ Strain Measurements. *Proceedings of the 47th Workshop on Geothermal Reservoir Engineering*.

Haimson, B. C., & Cornet, F. H. (2003). ISRM suggested methods for rock stress estimation—part 3: Hydraulic fracturing (hf) and/or hydraulic testing of pre-existing fractures (HTPF). *International Journal of Rock Mechanics and Mining Sciences*, *40*(7–8), 1011–1020. https://doi.org/10.1016/j.ijrmms.2003.08.002

Haimson, B. C., & Fairhurst, C. (1967). Initiation and extension of hydraulic fractures in rocks. *Society of Petroleum Engineers Journal*, *7*(3), 310–318. https://doi.org/10.2118/1710-PA

Han, H., & van der Baan, M. (2024). Constraint strategies for estimating in-situ stress from borehole measurements. *Geomechanics for Energy and the Environment*, *37*, 100518. https://doi.org/10.1016/j.gete.2023.100518

Hardy, M. P. (1973). *Fracture mechanics applied to rock* [Doctoral dissertation, University of Minnesota].

Heidbach, O., Rajabi, M., Di Giacomo, D., Harris, J., Lammers, S., Morawietz, S., Pierdominici, S., Reiter, K., Storchak, D., von Specht, S., & Ziegler, M. O. (2025). World stress map 2025. https://doi.org/10.5880/WSM.2025.002

Hubbert, M. K., & Willis, D. G. (1957). Mechanics of hydraulic fracturing. *Petroleum Transactions, AIME*, *210*, 153–168.

Irwin, G. R. (1957). Analysis of stresses and strains near the end of a crack traversing a plate. *Journal of Applied Mechanics*, *24*, 361–364.

Ito, T. (2008). Effect of pore pressure gradient on fracture initiation in fluid saturated porous media: Rock. *Engineering Fracture Mechanics*, *75*(7). https://doi.org/https://doi.org/10.1016/j.engfracmech.2007.03.028

Ito, T., & Hayashi, K. (1991). Physical background to the breakdown pressure in hydraulic fracturing tectonic stress measurements. *International Journal of Rock Mechanics and Mining Sciences & Geomechanics Abstracts*, *28*(4), 285–293. https://doi.org/10.1016/0148-9062(91)90538-Q

Jaeger, J. C., & Cook, N. G. W. (1979). *Fundamentals of rock mechanics* (3rd ed.). Chapman and Hall.

Jung, H., Sharma, M. M., Cramer, D. D., Oakes, S., & McClure, M. W. (2016). Re-examining interpretations of non-ideal behavior during diagnostic fracture injection tests. *Journal of Petroleum Science and Engineering*, *146*, 942–957. https://doi.org/10.1016/j.petrol.2016.07.038

Kirsch, G. (1898). Die theorie der elastizität und die bedürfnisse der festigkeitslehre. *Zeitschrift des Vereines deutscher Ingenieure*, *42*, 797–807.

Lee, M. Y., & Haimson, B. C. (1989). Statistical evaluation of hydraulic fracturing stress measurement parameters. *International Journal of Rock Mechanics and Mining Sciences & Geomechanics Abstracts*, *26*(6), 447–456. https://doi.org/10.1016/0148-9062(89)91494-3

McClure, M., & Horne, R. N. (2014). An investigation of stimulation mechanisms in enhanced geothermal systems. *International Journal of Rock Mechanics and Mining Sciences*, *72*, 242–260. https://doi.org/10.1016/j.ijrmms.2014.07.011

McClure, M., Jung, H., Cramer, D., & Sharma, M. (2016). The fracture-compliance method for picking closure pressure from diagnostic fracture-injection tests. *SPE Journal*, *21*(4), 1321–1339.

McClure, M. (2017). *DFIT, LOT, XLOT, Mini-Frac, Micro-Frac, fracture calibration test: Navigating terminology* [Blog post]. ResFrac Corporation. Retrieved March 8, 2025, from https://www.resfrac.com/blog/dfit-lot-xlot-minifrac-microfrac-fracture-calibration-test-navigating-terminology

McClure, M., Bammidi, V., Cipolla, C., Cramer, D., Martin, L., Savitski, A. A., Sobernheim, D., & Voller, K. (2019). A collaborative study on DFIT interpretation: Integrating modeling, field data, and analytical techniques. *Proceedings of the Unconventional Resources Technology Conference (URTeC)*, URTeC–123. https://doi.org/10.15530/urtec-2019-123

Mechelse, E. (2017). *The in-situ stress field in the netherlands: Regional trends, local deviations and an analysis of the stress regimes in the northeast of the netherlands* [Master's thesis, Delft University of Technology].

Mijnbouwwet (2023). https://wetten.overheid.nl/BWBR0014168/

Morgenstern, N. (1962). A relation between hydraulic fracture pressures and tectonic stresses. *Pure and Applied Geophysics*, *52*.

Muntendam-Bos, A., Hoedeman, G., Polychronopoulou, K., Draganov, D., Weemstra, C., van der Zee, W., Bakker, R., & Roest, H. (2022). An overview of induced seismicity in the Netherlands. *Netherlands Journal of Geosciences*, *101*, e1. https://doi.org/10.1017/njg.2021.14

Nolte, K. G. (1979). Determination of fracture parameters from fracturing pressure decline. *SPE Annual Technical Conference and Exhibition*. https://doi.org/https://doi.org/10.2118/8341-MS

Peška, P., & Zoback, M. (1995). Compressive and tensile failure of inclined well bores and determination of in situ stress and rock strength. *Journal of Geophysical Research*, *12*(3). https://doi.org/https://doi.org/10.1029/95JB00319DigitalObjectIdentifier(DOI)

Planbureau voor de Leefomgeving. (2025). *Toekomstverkenning WLO 2025: Cahier klimaat en energie* (PBL-publicatienummer 5455).

Raaen, A. M., Skomedal, E., Kjærholt, H., Markestad, P., & Økland, D. (2001). Stress determination from hydraulic fracturing tests: The system stiffness approach. *International Journal of Rock Mechanics and Mining Sciences*, *38*(4), 529–541. https://doi.org/10.1016/S1365-1609(01)00020-X

Raaen, A. M., Horsrud, P., Kjørholt, H., & Økland, D. (2006). Improved routine estimation of the minimum horizontal stress component from extended leak-off tests. *International Journal of Rock Mechanics and Mining Sciences*, *43*(1), 37–48. https://doi.org/10.1016/j.ijrmms.2005.04.004

Schmitt, D. R., & Zoback, M. D. (1989). Poroelastic effects in the determination of the maximum horizontal principal stress in hydraulic fracturing tests: A proposed breakdown equation employing a modified effective stress relation for tensile failure. *International Journal of Rock Mechanics and Mining Sciences & Geomechanics Abstracts*, *26*(6), 499–506. https://doi.org/10.1016/0148-9062(89)91427-7

Sneddon, I. N. (1946). The distribution of stress in the neighbourhood of a crack in an elastic solid. *Proceedings of the Royal Society of London. Series A. Mathematical and Physical Sciences*, *187*(1009), 229–260. https://doi.org/10.1098/rspa.1946.0077

Stephens, G., & Voight, B. (1982). Hydraulic fracturing theory for conditions of thermal stress. *International Journal of Rock Mechanics and Mining Sciences & Geomechanics Abstracts*, *19*(6), 279–284. https://doi.org/10.1016/0148-9062(82)91364-X

Van der Voort, N., & Vanclay, F. (2015). Social impacts of earthquakes caused by gas extraction in the province of Groningen, the Netherlands. *Environmental Impact Assessment Review*, *50*, 1–15.

Van Eekelen, H. A. M. (1982). Hydraulic fracture geometry: Fracture containment in layered formations [SPE-9261-PA]. *SPE Journal*, *22*(3), 341–349. https://doi.org/10.2118/9261-PA

Van Oort, E., & Vargo, R. (2008). Improving formation strength tests and their interpretation. *SPE Drilling & Completion*, *23*(3), 284–294. https://doi.org/10.2118/105193-PA

Verdon, J. (2021). Managing the seismic risk of geologically stored CO_2 and geothermal energy extraction. *Nature Reviews Earth & Environment*, *2*(5), 310–323. https://doi.org/10.1038/s43017-021-00151-9

Verweij, J. (2015). *Integrated pressure information system for the onshore and offshore Netherlands* (tech. rep.). TNO. https://www.nlog.nl/sites/default/files/2020-05/TNO-Report-2015-R10065-final-public2020.pdf

Wang, H., & Sharma, M. M. (2019). Determine in-situ stress and characterize complex fractures in naturally fractured reservoirs from diagnostic fracture injection tests. *Rock Mechanics and Rock Engineering*, *52*(12), 5025–5045. https://doi.org/10.1007/s00603-019-01793-w

Wang, H., & Sharma, M. M. (2017). A non-local model for fracture closure on rough fracture faces and asperities. *Journal of Petroleum Science and Engineering*, *154*, 425–437. https://doi.org/10.1016/j.petrol.2017.04.024

Weijers, L. (1995). *The near-wellbore geometry of hydraulic fractures initiated from horizontal and deviated wells* [Doctoral dissertation, Delft University of Technology].

White, A. J., Traugott, M. O., & Swarbrick, R. E. (2002). The use of leak-off tests as means of predicting minimum in-situ stress. *Petroleum Geoscience*, *8*(3), 189–193. https://doi.org/10.1144/petgeo.8.3.189

Widodo, N., Rai, M., & Kramadibrata, S. (2003). Analysis of pressurizing borehole wall in a hydraulic fracturing test in laboratory. *Rock Stress '03*, 145–151.

Wu, F., Li, D., Fan, X., Liu, J., & Li, X. (2020). Analytical interpretation of hydraulic fracturing initiation pressure and breakdown pressure. *Journal of Natural Gas Science and Engineering*, *76*, 103185. https://doi.org/10.1016/j.jngse.2020.103185

Zang, A., & Stephansson, O. (2010). *Stress field of the earth's crust*. Springer.

Zhang, X., Wang, J., Gao, F., Ju, Y., & Liu, J. (2017). Impact of water and nitrogen fracturing fluids on fracturing initiation pressure and flow pattern in anisotropic shale reservoirs. *Computers and Geotechnics*, *81*, 59–76. https://doi.org/10.1016/j.compgeo.2016.08.004

Zimmerman, R. W. (2018). *Fluid flow in porous media*. World Scientific.

Zoback, M. D. (2010). *Reservoir geomechanics*. Cambridge University Press.

Zoback, M. D., Barton, C. A., Brudy, M., Castillo, D. A., Finkbeiner, T., Grollimund, B. R., Moos, D. B., Peska, P., Ward, C. D., & Wiprut, D. J. (2003). Determination of stress orientation and magnitude in deep wells. *International Journal of Rock Mechanics and Mining Sciences*, *40*(7–8), 1049–1076. https://doi.org/10.1016/j.ijrmms.2003.07.001

A

Derivation of one-dimensional linear diffusion in porous media

This appendix derives the one-dimensional linear pressure diffusion equation for single-phase fluid flow in porous media following the derivation of Zimmerman (2018).

Assumptions

The derivation is based on the following assumptions:

- Single-phase, slightly compressible fluid.
- One-dimensional flow in a homogeneous, isotropic porous medium.
- Darcy flow (laminar, low Reynolds number).
- Constant permeability k, porosity ϕ, and viscosity μ.
- Small pressure gradients such that nonlinear terms can be neglected.
- Deformation of the solid matrix is captured implicitly through pore compressibility.

Under these assumptions, pressure evolution is governed by diffusion rather than wave propagation.

Conservation of mass

Consider one-dimensional flow through a porous medium with constant cross-sectional area A. Conservation of mass requires that the net mass flux into a representative elementary volume equals the rate of change of fluid mass stored within it:

$$\text{mass in} - \text{mass out} = \frac{\partial m}{\partial t}. \tag{A.1}$$

The mass flux is given by ρq, where ρ is fluid density and q is the Darcy flux. For 1D flow, conservation of mass becomes

$$-\frac{\partial(\rho q)}{\partial x} = \frac{\partial(\rho \phi)}{\partial t}, \tag{A.2}$$

which is exact and applies irrespective of the constitutive law for flow.

Darcy's law

For single-phase flow in the horizontal direction, Darcy's law relates flux to the pressure gradient:

$$q = -\frac{k}{\mu}\frac{\partial p}{\partial x}, \tag{A.3}$$

where k is permeability and μ is fluid viscosity.

Substituting Eq. (A.3) into Eq. (A.2) yields

$$\frac{\partial}{\partial x}\left(\rho\,\frac{k}{\mu}\,\frac{\partial p}{\partial x}\right)=\frac{\partial(\rho\phi)}{\partial t}. \tag{A.4}$$

Linearisation and diffusion form

The storage term on the right-hand side can be expanded using the chain rule:

$$\frac{\partial(\rho\phi)}{\partial t}=\rho\phi\left(\frac{1}{\rho}\frac{d\rho}{dp}+\frac{1}{\phi}\frac{d\phi}{dp}\right)\frac{\partial p}{\partial t}=\rho\phi(c_f+c_\phi)\frac{\partial p}{\partial t}, \tag{A.5}$$

where c_f is the fluid compressibility and c_ϕ the pore compressibility. The total compressibility is defined as

$$c_t=c_f+c_\phi. \tag{A.6}$$

On the left-hand side of Eq. (A.4), density variations with pressure introduce a nonlinear term proportional to $(\partial p/\partial x)^2$. For slightly compressible liquids and typical reservoir pressure gradients, this term is negligible and can be omitted. The governing equation then reduces to

$$\frac{\partial p}{\partial t}=\frac{k}{\phi\mu c_t}\frac{\partial^2 p}{\partial x^2}. \tag{A.7}$$

Equation (A.7) is the one-dimensional linear pressure diffusion equation. The coefficient

$$D_H=\frac{k}{\phi\mu c_t} \tag{A.8}$$

is the hydraulic diffusivity and controls the rate at which pressure disturbances propagate through the porous medium.

B

Derivation of Carter leak-off from pressure diffusion

This appendix shows how the classical Carter leak-off scaling $q_\ell \propto 1/\sqrt{t}$ follows directly from the 1D linear pressure-diffusion equation in a semi-infinite porous medium (Carter, 1957). The key idealisation is that the pressure differential between fracture and formation is treated as constant during the early-time leak-off period.

Assumptions

- Single-phase, slightly compressible fluid; homogeneous porous medium.
- 1D flow normal to the fracture face (x-direction), semi-infinite domain $x \geq 0$.
- Constant properties k, ϕ, μ, c_t.
- Darcy flow.
- Constant pressure differential: $\Delta p = p_f - p_0$ is constant (early-time approximation).
- Fracture pressure is spatially uniform along the face (no along-fracture pressure gradients).

From PDE to ODE

Start from the 1D pressure diffusion equation

$$\frac{\partial p}{\partial t} = D_H \frac{\partial^2 p}{\partial x^2}, \qquad D_H = \frac{k}{\phi \mu c_t}, \tag{B.1}$$

with initial and boundary conditions

$$p(x,0) = p_0, \qquad x \geq 0, \tag{B.2}$$

$$p(0,t) = p_f = p_0 + \Delta p, \qquad t > 0, \tag{B.3}$$

$$p(x,t) \to p_0 \quad \text{as } x \to \infty. \tag{B.4}$$

Introduce the similarity variable

$$\eta = \frac{x}{2\sqrt{D_H t}}, \tag{B.5}$$

and seek a similarity solution of the form $p(x,t) = p_0 + \Delta p\, f(\eta)$, following the classical semi-infinite diffusion solution (Carslaw & Jaeger, 1959). Using

$$\frac{\partial \eta}{\partial x} = \frac{1}{2\sqrt{D_H t}}, \qquad \frac{\partial \eta}{\partial t} = -\frac{\eta}{2t},$$

the derivatives become

$$\frac{\partial p}{\partial t} = \Delta p\, f'(\eta)\, \frac{\partial \eta}{\partial t} = -\Delta p\, \frac{\eta}{2t} f'(\eta), \tag{B.6}$$

$$\frac{\partial^2 p}{\partial x^2} = \Delta p\, f''(\eta) \left(\frac{\partial \eta}{\partial x}\right)^2 = \Delta p\, f''(\eta)\, \frac{1}{4D_H t}. \tag{B.7}$$

Substituting into Eq. (B.1) and cancelling common factors yields the ODE

$$f''(\eta) + 2\eta f'(\eta) = 0. \tag{B.8}$$

Similarity solution

Let $g(\eta) = f'(\eta)$. Then Eq. (B.8) becomes

$$g' + 2\eta g = 0 \quad \Rightarrow \quad g(\eta) = C_1 e^{-\eta^2}. \tag{B.9}$$

Integrating once more,

$$f(\eta) = C_1 \int_0^\eta e^{-s^2}\, ds + C_2. \tag{B.10}$$

Apply the boundary conditions:

$$f(0) = 1 \Rightarrow C_2 = 1, \qquad f(\infty) = 0 \Rightarrow 0 = C_1 \int_0^\infty e^{-s^2}\, ds + 1.$$

Using $\int_0^\infty e^{-s^2} ds = \frac{\sqrt{\pi}}{2}$, we obtain $C_1 = -\frac{2}{\sqrt{\pi}}$. Therefore,

$$f(\eta) = 1 - \frac{2}{\sqrt{\pi}} \int_0^\eta e^{-s^2}\, ds = \operatorname{erfc}(\eta), \tag{B.11}$$

and the pressure field is

$$p(x,t) = p_0 + \Delta p\, \operatorname{erfc}\!\left(\frac{x}{2\sqrt{D_H t}}\right). \tag{B.12}$$

Leak-off flux and the $1/\sqrt{t}$ (Carter) scaling

Darcy flux normal to the fracture face is

$$q_\ell(t) = -\frac{k}{\mu} \left.\frac{\partial p}{\partial x}\right|_{x=0}. \tag{B.13}$$

Differentiate Eq. (B.12). Using

$$\frac{d}{d\eta} \operatorname{erfc}(\eta) = -\frac{2}{\sqrt{\pi}} e^{-\eta^2}, \qquad \frac{\partial \eta}{\partial x} = \frac{1}{2\sqrt{D_H t}},$$

gives

$$\frac{\partial p}{\partial x} = \Delta p \left(-\frac{2}{\sqrt{\pi}} e^{-\eta^2}\right) \frac{1}{2\sqrt{D_H t}} = -\frac{\Delta p}{\sqrt{\pi D_H t}} e^{-\eta^2}. \tag{B.14}$$

At the fracture face $x = 0$ we have $\eta = 0$ and $e^{-\eta^2} = 1$, so

$$\left.\frac{\partial p}{\partial x}\right|_{x=0} = -\frac{\Delta p}{\sqrt{\pi D_H t}}. \tag{B.15}$$

Substitute into Eq. (B.13):

$$q_\ell(t) = \frac{k}{\mu} \frac{\Delta p}{\sqrt{\pi D_H t}} = \Delta p \sqrt{\frac{k\phi c_t}{\pi \mu}}\, \frac{1}{\sqrt{t}}. \tag{B.16}$$

Equation (B.16) is the Carter leak-off scaling: the leak-off *flux per unit fracture area* decays as $t^{-1/2}$. It is common to write Eq. (B.16) as

$$q_\ell(t) = \frac{C_L}{\sqrt{t}}, \qquad C_L = \Delta p \sqrt{\frac{k\phi c_t}{\pi \mu}}, \tag{B.17}$$

where C_L is the (effective) Carter leak-off coefficient.

Factor 2 and factor 4: two fracture faces and integrated volume

A planar hydraulic fracture has two faces exposed to leak-off. If the leak-off flux on each face is $q_\ell(t)$ (per unit area), then the total leak-off *rate* from a fracture of one-face area A_f is

$$Q_\ell(t) = 2A_f\, q_\ell(t) = \frac{2A_f C_L}{\sqrt{t}}. \tag{B.18}$$

The factor 2 appears purely because there are two faces.

The cumulative leak-off volume after shut-in over a time interval $[0, t]$ is obtained by integrating:

$$V_\ell(t) = \int_0^t Q_\ell(\tau)\, d\tau = 2A_f C_L \int_0^t \tau^{-1/2}\, d\tau = 4A_f C_L \sqrt{t}. \tag{B.19}$$

The factor 4 is therefore the combination of (i) two faces and (ii) integrating $t^{-1/2}$ over time.

C

Hoop Stresses Around Deviated Wellbores

Introduction

Stress concentrations around a wellbore control wellbore stability, fracture initiation, and the interpretation of hydraulic stress tests such as leak-off tests (LOTs) and formation integrity tests (FITs). While vertical wells represent a simplified case in which the wellbore axis is aligned with a principal stress direction, most subsurface wells are deviated. In deviated wells, the in-situ stress tensor must be transformed into a local wellbore coordinate system prior to evaluating stresses acting at the borehole wall (Zoback, 2010).

This appendix presents the theoretical framework for calculating hoop stresses around deviated wellbores using linear elastic theory and the generalized Kirsch solution. The formulation closely follows the approaches described by Peška and Zoback (1995) and Zoback (2010) and provides the basis for interpreting tensile fracture initiation and for correcting LOT/FIT data obtained in deviated wells.

Far-Field Stress State

The in-situ stress state is assumed to be defined by three mutually orthogonal principal stresses:

$$S_P = \begin{bmatrix} S_{H\,\max} & 0 & 0 \\ 0 & S_{h\,\min} & 0 \\ 0 & 0 & S_v \end{bmatrix}, \tag{C.1}$$

where $S_{H\,\max}$ and $S_{h\,\min}$ are the maximum and minimum horizontal stresses, respectively, and S_v is the vertical stress. The orientation of $S_{H\,\max}$ is specified by its azimuth in the horizontal plane. This stress parameterization is standard in reservoir geomechanics and is widely adopted in wellbore stability analyses (Jaeger & Cook, 1979; Zoback, 2010).

Wellbore Coordinate System

For a point along the trajectory of a deviated wellbore, a local Cartesian coordinate system (x_b, y_b, z_b) is defined (Fig. C.1). The z_b-axis is aligned with the wellbore axis, the x_b-axis points radially from the center of the borehole toward the deepest point of the wellbore cross-section, and the y_b-axis completes a right-handed coordinate system in the plane normal to the wellbore axis (Peška & Zoback, 1995).

The well trajectory is described by the inclination δ (measured from the vertical) and the azimuth φ (measured clockwise from the geographical reference direction).

Stress Tensor Transformation

Let S_G denote the stress tensor expressed in the geographical coordinate system. The stress tensor in the wellbore coordinate system S_W is obtained by applying a rotation matrix $R_{GW}(\delta, \varphi)$:

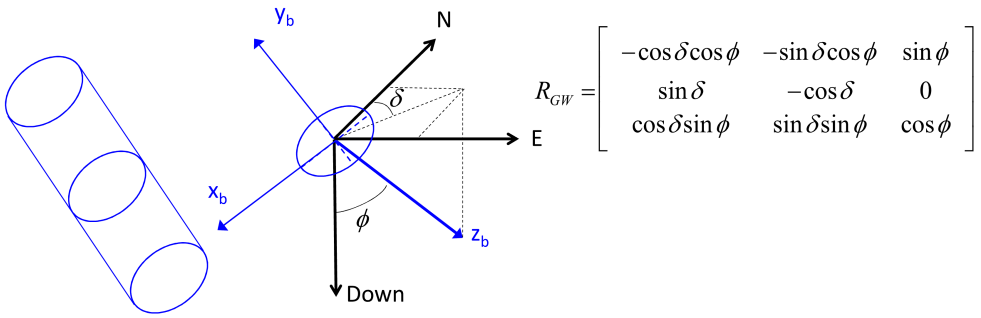

Figure C.1: Wellbore coordinate system for a deviated well.

$$S_W = R_{GW}\, S_G\, R_{GW}^T. \tag{C.2}$$

Alternatively, when stresses are defined in the principal stress coordinate system, the transformation can be written as:

$$S_W = R_{GW}\, R_{PG}^T\, S_P\, R_{PG}\, R_{GW}^T, \tag{C.3}$$

where R_{PG} is the rotation matrix from the principal stress coordinate system to the geographical coordinate system. These transformations follow standard tensor rotation rules used in borehole stress analysis.

The resulting stress tensor in the wellbore coordinate system is:

$$S_W = \begin{bmatrix} S_{11} & S_{12} & S_{13} \\ S_{21} & S_{22} & S_{23} \\ S_{31} & S_{32} & S_{33} \end{bmatrix}. \tag{C.4}$$

Effective Far-Field Stresses

Effective stresses acting on the wellbore wall are defined by subtracting the pore pressure P_p from the normal stress components:

$$\sigma_{11} = S_{11} - P_p, \tag{C.5}$$
$$\sigma_{22} = S_{22} - P_p, \tag{C.6}$$
$$\sigma_{33} = S_{33} - P_p, \tag{C.7}$$
$$\sigma_{12} = S_{12}, \tag{C.8}$$
$$\sigma_{13} = S_{13}, \tag{C.9}$$
$$\sigma_{23} = S_{23}. \tag{C.10}$$

These effective stresses represent the far-field boundary conditions used in the Kirsch solution.

Kirsch Solution for Deviated Wellbores

Assuming a circular wellbore of radius a drilled in a homogeneous, isotropic, linear-elastic medium, the generalized Kirsch equations provide the stress distribution at the borehole wall ($r = a$). In cylindrical coordinates (r, θ, z) aligned with the wellbore, the stresses are given by:

$$\sigma_{rr}(a,\theta) = P_w - P_p, \tag{C.11}$$
$$\sigma_{\theta\theta}(a,\theta) = \sigma_{11} + \sigma_{22} - 2(\sigma_{11} - \sigma_{22})\cos(2\theta) - 4\sigma_{12}\sin(2\theta) - (P_w - P_p), \tag{C.12}$$
$$\sigma_{zz}(a,\theta) = \sigma_{33} - 2\nu(\sigma_{11} - \sigma_{22})\cos(2\theta) - 4\nu\sigma_{12}\sin(2\theta), \tag{C.13}$$
$$\sigma_{\theta z}(a,\theta) = 2(\sigma_{23}\cos\theta - \sigma_{13}\sin\theta), \tag{C.14}$$

where P_w is the wellbore pressure, ν is Poisson's ratio, and θ is the circumferential angle around the borehole.

Closed-Form Minimum Hoop Stress

The circumferential stress $\sigma_{\theta\theta}(a,\theta)$ varies with θ. Its minimum value over the borehole wall admits a closed-form expression:

$$\min_{\theta} \sigma_{\theta\theta}(a,\theta) = \sigma_{11} + \sigma_{22} - 2\sqrt{(\sigma_{11} - \sigma_{22})^2 + (2\sigma_{12})^2} - (P_w - P_p). \tag{C.15}$$

This expression highlights the combined influence of stress anisotropy and far-field shear stress on tensile failure in deviated wells.

Tensile Failure Criterion and Critical Pressure

Tensile fracture initiation is assumed to occur when the minimum effective hoop stress equals the tensile strength T_0 of the rock:

$$\min_{\theta} \sigma_{\theta\theta}(a,\theta) = -T_0. \tag{C.16}$$

Substituting the closed-form minimum hoop stress yields the critical wellbore pressure required to initiate tensile failure:

$$P_{w,\mathrm{crit}} = P_p + (\sigma_{11} + \sigma_{22}) - 2\sqrt{(\sigma_{11} - \sigma_{22})^2 + (2\sigma_{12})^2} + T_0. \tag{C.17}$$

This equation forms the basis for predicting LOT and FIT pressures in deviated wells and is widely used in wellbore stability and hydraulic fracturing analyses.

Local Principal Stresses and Fracture Orientation

The local stress state at the borehole wall is defined by $(\sigma_{\theta\theta}, \sigma_{zz}, \sigma_{\theta z})$. The local principal stresses are obtained as the eigenvalues of:

$$\begin{bmatrix} \sigma_{\theta\theta} & \sigma_{\theta z} \\ \sigma_{\theta z} & \sigma_{zz} \end{bmatrix}. \tag{C.18}$$

The principal stress directions generally form an angle with respect to the wellbore axis. As a result, tensile fractures in deviated wells may initiate at an angle to the borehole axis and develop as short, inclined en-échelon fracture segments rather than a single longitudinal fracture.

Implications for Stress Test Interpretation

In vertical wells, LOT and FIT pressures are commonly interpreted as direct proxies for the minimum horizontal stress $S_{h\,\min}$. In deviated wells, however, measured pressures correspond to the condition at which the minimum hoop stress becomes tensile, which depends on both the stress state and the well trajectory.

Therefore, interpretation of stress tests in deviated wells requires explicit calculation of hoop stresses using the transformed stress tensor and the generalized Kirsch solution. The critical pressure equation may be inverted numerically to estimate $S_{h\,\min}$ from observed LOT or FIT pressures.

D

Sensitivity analysis of the Kirsch-based fracture initiation model

The analytical fracture initiation framework used in this study is based on the classical Kirsch solution for stresses around a cylindrical wellbore. Under simplified conditions for a vertical well, fracture initiation occurs when the effective circumferential stress at the borehole wall reaches the tensile strength of the rock. In this formulation, the initiation pressure can be expressed as

$$P_{\text{init}} = 3S_{h\,\min} - S_{H\,\max} - P_p + T_0, \tag{D.1}$$

where $S_{h\,\min}$ and $S_{H\,\max}$ denote the minimum and maximum horizontal stresses, P_p is the pore pressure, and T_0 is the tensile strength of the rock. Inverting this relation allows $S_{h\,\min}$ to be estimated from an observed leak-off or breakdown pressure under the assumptions of the model.

Because several parameters in this equation are uncertain in field applications, a sensitivity analysis was performed to evaluate how these uncertainties influence the inferred value of $S_{h\,\min}$. The analysis focuses on parameters that are either directly measured with uncertainty (e.g. leak-off pressure), or indirectly constrained and therefore highly uncertain (e.g. tensile strength and $S_{H\,\max}$).

Input parameters and assumptions

Four parameters were varied in the sensitivity analysis: leak-off pressure (LOP), maximum horizontal stress $S_{H\,\max}$, pore pressure P_p, and tensile strength T_0. These were selected because they directly enter the Kirsch-based initiation equation and are typically uncertain in field applications.

- **Leak-off pressure (LOP):** The LOP represents the observed pressure at which the formation begins to deviate from linear pressurization. Although it is measured, it is subject to interpretation uncertainty (e.g. picking method, data quality). A range of ± 5–10 bar around a nominal value was used to represent typical picking uncertainty observed in the dataset.
- **Maximum horizontal stress $S_{H\,\max}$:** This parameter is rarely measured directly and is typically inferred from regional stress models or borehole observations. A range of approximately ± 10–20 bar around a nominal stress gradient was assumed to reflect realistic uncertainty in regional stress estimates.
- **Pore pressure P_p:** Pore pressure is generally better constrained than stress magnitudes, especially in well-characterized formations. A relatively narrow range of ± 5 bar was used to reflect measurement and interpretation uncertainty.
- **Tensile strength T_0:** Tensile strength is one of the most uncertain parameters in field applications. Laboratory values often range between 0 and 10 MPa (0–100 bar), but in-situ values may be significantly lower due to microfractures, damage, or anisotropy. In this study, a broad range of 0–100 bar was used to reflect this uncertainty.

All parameters were assumed to be independent and uniformly distributed within their respective ranges. Although this is a simplification, it provides a first-order estimate of uncertainty propagation without introducing additional assumptions about parameter correlations.

Monte Carlo sensitivity analysis

A Monte Carlo simulation was used to propagate parameter uncertainty into the inferred stress magnitude. For each realization, values of LOP, $S_{H\,\max}$, P_p, and T_0 were randomly sampled within the ranges defined above and inserted into the inverted Kirsch equation to compute $S_{h\,\min}$.

Repeating this process for a large number of realizations produces a distribution of plausible stress values rather than a single deterministic estimate. Figure D.1 shows the resulting distribution.

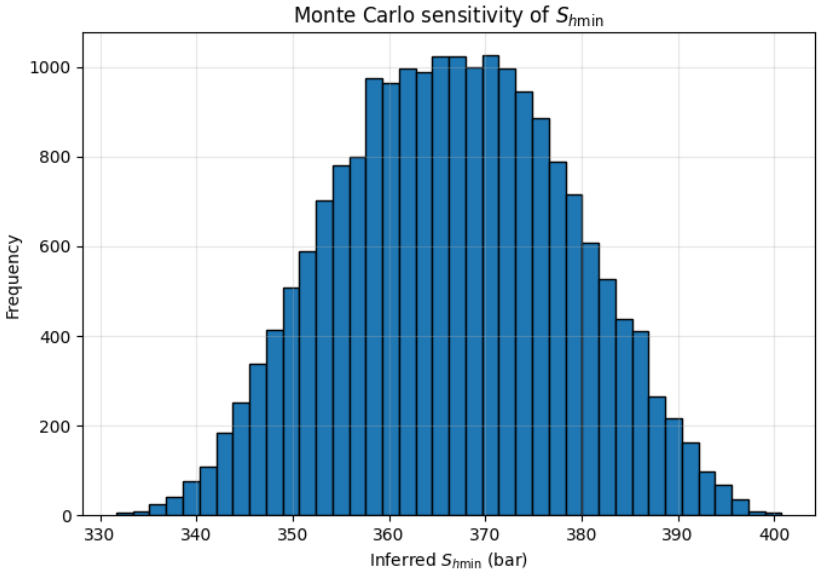

Figure D.1: Monte Carlo sensitivity analysis of the inverted Kirsch model. The histogram shows the distribution of inferred $S_{h\,\min}$ values resulting from uncertainty in leak-off pressure, maximum horizontal stress, pore pressure, and tensile strength.

The resulting distribution is approximately Gaussian and centred around the nominal stress estimate. Its width indicates that realistic parameter uncertainty can produce variations of several tens of bar in the inferred stress magnitude. This highlights that initiation-based stress estimates are highly sensitive to assumptions about poorly constrained parameters.

Relative parameter sensitivity

To assess the relative importance of each parameter, a tornado-style sensitivity analysis was performed. Each parameter was varied individually while others were held fixed at their nominal values.

Figure D.2 shows that tensile strength T_0 exerts the strongest influence on the inferred $S_{h\,\min}$ within the assumed ranges. Variations in $S_{H\,\max}$ and LOP also significantly affect the result, whereas pore pressure has a comparatively smaller impact.

The strong sensitivity to tensile strength reflects a fundamental limitation of initiation-based stress estimation, as this parameter is rarely known for in-situ conditions and may vary significantly due to rock damage and heterogeneity.

Sensitivity to well trajectory

The Kirsch formulation assumes a vertical well aligned with a principal stress direction. In deviated wells, however, the far-field stress tensor must be transformed into the borehole coordinate system. Fracture initiation then occurs when the most tensile effective stress at the borehole wall reaches the tensile strength criterion.

A numerical sensitivity study was performed by varying well inclination and azimuth while keeping the

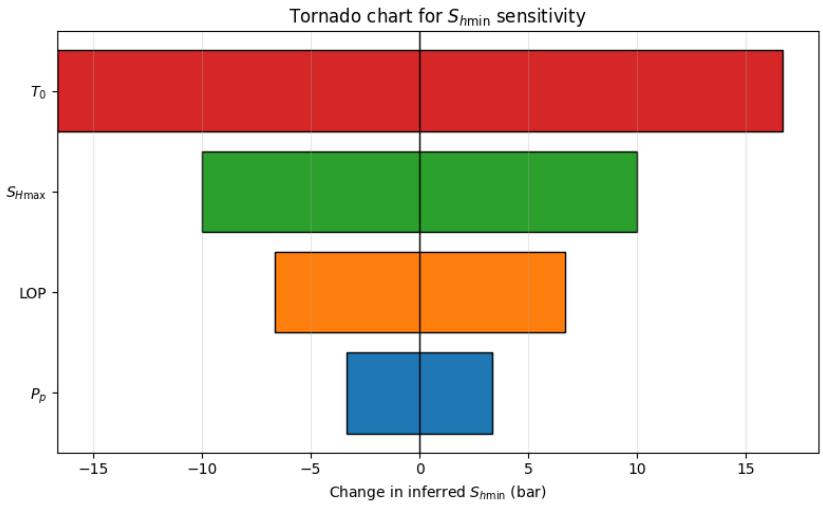

Figure D.2: Tornado chart showing the sensitivity of the inferred $S_{h\,\min}$ to uncertainty in the parameters of the Kirsch-based fracture initiation model.

far-field stress state constant. Figure D.3 shows that initiation pressure varies significantly with well inclination and azimuth.

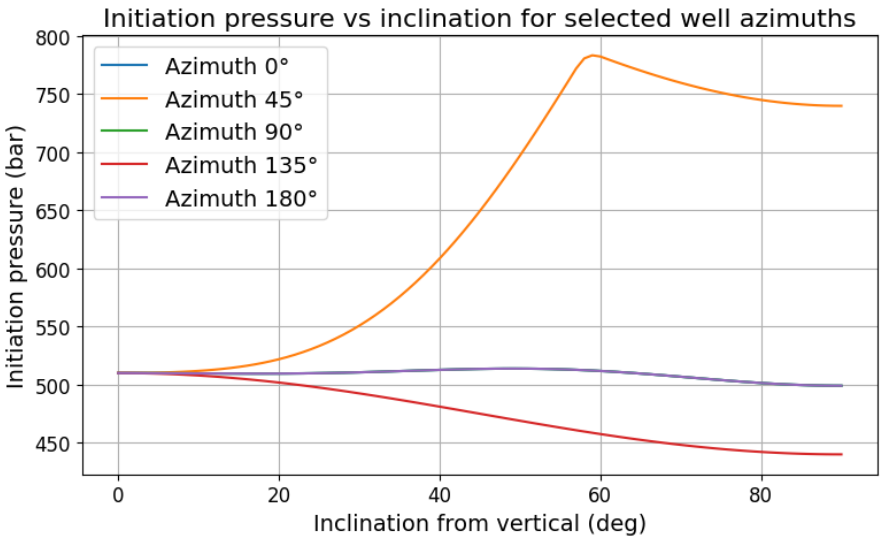

Figure D.3: Sensitivity of fracture initiation pressure to well inclination for several well azimuths. Note that some azimuths give similar results.

The full dependence is illustrated in Figure D.4, where initiation pressure is mapped as a function of well trajectory.

These results demonstrate that initiation pressure depends not only on stress magnitude but also on well orientation. Consequently, initiation-based pressures from different wells cannot be directly compared without accounting for trajectory effects.

Implications for stress estimation

The sensitivity analysis demonstrates that stress estimates derived from the Kirsch-based initiation model are inherently uncertain. Variations in tensile strength, $S_{H\,\max}$, and leak-off pressure can produce differences of several tens of bar in inferred $S_{h\,\min}$, while well trajectory introduces additional variability.

Together, these results show that initiation-based pressures do not uniquely constrain the far-field stress

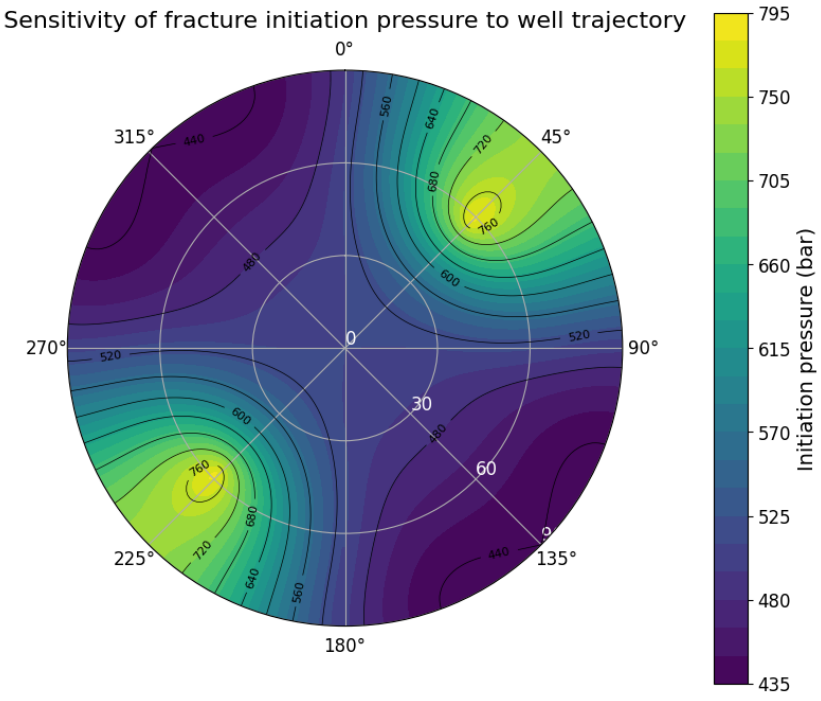

Figure D.4: Polar representation of fracture initiation pressure as a function of well trajectory.

state without additional assumptions. Closure-derived pressures from hydraulic fracture tests therefore remain the most reliable indicator of $S_{h\,\min}$, as they reflect mechanical equilibrium rather than local failure conditions.

E

AI Disclosure Statement

I hereby confirm that the present work is my original work. I declare that I have used AI tools only as allowed for this work. The AI tool used was ChatGPT (OpenAI).

Purpose of the AI tool deployment:

- Editing and improving readability, clarity of expression, and grammar of text written by the author.
- Brainstorming and structuring sections of the thesis (e.g., refinement of argument flow and formulation of research objectives).
- Exploratory consultation on general background information, comparable to the use of a search engine.
- Debugging and troubleshooting code written by the author (e.g., identifying syntax errors, improving code structure, and resolving implementation issues).

No AI tools were used for autonomous data analysis, independent generation of research results, or formulation of scientific conclusions. All analyses, interpretations, methodological decisions, coding implementations, and final written content are the original work of the author. All AI-generated outputs were critically reviewed, verified, and, where necessary, revised by the author.

I acknowledge my responsibility as a student to thoroughly verify all outputs and content produced by AI tools and accept full accountability for their accuracy and validity.